UNIVERSIDADE ESTADUAL DE CAMPINAS
Instituto de Biologia

LUIZ ALBERTO BANDEIRA FERREIRA

MECANISMO DE MORTE CELULAR E TOXICIDADE *IN VIVO* DE NANOPARTÍCULAS BIOSSINTÉTICAS DE PRATA

CELL DEATH MECHANISM AND *IN VIVO* TOXICITY OF BIOGENIC SILVER NANOPARTICLES

CAMPINAS
2019

LUIZ ALBERTO BANDEIRA FERREIRA

MECANISMO DE MORTE CELULAR E TOXICIDADE IN VIVO DE NANOPARTÍCULAS BIOSSINTÉTICAS DE PRATA

CELL DEATH MECHANISM AND *IN VIVO* TOXICITY OF BIOGENIC SILVER NANOPARTICLES

Thesis presented to the Institute of Biology of the University of Campinas in partial fulfillment of the requirements for the degree of Doctor in Science, in the area of Drugs, Medicines and Supplies for Health.

Tese apresentada ao Instituto de Biologia da Universidade Estadual de Campinas como parte dos requisitos exigidos para a obtenção do título de Doutor em Ciências, na área de Fármacos, Medicamentos e Insumos para Saúde.

Orientadores: MARCELO BISPO DE JESUS
Co-Orientadora: MARIA ALICE DA CRUZ HÖFLING

ESTE ARQUIVO DIGITAL CORRESPONDE A VERSÃO FINAL DA TESE DEFENDIDA PELO ALUNO LUIZ ALBERTO BANDEIRA FERREIRA E ORIENTADA PELO PROF. DR. MARCELO BISPO DE JESUS

CAMPINAS
2019

Ficha catalográfica
Universidade Estadual de Campinas
Biblioteca do Instituto de Biologia
Mara Janaina de Oliveira - CRB 8/6972

F413m

Ferreira, Luiz Alberto Bandeira, 1984-
Mecanismo de morte celular e toxicidade *in vivo* de nanoparticulas biossinteticas de prata / Luiz Alberto Bandeira Ferreira. – Campinas, SP : [s.n.], 2019.

Orientador: Marcelo Bispo de Jesus.
Tese (doutorado) – Universidade Estadual de Campinas, Instituto de Biologia.

1. Nanopartículas de prata. 2. N-acetilcisteína. 3. Quelantes. 4. Antídotos. 5. Regressão tumoral. I. Jesus, Marcelo Bispo de, 1980-. II. Universidade Estadual de Campinas. Instituto de Biologia. III. Título.

Informações para Biblioteca Digital

Título em outro idioma: Cell death mechanism and *in vivo* toxicity of biogenic silver nanoparticles
Palavras-chave em inglês:
Silver nanoparticles
N-acetylcysteine
Chelating agents
Antidotes
Tumor regression
Área de concentração: Fármacos, Medicamentos e Insumos para Saúde
Titulação: Doutor em Ciências
Banca examinadora:
Marcelo Bispo de Jesus [Orientador]
Talita Miguel Marin
Laura de Oliveira Nascimento
Juliana Minardi Nascimento
Ana Carolina Santos de Souza Galvão
Data de defesa: 29-08-2019
Programa de Pós-Graduação: Biociências e Tecnologia de Produtos Bioativos

Identificação e informações acadêmicas do(a) aluno(a)
- ORCID do autor: https://orcid.org/ 0000-0002-9466-1445
- Currículo Lattes do autor: http://lattes.cnpq.br/3529488141488849

Campinas, 29 de agosto de 2019.

COMISSÃO EXAMINADORA

Prof. Dr. Marcelo Bispo de Jesus (Presidente)

Profa. Dra. Talita Miguel Marin

Profa. Dra. Laura de Oliveira Nascimento

Profa. Dra. Juliana Minardi Nascimento

Profa. Dra. Ana Carolina Santos de Souza Galvão

Os membros da Comissão Examinadora acima assinaram a Ata de Defesa, que se encontram no processo de vida acadêmica do aluno.

A ata da defesa com as respectivas assinaturas dos membros da banca examinadora encontra-se no SIGA/Sistema de Fluxo de Dissertação/Tese e na Secretaria do Programa de Biociências e Tecnologia de Produtos Bioativos da Unidade Instituto de Biologia UNICAMP.

Dedicatoria

“Agradeço a Deus, pois sem ele eu não teria forças para percorrer essa longa jornada.
À minha amada mãe, meu maior exemplo de vida e superação”

Agradecimento

À minha família, principalmente minha mãe Marcia, por incentivar a minha profissão e dar todo o amparo necessário nesta caminhada;

Ao meu orientador Dr. Marcelo Bispo de Jesus, por ter acreditado no meu potencial, pelos ensinamentos, amizade e todo suporte necessário possível para realização deste trabalho.

Aos professores Dr. Nelson Durán e Wagner Fávaro pelas boas conversas e colaborações criadas ao decorrer deste trabalho.

À Profa. Dra. Maria Alice da Cruz-Höfling e a Dra. Monique Culturato Padilha Mendonça pela parceria e suporte nos estudos *in vivo*.

À Profa. Dra. Eneida de Paula e ao grupo do Laboratório de Biomenbranas pelas colaborações e suporte estrutural na caracterização de nanomateriais.

Ao Prof. Dr. Marco Aurélio Ramirez Vinolo e alunos pelos ensinamentos na extração de cultura primária de macrófagos e processos inflamatórios.

Os companheiros do laboratório NanoCell, Allan Radaic, Guilherme Campese, Fernanda Garcia Fóssa e Samara Bonesso e Juliana Mattoso pelas boas conversas, apoio nos momentos mais difíceis e grande amizade.

Ao Professor Carlos Bonafé e alunos Ancelmo e Marriam pela amizade e boas conversas.

Ao Programa de Pós-Graduação em Biociências e Tecnologia de Produtos Bioativos pela oportunidade de desenvolver este trabalho científico.

"O presente trabalho foi realizado com apoio da Coordenação de Aperfeiçoamento de Pessoal de Nível Superior - Brasil (CAPES) - Código de Financiamento 001"

Resumo

As nanopartículas de prata (AgNP) apresentam alta atividade antimicrobiana, propriedade essa de grande interesse científico-industrial. Em vista disso, cresce também a preocupação em relação ao uso, manipulação e eliminação desse nanomaterial, visando uma aplicação mais segura. Existem muitos estudos sobre os efeitos tóxicos causados por AgNP sintetizadas por métodos químicos ou biológicos. Entretanto, estudos da citotoxicidade de nanopartículas biossintéticas pode trazer particularidades. Um exemplo disso é a obtenção de AgNP pelo fungo *Fusarium oxysporum,* que leva a formação de nanopartículas com características únicas (*i.e.*, corona de proteínas fúngicas). Desta forma, as AgNP biossintéticas apresentam-se como uma alternativa promissora e pouco explorada em literatura, o que garante a originalidade deste presente trabalho. Ainda há poucos relatos sobre o seu efeito citotóxico, principalmente sobre os estudos do processamento celular e efeitos no metabolismo dessas partículas. Diante deste cenário, este trabalho teve como objetivo explorar, nas áreas da nanotoxicologia e nanomedicina, diferentes abordagens e aplicações para as AgNP biossintéticas, particularmente através dos estudos sobre os seus mecanismos moleculares de toxicidade, busca novos tratamentos contra a intoxicação por prata e aplicação oncológica no tratamento do câncer de bexiga. Nossos resultados mostraram que a complexação entre tiol-antioxidantes e nanopartículas metálicas pode gerar interpretações equivocadas nos mecanimos moleculares de citotoxicidade, principalmente envolvendo as intrpretações sobre o papel do estresse oxidativo. Este artefato exemplifica potenciais armadilhas na compreensão do mecanismo de nanotoxicidade. Em adicional, demonstramos que os tiol-antioxidantes, como a N-acetilcisteína (NAC), atuaram de forma preventiva contra os efeitos tóxicos das AgNP *in vivo*, sugerindo NAC como potencial candidato para intervenção precoce em casos de intoxicação por AgNPs. Por fim, direcionamos os achados sobre a citotoxicidade das AgNP biossintéticas para uma nova aplicação terapêutica. Os promissores resultados obtidos *in vitro* de genotoxicidade, indução de apoptose, redução da migração e proliferação celular, refletiram nos ensaios *in vivo* no modelo de câncer de bexiga não músculo invasivo, onde observamos relevante regressão tumoral. Assim, esses achados sugerem as AgNP como uma alternativa econômica e possível candidato a fármaco no tratamento do câncer de bexiga.

Palavras-Chave: nanopartículas de prata; biossintéticas; tiol-antioxidantes; NAC; quelante; antídoto; câncer de bexiga; regressão tumoral.

Abstract

Silver nanoparticles (AgNP) show high antimicrobial activity, a property of great scientific-industrial interest. Thus, there is a growing concern about the use, manipulation, and elimination of this nanomaterial, aiming at a safer application. Many studies investigate the toxic effects caused by AgNP synthesized by chemical or biological methods. However, studies of the cytotoxicity of biosynthetic nanoparticles may bring particularities. An example of this is the obtaining of AgNP by the fungus *Fusarium oxysporum*, which leads to the formation of nanoparticles with unique characteristics (i.e., the corona of fungal proteins). Hence, the biosynthetic AgNP presents as a promising alternative and little explored in the literature, which guarantees the originality of this present work. There are still few reports on its cytotoxic effect, mainly on the studies of cellular processing and impact on the metabolism of these nanoparticles. Given this scenario, this work aimed to explore, in the areas of nanotoxicology and nanomedicine, different approaches and applications for biosynthetic AgNP, mainly through studies on their molecular mechanisms of toxicity, search for new treatments against silver intoxication and oncological use in the treatment of bladder cancer. Our results showed that the complexation between thiol-antioxidants and metallic nanoparticles could generate misinterpretations in the molecular mechanisms of AgNP cytotoxicity, mainly involving the interpretations of the role of oxidative stress. This artifact exemplifies potential pitfalls in understanding the mechanism of nanotoxicity. Also, we demonstrated that thiol-antioxidants, such as N-acetylcysteine (NAC), prevented the toxic effects of AgNP *in vivo*, suggesting NAC as a potential candidate for early intervention in cases of AgNP poisoning. Finally, we address the findings on the cytotoxicity of biosynthetic AgNP for a new therapeutic application. The promising *in vitro* results of genotoxicity, induction of apoptosis, reduction of cell migration and proliferation were reflected in the *in vivo* assays in the non-muscle invasive bladder cancer model, where we observed relevant tumor regression. Thus, these findings suggest AgNP as an economical alternative and possible drug candidate in the treatment of bladder cancer.

Keywords: silver nanoparticles; biosynthetic; thiol-antioxidants; NAC; chelating; antidote; bladder cancer; tumor regression.

Lista de Ilustrações

CAPÍTULO 1

CAPÍTULO 2

CAPÍTULO 3

CAPÍTULO 4

CAPÍTULO 5

Lista de Tabela

CAPÍTULO 2

CAPÍTULO 3

CAPÍTULO 4

Lista de Abreviaturas e Siglas

AgNP - Silver nanoparticle (Nanopartículas de prata)

ROS - Reactive oxygem species (Espécies Reativas de oxigênio)

NAC - N-acetyl-L-Cysteine

L-Cys - L-Cysteine

GSH - Glutathione reduced

GSSG - Glutathione disulfide

TLX - Trolox

AA - Ascorbic acid

CM-H_2DCFDA - 6-chloromethyl-2',7'-dichlorodihydrofluorescein diacetate, acetyl ester

DNA - Deoxyribonucleic Acid

HuH-7 - Human Hepatocarcinoma cells

DMEM - Dulbecco's Modified Eagle's Medium

RMPI - Roswell Park Memorial Institute

FBS - fetal bovine serum

MTT - 3-(4,5-dimethylthiazol-2-yl)-2,5-diphenyltetrazolium bromid

IC50 - Half of the maximal inhibitory concentration

SPR - Surface Plasmon Resonance

DLS - Dynamic Light Scattering

NTA - Nanoparticle Tracking Analysis

PI - Propidium Iodide

PDI - Polydispersity Index

TEM - Transmission Electron Microscopy

XPS - X-ray Photoelectron Spectroscopy

i.v. - Intravenous

i.p. - intraperitoneal

AST - Aspartate Aminotransferase

ALT - Alanine Aminotransferase

ALP - Alkaline Phosphatase

BUN - Blood Urea Nitrogen

AMG - Autometallography

SOD-1 - Superoxide Dismutase-1

TBARS - Thiobarbituric Acid-Reactive Substances

HE - Hematoxylin-eosin

GF-AAS - Graphite Furnace Atomic Absorption Spectrometry

TMAH - Tetramethylammonium Hydroxide

GAPDH - Glyceraldehyde-3-phosphate dehydrogenase

cv - Central vein

pv - Portal vein

RBC - Red Blood Cells

Hb - Hemoglobin

Hct - Hematocrit

PLT - Platelets

WBC - White Blood Cells

MPS - Mononuclear Phagocyte System

FDA - Food and Drug Administration

CONCEA- Brazilian National Council to Control Animal Experimentation

CEUA - Institutional Committee for Ethics in Animal Use

BC - Bladder Cancer

NMIBC - Non-Muscle Invasive Bladder Cancer

MIBC - Muscle-Invasive Bladder Cancer

MNU - N-methyl-N-nitrosourea

pTis - Flat carcinoma *in situ*

pTa - Papillary carcinoma non-invasive

pT1 - Tumor invading mucosa or submucosa of the bladder wall

TURBT - Transurethral Resection of Bladder Tumor

BCG - Bacillus Calmette–Guerin

DBS - Double-Strand Breaks

ICAD - Inhibitor of caspase-activated DNAse

CAD - Caspase-activated DNAse

Sumário

CAPÍTULO 1 – Introdução

As nanopartículas de prata (AgNP) são conhecidas pelo largo espectro antimicrobiano e podem ser obtidas por processos químicos e bioquímicos. Devido a esta importante propriedade e facilidade de síntese, as AgNP são amplamente incorporadas em produtos na indústria de alimentos, agrícola, tintas, vestuário, cosméticos e utensílios médicos (Abbasi et al., 2016; Caro et al., 2010; Mytych et al., 2017). Na busca de uma alternativa para melhoria da estabilização coloidal e potencialização dos efeitos antimicrobianos, a biossíntese é uma importante ferramenta na produção de nanopartículas. (Abbasi et al., 2016; Nanda and Saravanan, 2009). O método consiste na utilização de agentes redutores orgânicos obtidos a partir fungos (Durán et al., 2005; Kowshik et al., 2003), bactérias (Sintubin et al., 2009), ou plantas (Krishnaraj et al., 2010) para a síntese de nanopartículas. A produção muitas vezes é realizada em condições de ambiente de temperatura, pressão e no pH fisiológico do organismo utilizado para a síntese, sem adição de solventes tóxicos e estabilizantes (Dhillon et al., 2011; Durán et al., 2010).

Para este estudo utilizamos nanopartículas biossintéticas obtidas a partir do extrato da biomassa do fungo *Fusarium oxysporum.* Neste método o nitrato de prata é adicionado em uma solução contendo redutases e outros substratos fúngicos, onde os íons prata (Ag^{+}) são reduzidos à prata metálica (Ag^{0}) (Durán et al., 2005, Durán et al., 2015). Este método de biossíntese possibilita a obtenção de AgNP esféricas com alto potencial antimicrobiano, faixa estreita de diâmetro hidrodinâmico (*i.e.*, monodispersas), estabilizadas por proteínas fúngicas, não sendo necessário a adição de surfactantes (Durán et al., 2007; Mohanpuria et al., 2008).

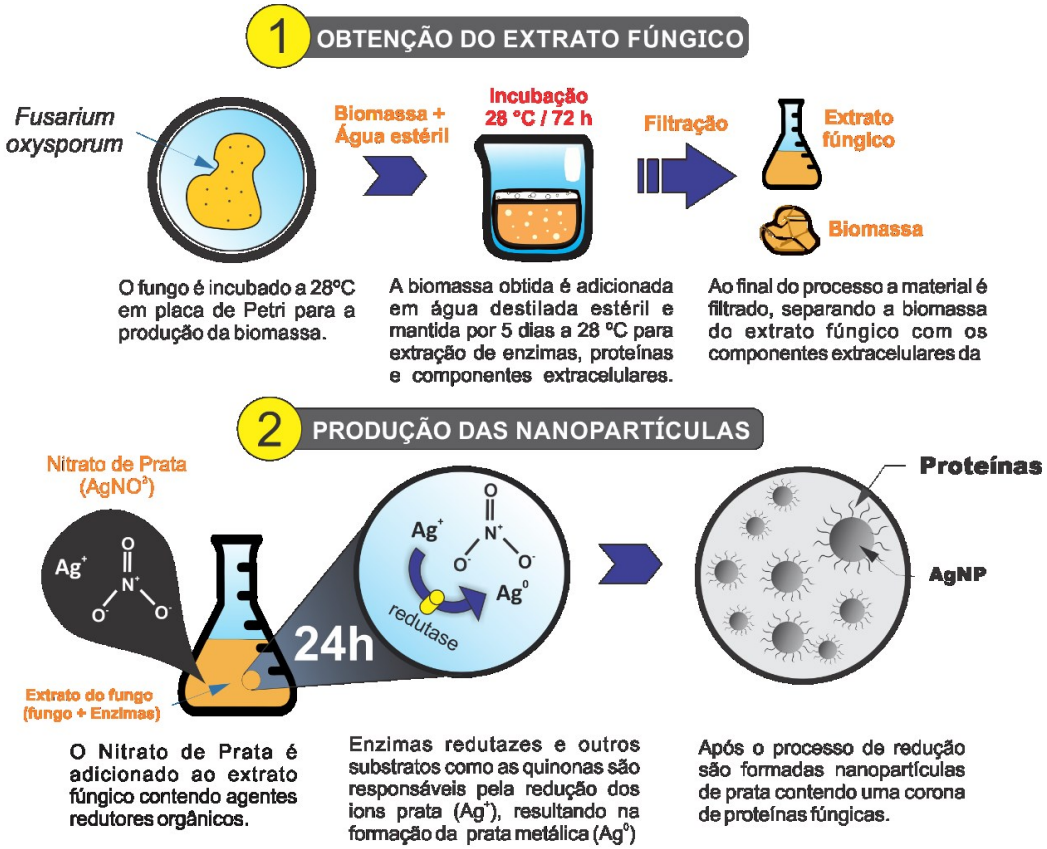

Figura 1. Biossíntese das nanopartículas de prata. *Ilustração do processo de biossíntese das AgNP.* **1**- Preparação do extrato fúngico: após o Fusarium oxysporum crescer ele é solubilizado em água e filtrado, assim formando uma solução contendo componentes extracelulares do fungo. **2**- Produção das AgNP biossintéticas: Nitrato de prata é adicionado ao extrato fúngico, no qual os íons prata (Ag^{+}) serão reduzidos por redutases contidas no filtrado fúngico, assim dando origem a prata metálica (Ag^{0}) que precipita na forma de nanopartículas revestidas por proteínas fúngicas. Adaptado: ERENO; MARCATO; RODRIGUES, 2013.

A biossíntese possui vantagens de produzir partículas com características únicas, muitas vezes as partículas apresentam em sua superfície proteínas provenientes dos organismos utilizados em sua síntese. Essas proteínas atuam de forma semelhante a surfactantes, impedindo colabação entre as partículas, reduzindo a agregação e precipitação (Durán et al., 2016, 2005). Além disso, estas proteínas podem modular o mecanismo de toxicidade, alterando vias de internalização celular e tipo de morte celular, ou ainda, podem atuar como imunomoduladores, favorecendo o seu reconhecimento por células de defesa (Chakraborty et al., 2016; Durán et

al., 2015). Desta forma, as AgNP biossintéticas apresentam-se como uma alternativa promissora e pouco explorada em literatura, o que garante a originalidade do presente trabalho.

Diante do aumento de produtos contendo AgNP e crescente preocupação a respeito do uso e eliminação desses nanomateriais, em adicional, dos inexplorados mecanismos de toxicidade devido as características particulares das nanopartículas biossintéticas, este trabalho teve como objetivo explorar diferentes abordagens e aplicações das AgNP oriundas do *Fusarium sp,* nas áreas da nanomedicina e nanotoxicologia, através da avaliação dos (i) mecanismos moleculares de toxicidade *in vitro* desencadeados pelas nanopartículas (e.g. estresse oxidativo e morte celular); (ii) mecanismos de toxicidade *in vivo* das nanopartícula e busca novos tratamentos contra a intoxicação por prata, com os estudos histopatológicos, hematológicos e avaliação bioquímica de marcadores de toxicidade; (iii) aplicação oncológica no tratamento do câncer de bexiga, através dos estudos *in vitro* dos mecanismos moleculares de toxicidade envolvidos na morte elular (apoptose/necrose), genotoxicidade, migração, proliferação e estudos histológicos em carcinoma de bexiga.

Deste modo, o Capítulo 2 aborda os principais efeitos citotóxicos causados pelas das biossintéticas nanopartículas de prata em células de hepatocarcinoma humano Huh-7, onde muitas vezes descrito que o estresse oxidativo é principal mecanismo de toxicidade para AgNP. Entretanto, nosso estudo gera uma nova reflexão e aponta possíveis equívocos de interpretação na associação de antioxidantes com AgNP. O inovador trabalho alerta para equivocadas interpretações de reversão da citotoxicidade, colocando em cheque a relação causa-efeito entre geração de espécies reativas de oxigênio e toxicidade de AgNP.

Observando os efeitos de interações entre as AgNP e tióis-antioxidantes, levantamos a hipótese de direcionarmos estes resultados para o tratamento da intoxicação por prata. O Capítulo 3 “Como um artefato pode se transformar em um antídoto” utiliza os princípios encontrados nos ensaios *in vitro* com antioxidantes e reverte para uma possível aplicação

terapêutica *in vivo*. Demonstramos que os efeitos observados dos tióis-antioxidantes eram capazes de reduzir significativamente a toxicidade *in vivo* estimuladas pelas AgNP.

No Capítulo 4 estudamos os mecanismos moleculares da citotoxicidade das AgNP em linhagem celular de carcinoma de bexiga. Em adicional, avaliamos atividade antitumoral das AgNP contra o câncer de bexiga não músculo invasivo, onde foi observado relevante redução tumoral. Este inovador trabalho apresentou resultados promissores no combate do câncer de bexiga, sugerindo uma nova alternativa de tratamento, neste cenário de grande incidência desta patologia com poucas possibilidades farmacológicas e terapêuticas.

Por fim, no Capítulo 5 realizamos a discussão de todo o trabalho em perspectiva, retomando os principais resultados e conceitos. Em seguida, finalizamos com a conclusão desta tese no Capítulo 6. Ao final do trabalho, em Apêndices, apresentamos os principais trabalhos publicados, depósito de patentes e resumos em congresso, representando toda a caminhada acadêmica neste trabalho de doutorado.

CAPÍTULO 2 - A influência de tióis-antioxidantes na avaliação da citotoxicidade das nanopartículas de prata

Thiol-antioxidants interfere with assessing silver nanoparticle cytotoxicity

[1]Luiz Alberto Bandeira Ferreira; [1]Samara Bonesso dos Reis; [3,4]Emanueli do Nascimento da Silva; [3]Solange Cadore, [2]Juliana da Silva Bernardes; [5,6]Nelson C. Durán; *[1]Marcelo B. de Jesus

[1]Nano-Cell Interactions Lab., Department of Biochemistry and Tissue Biology, Institute of Biology, University of Campinas, Campinas, SP, Brazil;

[2]Brazilian Center for Research in Energy and Materials, CNPEM, Campinas, Brazil;

[3]Institute of Chemistry, University of Campinas, Campinas, SP, Brazil;

[4]Department of Chemistry, Institute of Exact and Biologic Sciences, Federal University of Ouro Preto, Ouro Preto, MG, Brazil;

[5]NanoBioss, Institute of Chemistry, University of Campinas, Campinas, SP, Brazil;

[6]Nanomedine Units, Federal University of ABC (UFABC), Santo André, DP, Brazil.

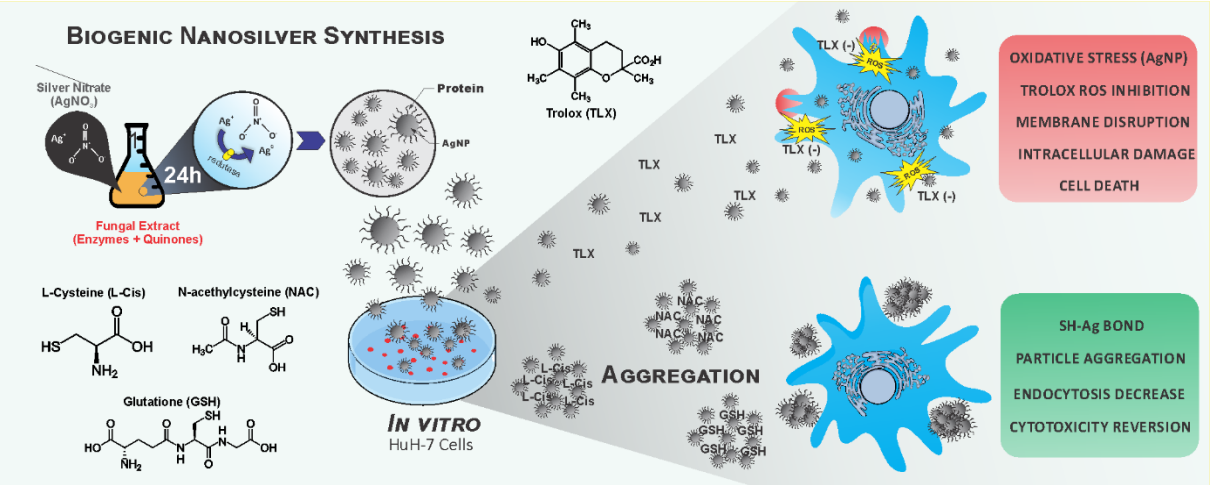

Abstract

Many studies have shown that silver nanoparticles (AgNP) induce oxidative stress, and it is commonly assumed that this is the main mechanism of AgNP cytotoxicity. Most of these studies rely on antioxidants to establish this cause-and-effect relationship; nevertheless, details on how these antioxidants interact with the AgNP are often overlooked. This work aimed to investigate the molecular mechanisms underlying the use of antioxidants with AgNP nanoparticles. Thus, we studied the molecular interaction between the thiol-antioxidants (N-acetyl-L-Cysteine, L-Cysteine, and glutathione) or non-thiol-antioxidants (Trolox) with chemically and biologically synthesized AgNP. Both antioxidants could mitigate ROS production in Huh-7 hepatocarcinoma cells, but only thiol-antioxidants could reverted prevent the cytotoxic effect, directly binding to the AgNP leading to aggregation. Our findings show that data interpretation might not be straightforward when using thiol-antioxidants to study the interactions between with metallic nanoparticles and cells. This artifact exemplifies potential pitfalls that could hinder the progress of nanotechnology and the understanding of the nanotoxicity mechanism.

Keywords: Silver nanoparticles; *in vitro*; oxidative stress; thiol-antioxidants; aggregation.

.

1. Introduction

Silver nanoparticles (AgNP) are known for their broad antimicrobial spectrum; hence, AgNP has been extensively incorporated into clothing, food, paints, cosmetics, and medical products (Chen and Schluesener, 2008; Galiano et al., 2008; Ge et al., 2014; Moore, 2006; Zhou et al., 2011). Continuous exposure to products containing AgNP raises concerns about its metabolism, elimination, and possible toxic effects. Many *in vitro* studies investigating the toxic effects of AgNP have reported several cytotoxic effects, including cell membrane damage (Zhornik et al., 2014), inflammatory response (Yang et al., 2012), DNA damage (Gromadzka-Ostrowska et al., 2012), genotoxicity (de Lima et al., 2012; Lima et al., 2013), and cell death by apoptosis or necrosis (Foldbjerg et al., 2009; Hsin et al., 2008). These cytotoxic effects are often related to the oxidative stress induced by AgNP exposure.

Oxidative stress has been investigated using several antioxidants that act through different mechanisms. One such antioxidant that has been used is N-acetyl-L-Cysteine (NAC), which inside the cells is deacetylated, resulting in L-Cysteine (L-Cys), an essential amino acid used in glutathione (GSH) synthesis. GSH participates in numerous physiological processes, maintaining cell functional capacity, morphological integrity, and detoxifying electrophilic xenobiotics (Samuni et al., 2013). These antioxidants have a nucleophilic free thiol group (R-SH) capable of interacting directly with the electrophilic groups of oxidizing radicals (*e.g.*, $^{\bullet}NO^{2}$, $CO^{3\bullet-}$, $O_2^{\bullet-}$,$^{\bullet}OH$, H_2O_2) (Issels et al., 1988; Xiao et al., 2016). Another example of antioxidant is Trolox (TLX; hydrophilic analog of vitamin E), which is frequently used to prevent oxidative stress induction by xenobiotics (Li et al., 2017).

Often antioxidants are used to demonstrate that the toxic mechanism of AgNP depends on ROS; this effect is suggested to be the most predominant mechanism of AgNP nanotoxicity (Kim and Ryu, 2013), even though, a large body of evidence indicates that silver and AgNP can interact with many chemical groups, including sulfide and chloride (Andersson Lars-Olov,

2003; Li and Lenhart, 2012). Although many studies to date make use of these antioxidants, no previous study has addressed how the most common antioxidants interact with silver nanoparticles. Additionally, we demonstrate that the principles determined here could be used to prevent the toxic effects induced by a sublethal intravenous dose of AgNP in Wistar rats (Mendonça et al., 2018). In light of these considerations, it is quite surprising that the effects of these antioxidants upon AgNP remain unclear. Therefore, in this work, we decided to investigate how antioxidants affect AgNP cytotoxic towards Huh-7 hepatocarcinoma cells, since hepatotoxicity has been reported for this nanoparticle.

2. Methods and Materials

2.1. Nanoparticle synthesis

For this study, biogenic and chemical synthesis stabilized in citrate (code 730807; Sigma-Aldrich, St. Louis, MO, USA) silver nanoparticles were used. Briefly, the biosynthesis of AgNP was obtained from the reaction with reductase enzymes and quinones contained in *Fusarium oxysporum* filtrate. After the fungus growth, approximately 10 g of biomass was poured into a conical flask containing 100 mL of distilled water, kept for 72 h at 28 ºC and then the aqueous solution components were separated by filtration. In fungal filtrated was added $AgNO_3$ (10^{-3} M) and kept for several hours at 28 °C. Metallic silver production (Ag^o) was followed by absorption measured in a UV-Vis at 300-700 nm using microplate reader Cytation 5 (Biotek Instruments, Winooski, VT, USA). Finally, the AgNP were size characterized by NTA, DLS (Supplementary, Table S1) and TEM, obtaining the concentration approximately of 100 nm. Silver concentrations were measured by inductively coupled plasma mass spectrometry (ICP-MS) using Optima 5300DV (PerkinElmer, USA) (Andrade et al., 2017; Durán et al., 2016, 2005), and the stock solution was standardized in 5 mM of silver.

2.2. Cell Culture

Human hepatocarcinoma cells (HuH-7, No. JCRB0403) were obtained from the Japanese Collection of Research Bioresources Cell Bank (JCRB, Japan) and cultured as a monolayer in Dulbecco's Modified Eagle's Medium (DMEM, Sigma-Aldrich, USA) supplemented with 10% fetal bovine serum (FBS, Sigma-Aldrich, St. Louis, MO), 1% penicillin, and streptomycin.

2.3. MTT assay

HuH-7 cells were seeded in 96-well plates (Corning Inc., USA) at the density of 1.0 x 10^4 cells per well in 200 µL of supplemented DMEM medium and incubated overnight. Then, cells were treated with increasing concentrations of AgNP (1-50 µM) diluted in serum-free medium at 37 °C. After 24 h, the medium was replaced by 100 µL of 0.5 mg/mL (3-(4,5-dimethylthiazol-2-yl)-2,5-diphenyltetrazolium bromide) tetrazolium (MTT) solution (Sigma-Aldrich, USA). After 2 hours of incubation, the medium was replaced with 100 µL of DMSO to dissolve the formazan crystals. Finally, the absorbance was determined by the microplate reader Cytation 5 (Biotek Instruments, USA) at $\lambda = 570$ nm.

2.4. Calcein/Propidium Iodide assay

HuH-7 cells were seeded in 96-well plates (Corning Inc., USA) at the density of 1.0 x 104 cells per well in 200 µL of supplemented DMEM medium and incubated overnight. Then, cells cells were treated with increasing concentrations of AgNP (1-50 µM) diluted in serum-free DMEM medium at 37 °C. After 24 h, the medium was replaced by Calcein-AM (1 µM, Thermo Fisher Scientific, USA), Hoechst 33342 (1 µM, Sigma-Aldrich, USA) and Propidium Iodide (PI, 1 µM, Abcam, UK) in Fluorobrite DMEM medium (Thermo Fisher Scientific, USA). After incubation, plates were imaged using a 10x objective by the Cytation 5 (Biotek

Instruments, USA) configured with DAPI, GFP, and PI light cubes. Images were analyzed using Gen5 software (Biotek, Winooski, VT, USA). In addition, Calcein fluorescence (ex/em ~492/517 nm) was used to estimate cell viability using the same Cytation 5 and the percentage of viable cells was normalized to non-treated cells.

2.5. Assessment of intracellular ROS

ROS generation was evaluated using the 6-chloromethyl-2',7'-dichlorodihydrofluorescein diacetate, acetyl ester (CM-H_2DCFDA; Thermo Fisher Scientific, Waltham, MA, USA). Cells were pre-treated with antioxidants for 30 min. followed by the treatment with AgNP IC_{50} (both diluted in Fluorobrite DMEM). ROS levels were acquired within 60 min (readings every 15 min) in ex/em: ~492–495/517–527 nm. Phorbol 12-Myristate 13-Acetate (PMA) was used as a positive control (ROS-inducing agent) and antioxidants NAC, L-Cys, GSH reduced and TLX, were used to pretreat cells followed by AgNP treatment.

2.6. Transmission Electron Microscopy (TEM)

AgNP suspension was diluted in ultrapure water or antioxidants and exposed on a copper TEM grid covered by an ultrathin carbon support film. The grids were dried under vacuum in a desiccator. Then, the images were acquired by JEOL JEM-2010HC transmission electron microscope (JEOL Co. Ltd., Japan) in accelerating voltage of 60 kV. TEM images were processed with ImageJ (National Institutes of Health, USA), using the ParticleSizer plugin (by Thorsten Wagner, Max Planck Institute Dortmund, Germany).

2.7. Dynamic Light Scattering and Zeta Potential

Dynamic Light Scattering (DLS) technique was employed to measure the average hydrodynamic diameter and polydispersity index of AgNP using a ZetaSizer Nano ZS 90

instrument (Malvern, UK). Measurements were performed using polystyrene cuvettes with a path length of 10 mm, at 25 ºC, in a scattering angle of 90°. The zeta potential was measured with the same instrument using capillary cells with a path length of 10 mm. The stock solution of AgNP suspension (5 mM) was diluted 1:100 in ultrapure water or antioxidant solution.

2.8. Nanoparticle tracking Analysis

Nanoparticle Tracking Analysis (NTA) measurements were performed with a NanoSight LM20 (Malvern, UK) equipped with a sample chamber with a 640-nm laser and a Viton fluoroelastomer O-ring. The stock solution of AgNP suspension (5 mM) was diluted (1:1000) in ultrapure water or antioxidant solution and injected into the sample chamber with sterile syringes. After manual shutter and gain adjustments, the samples were performed at room temperature with three measurements of 60 seconds. The values of concentration and mean size were obtained by the NTA 2.0 Build 127 software (Malvern, UK).

2.9. X-ray photoelectron spectroscopy (XPS)

Chemical surface analyses of AgNP nanoparticles were obtained by X-ray photoelectron spectroscopy (XPS) using a K-Alpha X-ray photoelectron spectrometer (Thermo Fisher Scientific, UK) equipped with a hemispherical electron analyzer and monochromatic Al Kα (1486.6 eV) radiation. Survey (full-range) and high-resolution spectra for S were acquired using pass energy of 200 and 50 eV, respectively. The data were analyzed using the Thermo Avantage Software (Version 5.921) and the XPS results presented in this work correspond to an average of three measurements taken in different regions of the samples.

2.10. AgNP internalization in presence of antioxidants

HuH-7 cells were seeded in 6-well plates at a density of 3,0 x 10^5 cells/well in 5 mL and kept under 5% CO2 at 37 °C overnight. Next, cells were treated with AgNP (IC_{50}) for 1/4, 1/2, 1, 3, 6, and 24 hours. For experiments in the presence of antioxidants, cells were pretreated with NAC (10 mM), L-Cys (1 mM), GSH (10 mM), TLX (1 mM), and glutathione oxidized (GSHox) and incubated for 30 minutes. Next, the AgNP (IC_{50}) were added over and incubated for 6 hours.

Cell Lysis and silver quantification: After treatments, cells were washed thrice with Phosphate Buffered Saline (PBS) and the 500 µl of RIPA buffer (Santa Cruz Biotechnology, USA) was added and incubated for 1 hour until complete cell lysis. Next, 500 µl of ultrapure water was added to the well and homogenize for 10 minutes on the orbital shaker. Finally, the silver concentrations were measured by inductively coupled plasma mass spectrometry (ICP-MS) using Optima 5300DV (PerkinElmer, USA) (Andrade et al., 2017; Durán et al., 2016, 2005).

3. Results and Discussion

3.1. AgNP cytotoxicity is prevented depending on thiol presence

We determined the half-maximal inhibitory concentration (IC_{50}) of AgNP upon Huh-7 cells after 24 h. We used two approaches (MTT assay and calcein/PI assay); these methods are based on different chemical principles, which increase the robustness of the results and help avoid artifacts (Azhdarzadeh et al., 2015; de Jesus and Kapila, 2014; Rösslein et al., 2015). Figure 1a shows that all techniques reported a comparable dose-response relationship and similar IC_{50} values: 10.61 µM for MTT, 9.10 µM for calcein, and 11.12 µM for PI. The impact of AgNP treatment on cell morphology is illustrated in Figure 1b. Control cells are mostly attached and depicted as a cuboidal epithelial-like morphology; upon AgNP treatment, cells are detached and accompanied by morphological changes (cell shrinkage and rounding). We also

observed that calcein-negative cells, indicating lost cellular viability, and PI-positive cells, indicating cell death. Similar cytotoxicity profiles were found for chemically synthesized AgNP (Supplementary, Figure S1).

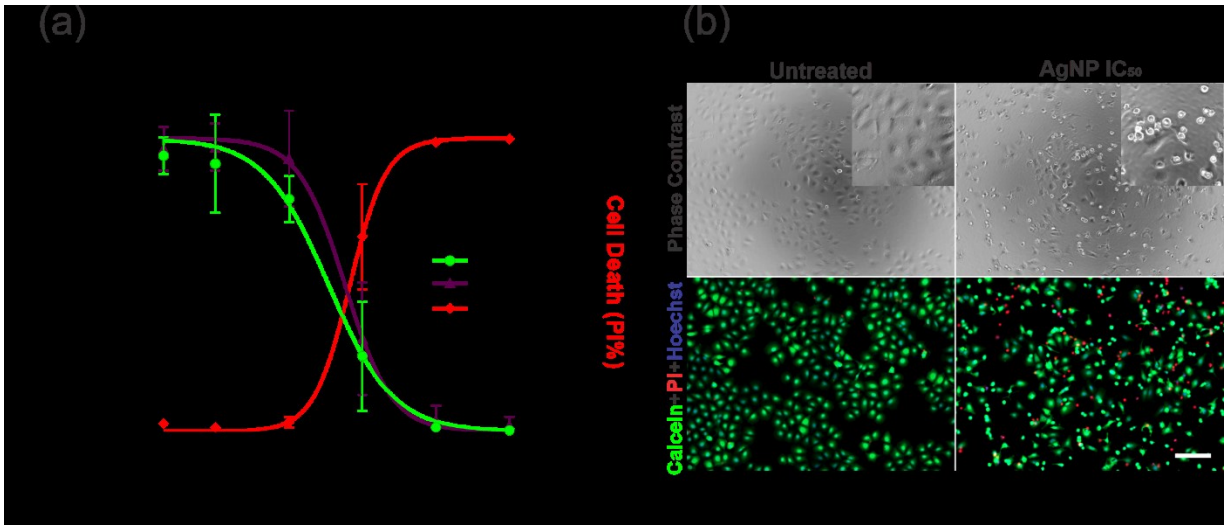

Figure 1. *AgNP cytotoxicity towards HuH-7 hepatocarcinoma cell.* (a) Cell viability measured by MTT (λmax = 570 nm), Calcein-AM (ex/em ~492/517nm), and PI (ex/em ~535/617 nm). Cells were treated with increasing concentrations of AgNP (1-50 µM) for 24 h. Each value represents the mean ± S.D. of three independent experiments (n = 3); cell viability was normalized to untreated control. (b) Representative images of IC50 by Calcein/PI assay obtained by phase contrast and the images below represent the merge of the DAPI, GFP, and PI light cubes. Scale bar: 200 µm.

After determining the IC_{50} concentration of AgNP in Huh-7 cells, we evaluated the oxidative stress production upon the AgNP treatment using the CM-H_2DCFDA probe. PMA was used as a positive control (ROS-inducing agent) and antioxidants NAC, L-Cys, GSH reduced, and TLX were used to pretreat cells followed by AgNP treatment. AgNP treatment led to an increase in ROS production by cells (*$p<0.05$, Figure 2a), similar to the positive control (PMA) levels. As expected, all antioxidants kept the ROS at basal levels, which is consistent with the previous studies (Kim et al., 2009, p.; Li et al., 2017; Shi et al., 2014).

To investigate the role of ROS generation in AgNP cytotoxicity, we next evaluate whether the basal ROS levels upon pretreatment with antioxidants could prevent the cytotoxic effects of AgNP. For this, cells were pretreated using a nontoxic concentration of antioxidants,

which was able to prevent ROS generation, followed by treatment with an IC_{50} dose of AgNP. Typically, NAC and GSH are used as a ROS scavenger in cytotoxic AgNP studies, and the employment of these antioxidants increased cell viability (Li et al., 2017; Shi et al., 2014). Treatment with NAC, L-Cys, and GSH indeed prevented the AgNP cytotoxicity (Figure 2b, #). Surprisingly, pretreatment with TLX could not prevent the cytotoxic effects (Figure 2b, ¢). These results were confirmed using fluorescence microscopy, as shown in Figure 2c. Similar results were obtained for chemically synthesized AgNP (Supplementary, Figure S2). In addition, we test the hypothesis of the free thiol being essential for the mitigation of AgNP cytotoxicity, for that we evaluated the cytotoxicity in the presence of glutathione disulfide (GSSG), which presents sulfide bonds between the GSH molecules. The GSSG was not capable of preventing the cytotoxicity of synthetic AgNP, and partially prevented the toxicity of the biogenic AgNP. Probably, the partial effect was observed because nonenzymatic thiol-disulfide exchange between GSSG and cysteine present on the surface of the biogenic AgNP (Supplementary, Figure S3). These results are intriguing because they point to the thiol as the responsible for the mitigation of AgNP cytotoxicity and suggest an absence of correlation between ROS production and cytotoxicity caused by AgNP.

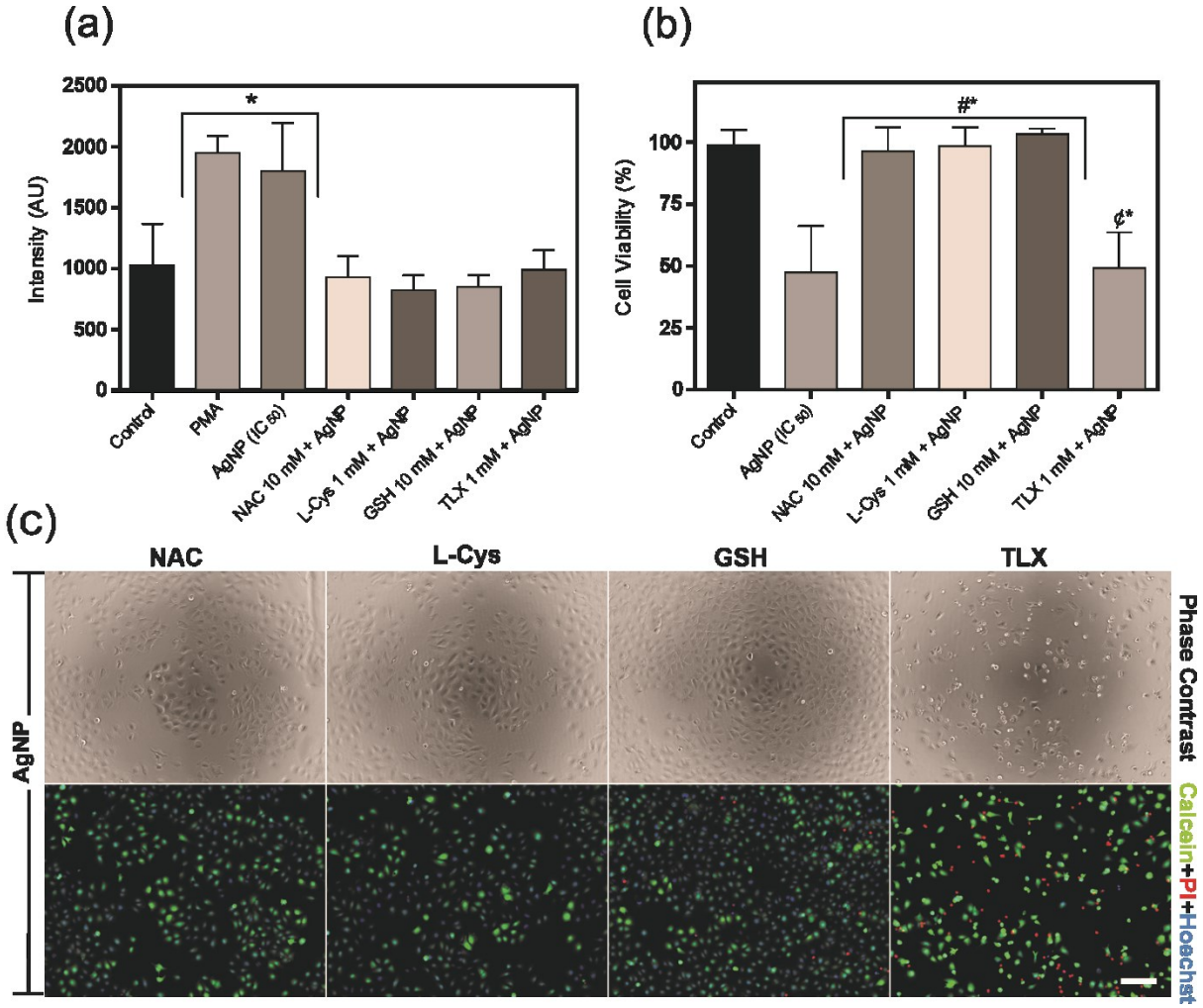

Figure 2. *ROS generation and cell viability of Huh-7 cells pretreated with thiol and non-thiol-antioxidants.* (a) Cells were treated with AgNP IC50 AgNP (1), and the generation of ROS species was evaluated by CM-H2DCFDA probe. Phorbol 12-myristate 13-acetate (PMA, 1 µM) was used as positive control of ROS production. The y-axis is the fluorescence intensity integrating (area under the curve) and all the values acquired by a 60-min period (readings every 15 min). Each value represents the mean ± S.D and *$p<0.05$ for significant difference of control vs. all, ANOVA followed by Tukey test. (b) Cells were treated with AgNP IC50 for 24h of incubation, and cell viability was assessed by the Calcein-AM assay. Each value represents the mean ± S.D. of three independent experiments (n=3), and the cell viability was normalized from the control (without treatment). # = $p<0.05$ significant difference AgNP vs. all; ¢ = $p<0.05$ significant difference Control vs. all. ANOVA followed by Tukey test. (c) Representative images of AgNP cell viability in the presence of antioxidants. Scale bar: 200 µm.

3.2. Thiol-antioxidants lead to AgNP aggregation

Intrigued by the difference in the antioxidant behavior and based on the literature that shows sulfidation could prevent the toxicity of AgNP towards microorganisms, we reasoned that the thiol-antioxidants were perhaps directly interacting with the AgNP and somehow

preventing the cytotoxic effects (Choi et al., 2009; Levard et al., 2013). To assess such possibility, we investigated the molecular interaction between the antioxidants and AgNP. Therefore, we used a Surface Plasmon Resonance (SPR) to identify interactions on the surface of nanoparticles and the alteration of colloidal stability (Lee et al., 2008). Thiol-antioxidants (NAC, L-Cys, and GSH) result in a decrease and enlargement of the SPR, indicating a surface interaction with AgNP (Supplementary, Figure S4 and S6). Further, we used the DLS and NTA techniques to evaluate the hydrodynamic size, zeta potential, and concentration of the nanoparticles in the presence of the antioxidants (Table 1). Incubation with non-thiol-antioxidants (TLX) led to no significant alterations in size, while thiol-antioxidants (NAC, L-Cys, and GSH) led to a significant increase in AgNP size. The increase in AgNP size followed by a decrease in concentration could be associated with aggregation induced by the thiol-antioxidants. The zeta potential results were not conclusive, possibly because all the antioxidants tested somehow interacted with the surface of the particle.

Further, insight into the interaction between antioxidants and AgNP was gained by Transmission Electron Microscopy (TEM). Figure 3 shows the aggregation promoted by NAC, L-Cys, and GSH on the AgNP, while TLX did not affect AgNP. Similarly, thiol-antioxidants induced the aggregation of chemically synthesized AgNP (Supplementary, Figure S5, S6 and Table 2). Interestingly, GSSG caused mild alteration on physichochemical propertiers of AgNP. This could be explained by the reversible disulfide bond formation, which could lead to free thiol formation, and allowing to AgNP interaction. Overall, the physicochemical data (SPR, DLS, NTA, and TEM) suggested that antioxidants containing the thiol group exhibit AgNP chelating activity.

Table 1. Characterization of biogenic silver nanoparticles in antioxidants solutions: NAC 10 mM; L-Cys 1mM; GSH 10 mM; TLX 1 mM. The diameter, zeta potential and PDI of AgNP suspensions were measured using a Zetasizer Nano (Malvern Instruments Ltd, USA) and concentration measured using Nanotracking Analysis (Malvern Instruments Ltd, USA). Each value represents the mean ±S.D (n = 3).

Groups	DLS Size (nm)	NTA Size (nm)	PDI	Zeta Potential (mV)	Concentration (particles/mL)
AgNP	101.7 ±3.8	79.3 ±39.7	0.267 ±0.009	-26,7 ±11,1	7.77^{11} ±2.69^{10}
AgNP + NAC	3624 ±551.7*	147.9 ±129.2	0.514 ±0.057	-5,9 ±4,8	4.73^{11} ±6.89^{10}
AgNP + L-Cys	5076 ±841.4*	147.3 ±119.6	0.689 ±0.113	-10,9 ±4,1	1.21^{11} ±1.03^{10}
AgNP + GSH	3100 ±175.0*	189.5 ±140.4	0.557 ±0.053	-5,6 ±3,1	1.98^{11} ± 1.44^{10}
AgNP + TLX	121.2 ±3.0	81.5 ±31.6	0.401 ±0.015	-14,1 ±9,4	5.10^{11} ± 2.17^{10}
AgNP+GSSG	134.6 ±0.9	145.6 ±65.8	0.288 ±0.068	-2.0 ±1.72	8.1011 ±3.6210

*ANOVA followed by Anova test (AgNP vs all).

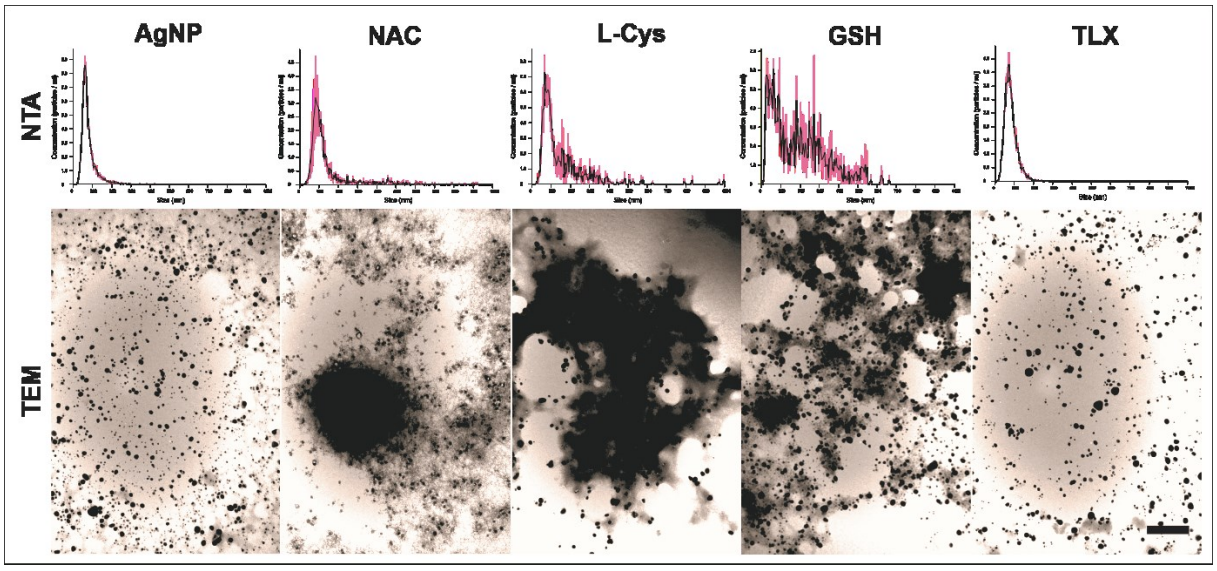

Figure 3. *AgNP aggregation in presence of thiol-antioxidants*. NTA measurements in the presence of antioxidants, 5 mM of biogenic AgNP were diluted (1:1000) in different media: ultrapure water; NAC (10 mM); L-Cys (1 mM); GSH (10 mM); TLX (1 mM). A representative TEM image of synthetic AgNP in antioxidant solution. A drop of nanoparticle suspension diluted in antioxidant solutions was deposited over the grid and let to dry overnight. The micrographs were obtained in magnification of 75,000x at a voltage of 60 kV. Scale bar: 200 nm.

3.3. Thiol group binds to AgNP

XPS measurements were used to gain additional understanding of molecular interactions between AgNP and thiol-antioxidants (Ag^0-Thiol binding), and the results are shown in Figure 4. Deconvolution of high-resolution S2p spectra reveal two different chemical states for S: (1) the spin-orbit doublet at 162.3 eV (S2p3/2) and 163.4 eV (S2p1/2) attributed to S in Ag-S chemical state, and (2) the spin-orbit pair (green curves) at 163.9 eV (S2p3/2) and 165.0 eV (S2p1/2) associated with S atoms of physisorbed thiol-antioxidants. As expected, no signal in the S2p region was detected for AgNP, AgNP-TLX (Figure 4d). The atomic percentage of sulfur atoms related to the Ag-S chemical state prevailed among the three thiol-antioxidants used in this work, ranging from 74% to 96%, as shown in Figure 4e, while the concentration of physisorbed species is lower and varies from 4% to 26%. These results confirm that AgNP nanoparticles are functionalized by the thiol-containing molecules, suggesting a replacement of the AgNP capping agent by Ag-SR species. This replacement may interfere with the colloidal stability, promoting aggregation and agglomeration of the nanoparticles as observed by NTA, DLS, and TEM techniques. The surface composition accessed through Survey Spectra reveals that Ag and S atomic percentages on the AgNP surfaces (Figure 4f) increase when the molecular volume of the anti-oxidants decreases (L-Cys< NAC< GSH), suggesting that a steric effect is relevant for the capping agent removal and consequently in the nanoparticle aggregation.

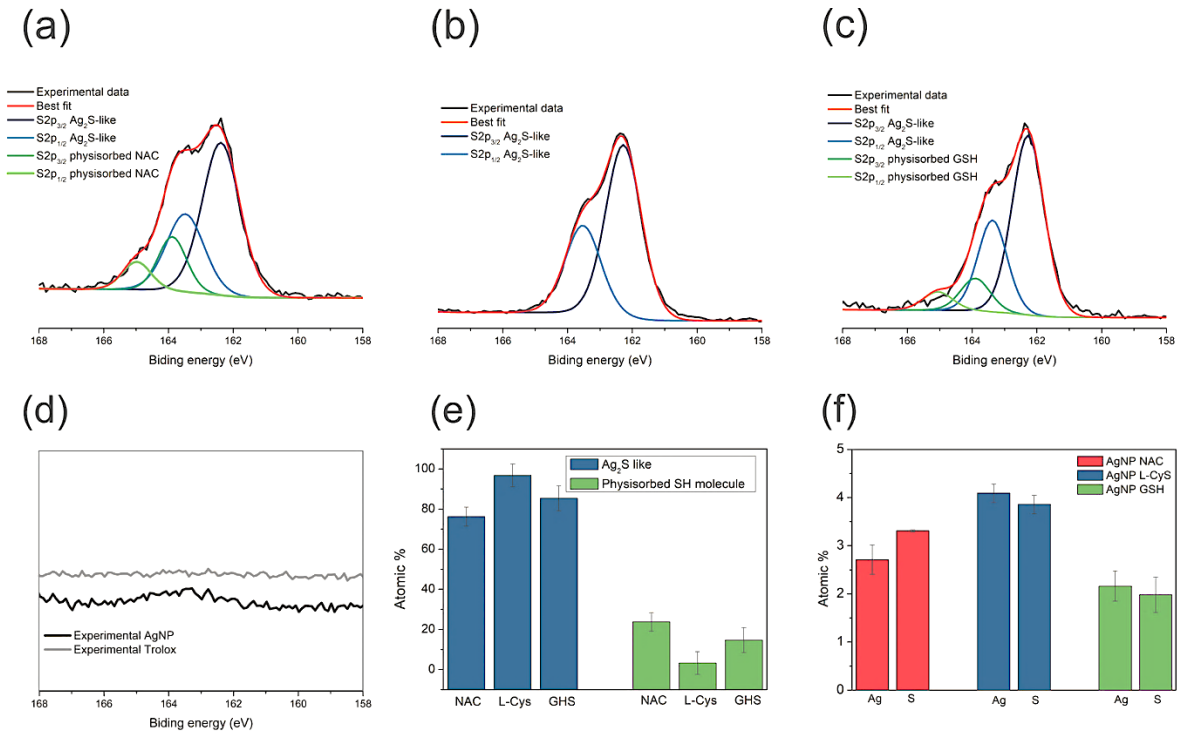

Figure 4. *High 2p spectra for AgNP in the presence of*: **(a)** NAC 10 mM **(b);** L-Cys 1 mM **(c)**; GSH 10 mM; **(d)** AgNP in water and TLX 1 mM; **(e)** Atomic percentage of Ag-S and physisorbed SH molecules; **(f)** Ag and S atomic percentage on AgNPs surface.

3.4. Internalization silver nanoparticles decrease

To gain further understanding of how thiol-antioxidants prevented the AgNP cytotoxicity, we evaluated whether the antioxidants affected the cellular uptake of AgNP. First, we determined the internalization kinetics of AgNP in Huh-7 cells (Figure 5a). The results showed the increase of the intracellular silver concentration, where the highest concentration was obtained in 6 hours. After defining the internalization time, we evaluated the interference of the antioxidants in the uptake of the nanoparticles (Figure 5b). AgNP-treated cells in the presence of NAC, L-Cys, and reduced GSH significantly reduced decreased the internalization of silver nanoparticles (* $p < 0.05$ of AgNP; Figure 5b), while in the presence of Trolox TLX were similar to the control levels. The GSSG showed an intermediated profile, as observed in cytotoxicity probably because of transient reduction of GSSG by cysteine of biogenic AgNP (Figure S3). Thus, we suggest that thiol-antioxidants precludes the interaction of both biogenic

and synthetic AgNP with cells. Hence, we have used NAC for managing rats intoxicated with sublethal dose of AgNP, interestingly we reverted prevented the toxic effects and increase the clearance of AgNP (Mendonça, et. al, 2018).

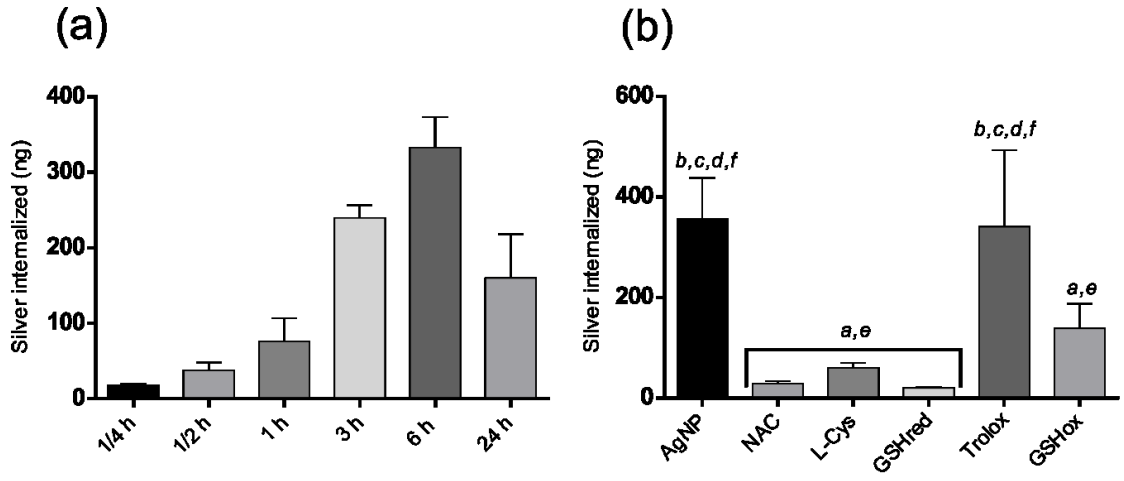

Figure 5. *Influence of thiol-antioxidants in the internalization.* **(a)** Cells were treated with AgNP IC^{50} at increasing times and the AgNP internalized was analyzed by ICP-OES. **(b)** Cells were treated with AgNP IC^{50} in presence of antioxidants (NAC, L-Cys, GSHred, TLX and GSHox) by 6 hours of incubation. Each value represents the mean ± S.D and *$p<0.05$ for significant difference of AgNP vs all, ANOVA followed by Tukey test.

4. Conclusion

Our results shed light on the use of molecules with free thiol and AgNP; in these cases, data interpretation might not be straightforward. For example, cytotoxicity mitigation in the presence of thiol-antioxidants was the result of the direct binding of the thiol group to the AgNP rather than ROS inhibition. In addition, other metallic nanoparticles (CuNP, AuNP, FeNP, PbNP, TiNP) may suffer from the same limitations shown here for AgNP; in a similar fashion other inhibitor containing free thiol (*e.g.*, Necrostatin) could have similar drawbacks. Based on our findings, we suggest the reduction of the plasmon band as an initial and straightforward way to verify any interference with AgNP. Finally, these results open the door for the targeting of the drug NAC, L-Cys, and GSH, for treating diseases related to AgNP since they could neutralize the effects or favor their excretion.

5. Supplementary Information

5.1. Synthetic silver nanoparticle cytotoxicity

For improving the robustness and confirming the results found for biogenic AgNP, we have repeated the core experiments using synthetic nanoparticles (Sigma Aldrich, St. Louis, MO). Initially, we determined the cytotoxicity of synthetic AgNP towards Huh-7 cells (Figure S1). Figure S1a shows the sigmoidal regression used for determining the IC_{50} values: 19.28 µM for MTT, 16.25 µM for Calcein, and 15.07 µM for PI, demonstrating both nanoparticles showed similar toxicity towards Huh-7 cells. The effects of synthetic AgNP treatment on cell morphology were comparable to that found for biogenic AgNP (Figure S1b). Control cells are mostly attached and depicted a cuboidal epithelial-like morphology; upon AgNP treatment, some cells are detached and show morphological changes (*e.g.*, cell shrinkage and rounding).

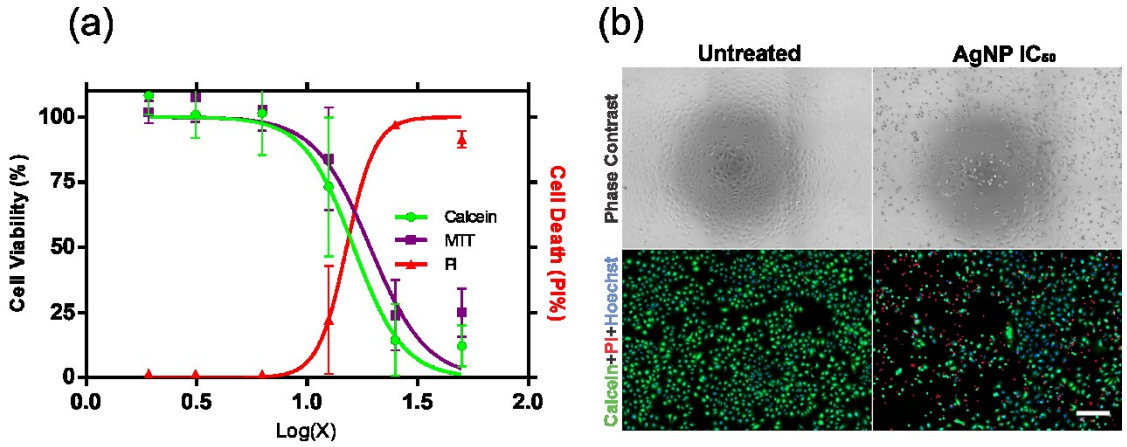

Figure S1. *Synthetic AgNP cytotoxicity towards HUH7 hepatocarcinoma cell*. (a) Cell viability assessed by MTT (λmax = 570 nm), Calcein-AM (ex/em 494/517 nm), and PI (ex/em 535/617 nm). Cells were treated with increasing concentrations of AgNP (1-50 µM) for 24 h. Each value represents the mean ± S.D. of three independent experiments (n = 3), cell viability was normalized to untreated control. (b) *Representative images of IC_{50} by Calcein/PI assay*. The above images were obtained by phase contrast, and the images below represent the merge of the GFP, DAPI, and PI filters. Column: Control group; IC_{50} treatment. Top: Phase contrast; Botton: Calcein+PI+Hoechst 33342. Scale bar: 200 µm.

5.2. Synthetic Silver nanoparticle viability in presence of antioxidants

The mitigation of cytotoxicity in the presence of thiol-antioxidants was also observed for synthetic AgNP. Cells were pretreated using a nontoxic concentration of antioxidants (Figure S2a), which were still able to prevent the ROS generation, followed by the treatment with synthetic AgNP IC_{50} concentration. The results of AgNP treatment associated with NAC, L-Cys, or GSH prevented nanosilver cytotoxicity (Figure S2b, #*). Conversely, pretreatment with TLX could not prevented the cytotoxic effects (Figure S2b, ¢*). These results were confirmed observing the cells using fluorescence microscopy (Figure S2c). The pretreatment with thiol-antioxidants (NAC, L-Cys, or GSH) showed similar morphology to the untreated cells, while in the pretreatment with non-thiol-antioxidant (TLX) we found nonviable cells and dead cells.

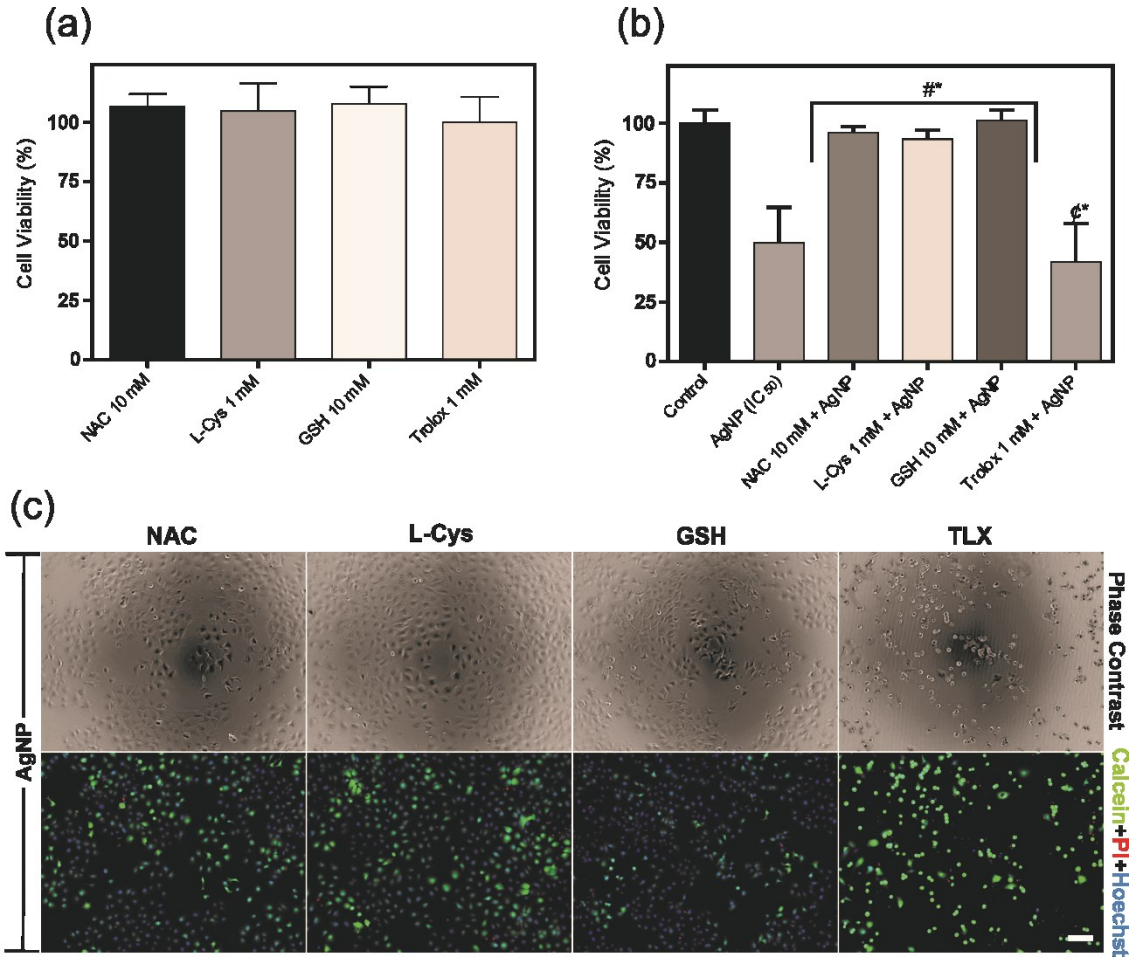

Figure S2. *Assessment of intracellular ROS and cell viability of Huh-7 cells pretreated with thiol and non-thiol-antioxidants and treated with synthetic AgNP.* (a) Cells were treated with antioxidants NAC (10 mM), L-Cys (1 mM), GSH (10 mM), and TLX (1 mM) for 24h, and cell viability was assessed by Calcein-AM assay (b) Cells were treated with synthetic AgNP IC50 for 24h of incubation, and cell viability was assessed by Calcein-AM assay. Each value represents the mean ± S.D. of three independent experiments (n=3), and the cell viability was normalized from the control (without treatment). #= <0.05 significant difference AgNP vs. All; ¢ = p<0.05 significant difference Control vs. All. ANOVA followed by Tukey test. (c) Representative images of AgNP cell viability in the presence of antioxidants. The above images were obtained by phase contrast, and the images below represent the merge of the GFP, DAPI, and PI filters. Groups: AgNP + NAC 10 mM; AgNP +L-Cys 1 mM; AgNP + GSH 10 mM; AgNP + GSH 10 mM; AgNP + GSH 10 mM. Top: Phase contrast; Bottom: Hoechst + Calcein + PI. Scale bar: 100 μm.

5.3. Viability with GSH oxidized

We reasoned that the presence of free thiol mediated the mitigation of AgNP cytotoxicity in the presence of thiol-antioxidants. To assess such possibility, we investigated the toxicity of synthetic and biogenic AgNP in the presence of glutathione disulfide (GSSG). The GSSG contains two molecules of GSH bound by a disulfide bond, resulting in the loss the GSH free thiol. Figure S3 shows the cell viability of Huh-7 cells treated with biosynthetic (Figure S3a) and synthetic (Figure S3b) AgNP in the presence of GSSG. First, we assure that the GSSG concentrations used had no cytotoxicity (Figure S2a). Next, we observe that the biogenic AgNP cytotoxicity in the presence of GSSG could not prevented the toxic effects like demonstrated for GSH (Figure 2). Although higher concentrations of GSSG (5 and 10 mM) partially prevented the toxicity, this could be explained by the nonenzymatic thiol-disulfide exchange between GSSG and cysteine present on the surface of biogenic AgNP. The GSSG could not prevented the cytotoxic effects of synthetic AgNP regardless of the concentrations (Figure S3b). Therefore, these results support our hypothesis of the importance of free thiol in preventing AgNP cytotoxicity.

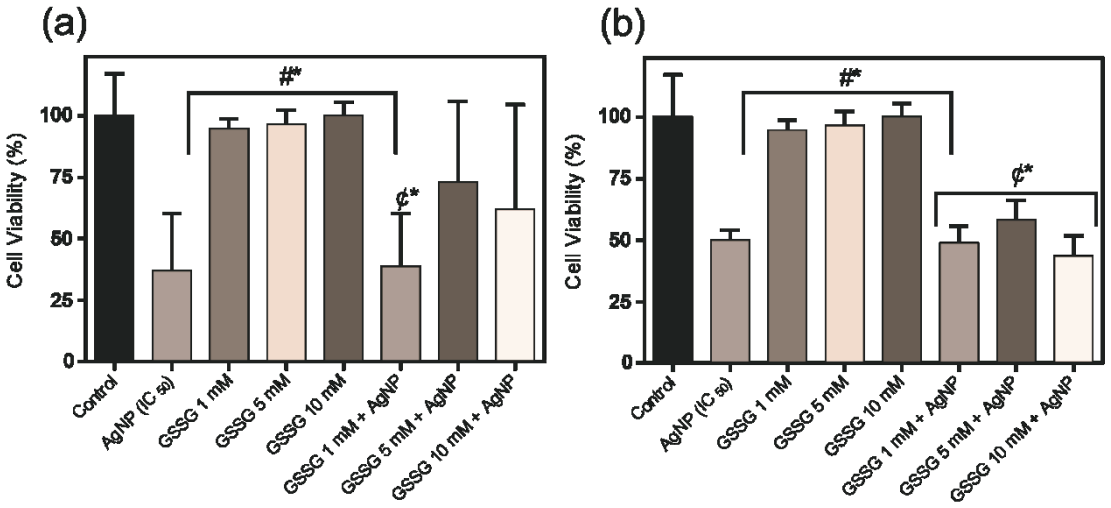

Figure S3. *Viability of AgNP biosynthetic and synthetic in presence of GSSG*. Cells were treated pretreated with GSSG and follow the treatment of biogenic (a) and synthetic (b) AgNP IC50 for 24h of incubation, and cell viability was measured by the Calcein-AM assay. Each value represents the mean ± S.D. of three independent experiments (n=3), and the cell viability was normalized from the control (without treatment). # = $p<0.05$ significant difference AgNP vs. All; ¢ = $p<0.05$ significant difference Control vs. All. ANOVA followed by Tukey test.

5.4. SPR modification by thiol-antioxidants in biogenic AgNP

To monitor the biogenic AgNP nanoparticle surface and aggregation state, we used Surface Plasmon Resonance (SPR) 1 (Figure S4). The scattering spectrum of biogenic AgNP exhibit λ max of 440 nm (Figure S4a) (Durán et al., 2005; Marcato et al., 2015). Upon the addition of NAC, L-Cys, or GSH to AgNP, we can see a positive correlation between the antioxidant concentration and the decrease and enlargement of the SPR (Figure S4b, c, and d), while the addition of TLX, regardless of the concentration used (1-100 mM), did not affect the AgNP scattering spectrum (Figure S4e). Low concentration of GSSG (1 mM) was not capable of decreasing the SPR, but higher concentrations (10 and 100 mM) could significantly reduce it (Figure S4f). This effect could be caused by reversible disulfide bond formation, regenerating the free thiol, and leading to AgNP interaction.

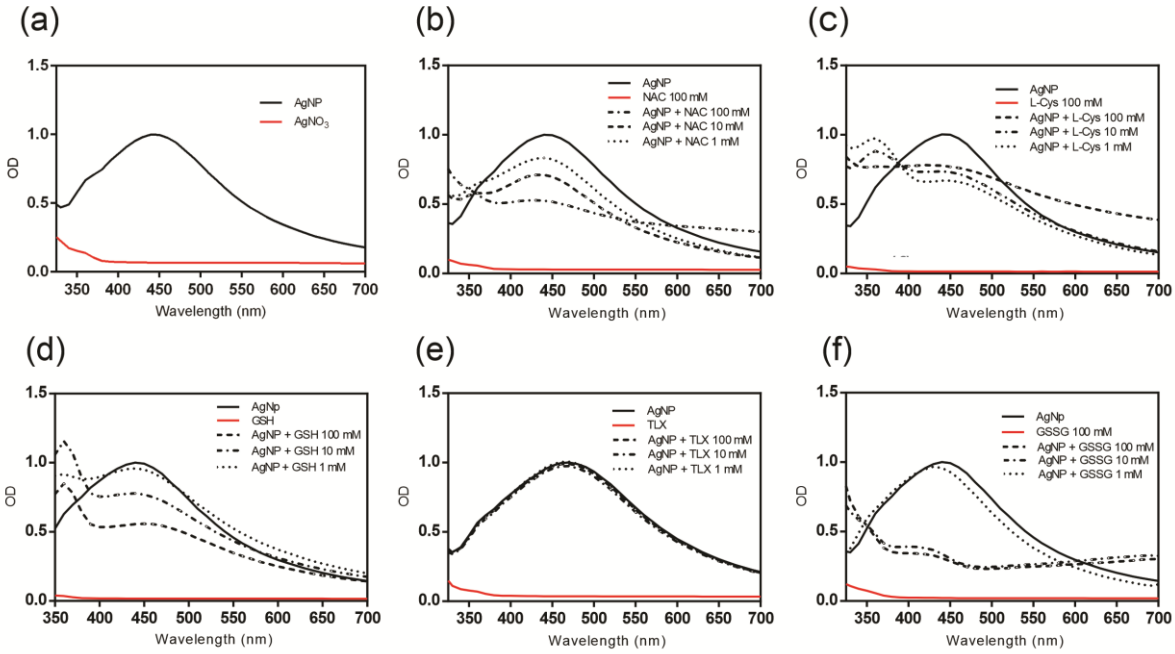

Figure S4. *Antioxidants interference in surface plasmon resonance of biogenic AgNP*. The UV-vis spectrum represents the Plasmon band of biogenic AgNP in the presence of increase concentrations antioxidants. (a) AgNP in water; (b) AgNP + NAC (1-100 mM); (c) AgNP + L-Cys (1-100 mM); (d) AgNP + GSH (1-100 mM); (e) AgNP + TLX (1-100 mM) and (f) AgNP + GSSG (1-100 mM). UV-Vis spectra acquired wavelength absorbance 300-700 nm.

5.5. Synthetic silver nanoparticles characterization

NTA technique was used to evaluate the hydrodynamic size and concentration of the nanoparticles in the presence of the antioxidants. Synthetic AgNP median hydrodynamic diameter was 46.1±33.5 nm, and the concentration of 1.51^{11} ±1.10^{10} particles/ml (Table S1). Incubation with non-thiol-antioxidant (TLX) led to no significant alterations in size, while thiol-antioxidants (NAC, GSH, and GSSG) increased AgNP size. Both results in the presence of thiol-antioxidants, *i.e.* increase in nanoparticles size and concentration decrease, could be explained by nanoparticle aggregation, as observed by TEM (Figure S5). By contrast, L-Cys was not capable of inducing aggregation of synthetic AgNP, which may be due to the lower concentration of synthetic AgNP compared to the biogenic AgNP.

Table S1. Physicochemical characterization of synthetic silver nanoparticles in the presence of antioxidants: NAC (10 mM), L-Cys (1mM), GSH (10 mM), and TLX (1 mM). The diameter and concentration of AgNP suspensions was measured using Nanotracking Analysis (Malvern Instruments Ltd, USA). Each value represents the mean ±S.D (n = 3).

Groups	NTA Size (nm)	Concentration (particles/mL)
AgNP	46.1±33.5	1.51^{11} ±1.10^{10}
AgNP + NAC	105.3 ±46.1	3.78^{10} ±8.51^{08}
AgNP + L-Cys	54.2 ±77.8	1.32^{11} ±1.44^{10}
AgNP + GSH	171.2±91.2	1.99^{10} ± 2.20^{09}
AgNP + TLX	44.7 ±28.5	1.22^{11} ± 2.17^{10}
AgNP + GSSG	170.1 ±68.9	8.7710 ±9.039

Further insight into the interaction between thiol-antioxidants and synthetic AgNP was gained by TEM. The median size of synthetic AgNP was 46.89 ±12.20 nm (Figure S5a and b), similar to what was described by the manufacturer (40 nm, Sigma-Aldrich, USA). Figure S5c II shows the aggregation of synthetic AgNP promoted by the addition of NAC, in contrast to what observed upon the addition of TLX 1 mM (S5(c) III), which presented the similar behavior of AgNP diluted in ultrapure water (S5(c) I).

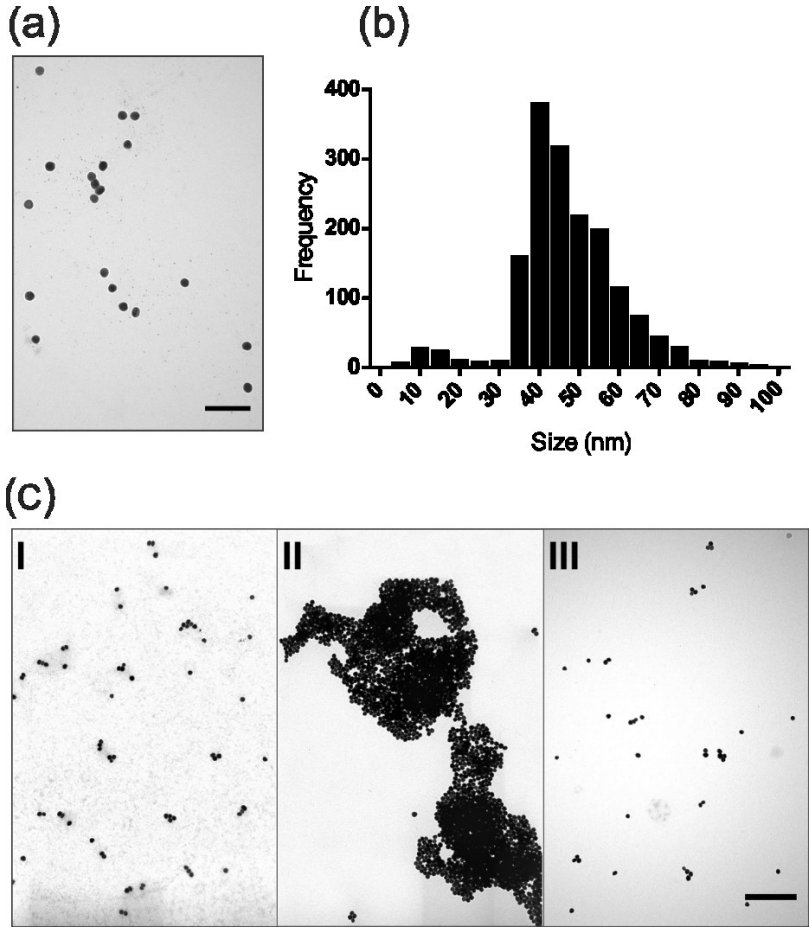

Figure S5. *TEM of synthetic AgNP in the presence of NAC.* (a) Representative TEM image of synthetic AgNP. A drop of nanoparticles suspension was deposited on the grid and let it dry overnight. Micrographs were obtained at magnification 75000x at a voltage of 60 kV, scale bar = 200 nm. (b) Size frequency analysis of AgNP. TEM images were analyzed in the software ImageJ by the NanoDefine ParticleSizer plugin (n = 1613 particles) (c) Representative TEM image of synthetic AgNP in the presence of antioxidants. A drop of nanoparticles suspension diluted in antioxidant solutions was deposited on the grid and let it dry overnight. Micrographs were obtained at magnification 27800x at a voltage of 60 kV, scale bar = 500 nm. Groups: I - ultrapure water; II - NAC (10 mM); III - TLX (1 mM).

5.6. SPR modification by thiol-antioxidants in Synthetic AgNP

SPR was also used to investigate the interaction between thiol-antioxidants and synthetic AgNP. The scattering spectrum of biogenic AgNP exhibit λ max of 420 nm (Figure S6a). The addition of NAC, L-Cys, or GSH to AgNP resulted in the decrease in the SPR scattering spectrum (Figure S6b, c, and d), in particular at higher concentrations (100 mM). These changes were probably due to surface interaction and aggregation induction, which

supports with NTA results. Interestingly, TLX at lower concentrations (1 and 10 mM) slightly modified the SPR scattering spectrum of AgNP and at higher concentration (100 mM) decreased the band intensity (Figure S6e). Nevertheless, the explanation for this observation is not clear because we have no sign of aggregation, neither by NTA nor TEM, like thiol-antioxidants. GSSG interference (Figure S6f) in the SPR profile showed an intermediate pattern compared to GSH (Figure S6d), which could support the idea that GSSG can reversibly regenerate free thiol and interact with the AgNP.

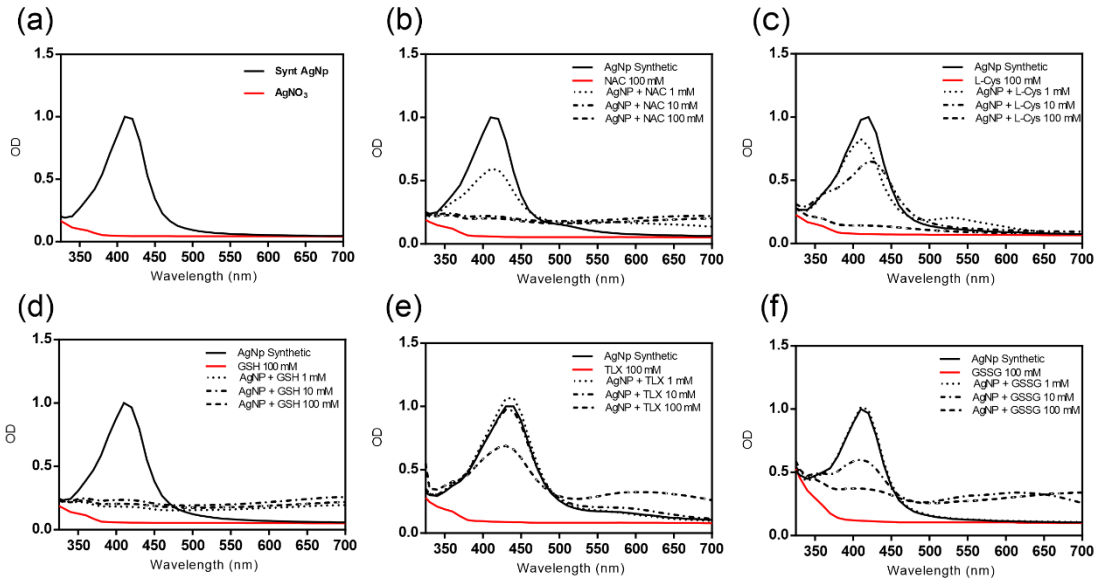

Figure S6. *Antioxidants interference in surface plasmon resonance of synthetic AgNP*. The UV-vis spectrum represents the SPR of biogenic AgNP in the presence of increase concentrations antioxidants. (a) AgNP in water; (b) AgNP + NAC (1-100 mM); (c) AgNP + L-Cys (1-100 mM); (d) AgNP + GSH (1-100 mM); (e) AgNP + TLX (1-100 mM) and (f) AgNP + GSSG (1-100 mM). UV-Vis spectra acquired wavelength absorbance 300-700 nm.

CAPÍTULO 3 - Como um artefato pode se transformar num antídoto.

N-Acetylcysteine reverses silver nanoparticle intoxication in rats

Luiz Alberto Bandeira Ferreira[a§], Monique Culturato Padilha Mendonça[a§], Cintia Rizoli[a], Ângela Giovana Batista[b], Mário Roberto Maróstica Júnior[b], Emanueli do Nascimento da Silva[c], Solange Cadore[c], Nelson Durán[c,d], Maria Alice da Cruz-Höfling[a], Marcelo Bispo de Jesus[a]*

[§] Both authors contributed equally to this manuscript

[a]*Department of Biochemistry and Tissue Biology, Institute of Biology, University of Campinas, Campinas, São Paulo, 13083-970, Brazil;*

[b]*Department of Food and Nutrition, University of Campinas, Campinas, São Paulo, 13083-862, Brazil;*

[c]*Institute of Chemistry, University of Campinas, Campinas, São Paulo, 13083-970, Brazil;*

[d]*Nanomedine Units, Federal University of ABC (UFABC), Santo André, São Paulo, 09210-58, Brazil;*

Nanotoxicology

ISSN: 1743-5390 (Print) 1743-5404 (Online) Journal homepage: http://www.tandfonline.com/loi/inan20

N-Acetylcysteine reverses silver nanoparticle intoxication in rats

Monique Culturato Padilha Mendonça, Luiz Bandeira Ferreira, Cintia Rizoli, Ângela Giovana Batista, Mário Roberto Maróstica Júnior, Emanueli do Nascimento da Silva, Solange Cadore, Nelson Durán, Maria Alice da Cruz-Höfling & Marcelo Bispo de Jesus

Abstract

The increasing use of silver nanoparticles (AgNPs) in consumer products raises the risk of human toxicity. Currently, there are no therapeutic options or established treatment protocols in cases of AgNPs intoxication. We demonstrated previously that thiol antioxidants compounds can reverse the cytotoxicity induced by AgNPs in Huh-7 hepatocarcinoma cells. Here, we investigated the use of N-acetylcysteine (NAC) against the systemic toxic effects of AgNPs (79.3 nm) in rats. Biochemical, histopathological, hematological, and oxidative parameters showed that a single intravenous injection of AgNPs (5 mg/kg b.w.) induced deleterious effects such as hepatotoxicity, potentially as a result of AgNPs accumulation in the liver. Treatment with a single intraperitoneal injection of NAC (1 g/kg b.w.) one hour after AgNPs exposure significantly attenuated all toxic effects evaluated and altered the bioaccumulation and release patterns of AgNPs in rats. The findings show that NAC may be a promising candidate for clinical management of AgNPs intoxication.

Keywords: nanotoxicology, metallic nanoparticles, thiol compounds, glutathione, ascorbic acid.

1. Introduction

Silver nanoparticles (AgNPs) are the most commonly used nanomaterial in consumer products (Vance et al., 2015). The primary application of AgNPs is related to their remarkable antimicrobial activity (Nelson. Durán et al., 2016; Franci et al., 2015; Kim et al., 2007), and they are applied to a variety of products including textiles (Windler et al., 2013), cosmetics (Kokura et al., 2010), food packaging (Peters et al., 2016; Rhim et al., 2013), and medical devices (Dayyoub et al., 2017; Shrestha and Kishen, 2016). The widespread production and use of AgNPs have resulted in a growing number of workers and consumers exposed to these nanoparticles. Currently, data from assessments of AgNPs exposure in workplaces and their release from consumer products are limited (Savery et al., 2017; Weldon et al., 2016).

Therapeutic, occupational, accidental or self-inflicted intoxication with high doses of silver has been documented (Drake and Hazelwood, 2005; Hadrup and Lam, 2014; Jung et al., 2017; Trop et al., 2006). Hadrup *et al.* in a recent review reported that adverse effects of silver in humans start to occur at cumulative doses in the range of 60-70 mg silver/kg body weight (Hadrup et al., 2018). For the general population, the estimated dietary human intake of silver has been described to be 70-90 μg per day (Wijnhoven et al., 2009); although, this number is likely underestimated nowadays since the actual exposure levels are higher due to the widespread production and use of silver. From 2005 to 2017, the silver production worldwide increased by 20% (Statista, 2018).

Considerable efforts have been made to understand the AgNPs toxicity. The AgNPs toxicity is closely related to the release of Ag ions (Ag^+) (Nelson. Durán et al., 2016; McShan et al., 2014). However, it is difficult to determine whether the toxicity is solely a result of the Ag^+ or whether the AgNPs themselves cause toxic effects. Inside the cell, AgNPs can induce production of reactive oxygen species (ROS), disruption of energy metabolism and gene transcription, and binding with the free thiol groups of enzymes and cellular proteins. These

mechanisms lead to pro-inflammatory cytokine induction, DNA damage and eventually cell death by apoptosis or necrosis (McShan et al., 2014; Wang et al., 2015). In parallel, *in vivo* rodent studies revealed that AgNPs might cause toxicity to several vital organs including brain, heart, lung, liver, kidney, and non-vital ones such as spleen. These toxic effects have been observed either after single or repeated exposure, regardless the route of administration (Bostan et al., 2016; Mao et al., 2016; Recordati et al., 2015; Yang et al., 2017). While there is evidence that AgNPs are toxic, toxicity studies of AgNPs have resulted in inconclusive data as several studies have reported either beneficial or harmful effects of these nanomaterials. These discrepancies have been attributed to AgNPs physicochemical characteristics, dose, route of administration, or the tested animal species (Marin et al., 2015). Besides all of these potential factors, there is one that is crucial but, in many cases, ignored. This factor is AgNPs structure that can be determinate by different techniques such as X-ray diffraction pattern (Nelson Durán et al., 2016b). Despite the controversies and knowledge about AgNPs toxicity; there are still no therapeutic options or established treatment protocols in cases of AgNPs intoxication.

Previously, we demonstrated that non-thiol antioxidant compounds, such as Trolox (water-soluble analog of vitamin E) and ascorbic acid (AA) prevented ROS production but not cell death in Huh-7 hepatocarcinoma cells. Conversely, we showed that thiol antioxidants such as N-acetylcysteine (NAC), L-cysteine, and glutathione (GSH) acted as metal chelators and inhibited the cytotoxic effects of AgNPs (Ferreira et al., 2018). To further substantiate these *in vitro* findings, we performed a more extensive and detailed study to assess whether or not the NAC protective effect would also be effective for the *in vivo* condition. Such an approach may reinforce the view that thiol groups are involved in modulation of the neutralization of AgNPs toxic effects.

In this study, we exposed Wistar rats to a sublethal intravenous (i.v.) dose of AgNPs and evaluated whether or not systemic toxic effects were triggered and if NAC therapy initiated

1 h following this would neutralize such effects. To answer this question, biochemical, hematological, and histopathological analyses were performed 24 h post-administration. Furthermore, we investigated the antioxidant defense system and the fate and excretion of AgNPs to elucidate the main routes of AgNPs bioaccumulation and release. To the best of our knowledge, this is the first study to demonstrate that NAC can act as an antidote to treat AgNPs intoxication.

2. Materials and Methods

2.1. Materials

Reagents were purchased from Sigma-Aldrich (St. Louis, MO, USA), unless specified otherwise.

2.2. Synthesis and characterization of AgNPs

Synthesis and characterization of the AgNPs used for this study have been reported previously (Durán et al., 2005; Fanti et al., 2018; Ferreira et al., 2018). In brief, the fungus *Fusarium oxysporum* was grown in a medium containing 2 % malt extract and 0.5 % yeast extract at 28 °C for six days. The grown biomass was filtered and washed on filter paper using a Büchner funnel. Approximately 10 g of the humid biomass obtained was transferred to a conical flask containing 100 mL distilled water and kept at 28 °C for 72 h. After this time, 10 mM silver nitrate ($AgNO_3$) was added in the filtrate and maintained at 28 °C for 72 h. The reduction of silver ions in AgNPs suspension was monitored by ultraviolet-visible spectroscopy (UV-vis) between 300 and 700 nm using a Cytation 5 Cell Imaging Multi-Mode Reader (Biotek, Sunnyvale, CA, USA). The silver concentration in suspension was determined by inductively-coupled plasma mass spectrometry using an Optima 8300DV optical emission spectrometer (PerkinElmer, Waltham, MA, USA). The recovered AgNPs were characterized

by transmission electron microscopy, nanoparticle tracking analysis (NTA), and X-ray photoelectron spectroscopy (Ferreira et al., 2018). In this study, we obtained additional information regarding the surface charge (zeta potential) and polydispersity index of the AgNPs using dynamic light scattering (Malvern NanoZS, Malvern Instruments, Worcestershire, UK).

2.3. Animals and Treatment

All experimental procedures were approved by the Institutional Committee for Ethics in Animal Use (CEUA/UNICAMP, protocol no. 4410-1) following the Brazilian National Council for Animal Experimentation Control. Male Wistar rats, 6-7 weeks old, weighing 200-250 g, were used in this study. The animals were housed using a standard 12 h light/dark cycle, in a temperature-controlled environment (22 ± 2 °C), with access to water and chow (Nuvital, Curitiba, PR, Brazil) *ad libitum* (n=5 animals/plastic cage).

After one week of acclimatization, the rats were divided randomly into five groups comprising: (i) controls (physiological saline solution), (ii) $AgNO_3$ (used as a reference material to indicate if the effects are caused by free silver ions), (iii) AgNPs, (iv) NAC, and (v) AgNPs+NAC. Additionally, to assess whether the thiol groups play a key role in the reversion of AgNPs toxicity, the effects of the thiol antioxidant compound GSH and the non-thiol antioxidant compound AA were comparatively investigated.

The animals from control, $AgNO_3$, and AgNPs groups received a single i.v. injection of 0.9% sterile saline solution, $AgNO_3$ or AgNPs (5 mg/kg body weight), respectively. The dose was selected based on the results of a dose-response pilot study in which nine rats were exposed to AgNPs at doses of 5, 7.5 and 10 mg/kg (n=3/dose) for 24 h. The starting dose was based on a literature review (Savery et al., 2017). From six rats tested for the two highest doses (7.5 and 10 mg/kg), four animals (n=2/dose) died immediately after the administration. Those animals that received the lowest dose (5 mg/kg) survived throughout treatment period but

presented marked signs of toxicity such as abnormal posture, tremor, skin alteration (cyanosis), ataxia, and other motor abnormalities.

One hour after AgNPs administration, the rats were injected intraperitoneally with 1 g/kg body weight of NAC, GSH or AA. This dose was chosen according to previous studies (Kondakçı et al., 2017; Mansour et al., 2008). The animals were euthanized 24 h after treatment.

2.4. Histopathology and immunohistochemistry

Animals (n=3/group) were anesthetized by intraperitoneal injection of ketamine (Dopalen®, 270 mg/kg body weight) and xylazine (Anasedan®, 30 mg/kg body weight) (both obtained from Fortvale, Valinhos, SP, Brazil). Next, animals were perfused transcardially with physiological saline followed by 4 % paraformaldehyde in 0.1 M phosphate buffered saline (PBS, pH 7.4). The liver was excised immediately, post-fixed overnight in the same fixative and embedded in paraffin. Sections (5 μm thickness) were routinely stained with Hematoxylin-eosin (HE) for histopathological analysis.

The expression of anti-CD 68 was evaluated by immunohistochemistry in paraffin-embedded liver sections to identify resident macrophages. Liver tissues were dewaxed, hydrated, and immersed in 3 % hydrogen peroxide twice for 10 min to inactivate endogenous peroxidase activity. For epitope retrieval, tissues were incubated in 10 mM sodium citrate buffer (pH 6.0), in a steamer (95-99°C) for 30 min. Non-specific binding of antibodies was blocked by incubation with 5% skimmed milk powder for 1 h at room temperature. Tissues were then incubated overnight with 1:50 anti-CD 68 (AbD Serotec, Raleigh, NC, USA) in a humidified chamber at 4 °C. After washing twice with PBS, tissues were incubated with the biotinylated secondary antibody (EnVision_HRP link, Dako Cytomation, CA, USA) for 30 min at room temperature. Peroxidase activity was detected using diaminobenzidine chromogenic solution (DAB+, Dako Cytomation) counterstained with Harris hematoxylin. After ethanol dehydration,

the slides were mounted in Entellan (Merck, Darmstadt, Germany). All images were captured using an Olympus BX51 photomicroscope (Shinjuku, Tokyo, Japan).

Image analysis (n=3/group; 4 fields per animal) was done using Image J with IHC Toolbox plugin (http://rsb.info.nih.gov/ij/plugins/ihc-toolbox/index.html.) that detected the brown color of H-DAB stained images and separated from Harris hematoxylin. This color image segmentation makes possible to determine the total percentage of pixels stained by anti-CD-68.

2.5. Blood samples

Blood (4 mL) from each anesthetized rat (n=4-10/group) were collected by cardiac puncture before perfusion into EDTA or gel separator tubes. Each blood sample in the EDTA tubes was analyzed immediately using a Coulter T540 hematology system (Fullerton, CA, USA). Blood in the gel separator tubes was centrifuged at 1500 g for 15 min for serum extraction. The biochemical analysis of aspartate aminotransferase (AST), alanine aminotransferase (ALT), alkaline phosphatase (ALP), blood urea nitrogen (BUN), and creatinine were performed in a Cobas® 6000 C501 Clinical Chemistry Analyzer (Roche Diagnostics, Mannheim, Germany) on the day of collection. Serum samples for antioxidant analysis were aliquoted and frozen at −80°C prior to use.

2.6. Western blotting

Liver samples (n=5/group) were frozen in liquid nitrogen and homogenized in an extraction buffer (10 mM EDTA, 2 mM PMSF, 100 mM NaF, 10 mM sodium pyrophosphate, 10 mM $NaVO_4$, 0.1 mg aprotinin/mL and 100 mM Tris, pH 7.4). The tissue homogenates were centrifuged, and a sample of each homogenate was quantified by Bradford assay (Bio-Rad Laboratories, Hercules, CA, USA). The supernatants were mixed (1:1) with Laemmli

buffer and transferred to a dry bath at 100°C for 5 min. Equal amounts of protein (40 μg) were separated on a 12% sodium dodecyl sulfate-polyacrylamide gel and electroblotted onto nitrocellulose membranes (Bio-Rad). The membranes were blocked with 5% skimmed milk powder in 0.1% Tris-buffered saline conatining 0.05 % Tween 20, pH 7.4 (TBS-T) for 1 h at room temperature, and then probed overnight with primary antibodies against catalase (1:500, sc-50508, Santa Cruz Biotechnology, CA, USA) and superoxide dismutase-1 (SOD-1) (1:500, sc-11407, Santa Cruz Biotechnology). Subsequently, the membranes were incubated with HRP-conjugated secondary antibodies for 2 h. The blots were detected by incubation in a chemiluminescence solution (Super Signal West Pico Chemiluminescent Substrate; Pierce Biotechnology, Rockford, IL, USA), followed by luminescent signal capture using the Gene Gnome equipment (Syngene Bio Imaging, Cambridge, UK). Band intensities were quantified by densitometry using Image J 1.8.0 (NIH, Bethesda, MD, USA). The blots were stripped and reprobed for GAPDH as an endogenous control to monitor protein loading, the efficiency of blot transfer, and non-specific changes in protein levels. The protein results were expressed as a ratio relative to endogenous control.

2.7. Antioxidant analysis

The concentration of thiobarbituric acid-reactive substances (TBARS), and the activities of GSH, SOD, and catalase in serum and liver homogenates were measured as described previously (Batista et al., 2014).

2.8. Autometallography (AMG)

Localization of AgNPs was performed using histological sections of paraffin-embedded tissue samples with AMG staining as described previously (Miller et al., 2016). After dewaxing, the sections were dried for 1 h at 40 °C and then placed in jars filled with AMG

developer (25 % Arabic gum, 50% citrate buffer, 5.6% hydroquinone, and 0.1% $AgNO_3$). Silver development was terminated after 1 h by replacing the developer with 2.5% w/v sodium thiosulphate for 10 min. Next, the sections were placed under running tap water for 20 min followed by washing in distilled water. All sections were stained with HE, mounted with Entellan and examined under an Olympus BX51 light microscope.

2.9. Quantification of silver concentration

Total silver concentrations were determined in organs (liver, kidney, spleen and lungs), urine and feces by graphite furnace atomic absorption spectrometry (GF-AAS) using an AAnalyst 600 spectrometer (Perkin-Elmer, Norwalk, USA) (n=3-6/group).

For GF-AAS measurements in tissue and feces, 0.05-0.15 g of lyophilized samples (depending on the available tissue amount) were homogenized in 9.5 mL of deionized water (depending on the available tissue amount) and incubated for 5 min. Subsequently, 0.5 mL of 25 % tetramethylammonium hydroxide (TMAH) was added to the solution and incubated in an ultrasound cleaning apparatus until complete solubilization of the samples. The absorbance was determined at the 328.1-nm resonance line, and some posterior dilution was made if necessary. Analysis of urine samples was performed without adding TMAH. The analytical calibration curve was generated at 10-60 µg/L using aqueous metallic silver standards and a 3 µg solution of 5 µg/mg Pd $(NO_3)_2$ as a chemical modifier. The pyrolysis and atomization temperatures were 800°C and 1700°C, respectively. All readings were performed in triplicate.

All GF-AAS instrumental conditions were optimized using recovery tests at 25 µg/L and suitable recoveries were obtained (95 ± 2 %), as well as adequate relative deviations (<10 %). The limits of detection and quantification were 0.42 and 1.4 µg/ L, respectively.

2.10. Statistical analysis

Data were analyzed using GraphPad Prism version 5.0 (GraphPad Software, San Diego, CA). One-way ANOVA followed by Tukey *post-hoc* test was used to determine the statistical significance between three or more groups. Student's *t*-test was used for comparisons between two groups. Differences were considered statistically significant at $p < 0.05$. All values were expressed as the mean ± standard error of the mean (SEM).

3. Results and Discussion

3.1. Nanoparticle characterization

A detailed physicochemical and morphological characterization of AgNPs has been reported previously by our group (Ferreira et al., 2018). Briefly, the AgNPs showed a spherical structure and monodispersed state, which was corroborated by a polydispersity index of 0.386 ± 0.03. Assessments by NTA showed that an average size of 79.3 ± 39.7 nm, a concentration of 7.77^{11} ± 2.69^{10} particles/mL and a negative zeta potential of -31.3 ± 0.3 mV. The main properties of AgNPs were confirmed before *in vivo* experiments since physicochemical properties such as shape, size, size distribution, surface chemistry and composition can influence their biodistribution and biological activity (Zhang et al., 2016).

3.2. Thiol antioxidants reverse the hepatotoxic effect of AgNPs in rats

In line with our previous research (Ferreira et al., 2018), we hypothesized that thiol-containing antioxidants could act as chelating agents *in vivo* (Supplementary Information, Figure S1), thereby preventing the toxic effects caused by the AgNPs. First, we evaluated serum biochemical parameters of the hepatic function in male Wistar rats i.v.-administered AgNPs. The liver is an important organ of detoxification and has been described as the primary organ for silver bioaccumulation (Dziendzikowska et al., 2012; Ramadi et al., 2016).

As shown in Figure 1(a-c), the levels of AST, ALT, and ALP were increased in AgNPs-treated rats compared to control (physiological saline) and $AgNO_3$ groups. All biochemical parameters decreased after administration of the thiol-compounds NAC or GSH 1 h after injection of AgNPs, neither NAC nor $AgNO_3$ alone affected any of the biochemical parameters, indicating that silver salt was less toxic to the animals than AgNPs. On the other hand, the treatment with the non-thiol compound AA was not able to attenuate the increased serum enzymes activities found in the AgNPs-treated animals, supporting at least partial specificity of the effects for thiol (-SH) group. Thiol groups bind with high affinity to silver ions, thus increasing the dissolution rate of AgNPs due to the silver-thiol complex formation and resulting in a progressive decrease of AgNPs body concentrations (Behra et al., 2013; Bell and Kramer, 1999; Flora and Pachauri, 2010; Gondikas et al., 2012).

Next, we performed histopathological analysis of the liver to gain additional understanding of the thiol-containing antioxidant protective effect. We found normal cytoarchitecture in control (Figure 1(d)), NAC (Figure 1(e)), and $AgNO_3$ (Figure 1(f)) groups, and no visible alterations were observed next to portal space, the centrilobular vein or throughout the hepatic lobule (Figure 1(d) to 1(f)). In contrast, livers from the AgNPs group exhibited inflammatory cell infiltration at the hepatic portal system (Figure 1(g), (h)). Intravenous exposure of mice to AgNPs, but not $AgNO_3$, induce inflammation in the liver, kidney, and lung suggesting that Ag particulates have unique mechanisms that cause the peripheral inflammation (Guo et al., 2016). In accordance with liver biochemistry results, the hepatic tissue showed normal morphology upon AgNPs+NAC treatment (Figure 1(i)) and, in agreement with our thiol group protective effect hypothesis, similar alterations to those found in AgNPs-injected rats were found in AgNPs+AA (Figure 1(j)) and not in the AgNPs+GSH group (Figure 1(k)).

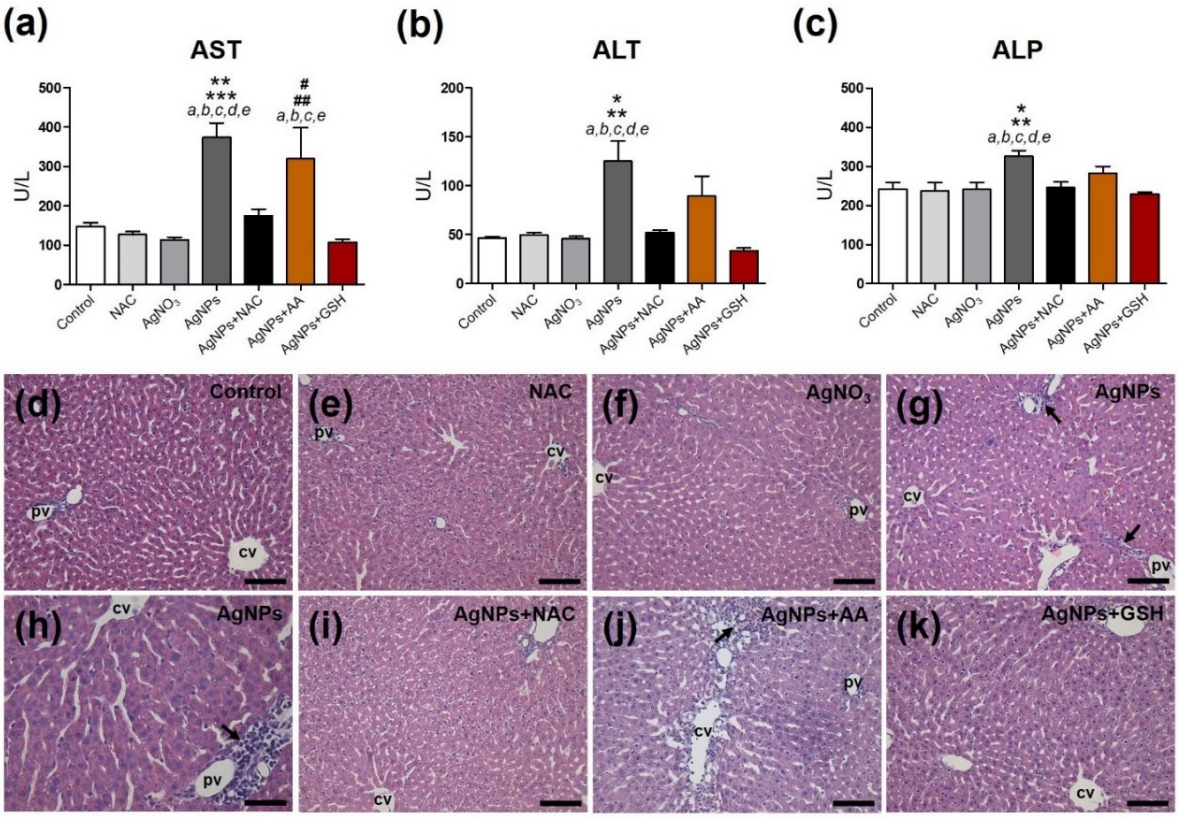

Figure 1. *Effects of N-acetylcysteine (NAC), ascorbic acid (AA) and glutathione (GSH) in hepatic tissue after silver nanoparticle (AgNPs) i.v. administration***.** Rats received a single intravenous injection of 0.9% saline (control), AgNPs or silver nitrate ($AgNO_3$) (5 mg/kg), followed by single i.p. administration of NAC, AA, or GSH (1 g/kg). Twenty-four hours post-treatment, the concentration of (**a**) aspartate transaminase (AST), (**b**) alanine transaminase (ALT), and (**c**) alkaline phosphatase (ALP) were determined. (**d-k**) Representative photomicrographs of the hepatic parenchyma stained with Hematoxylin-eosin after administration of (**d**) 0.9% saline, (**e**) NAC, (**f**) $AgNO_3$, (**g,h**) AgNPs, (**i**) AgNPs+NAC, (**j**), AgNPs+AA, or (**k**) AgNPs+GSH administration. Bars = 100 µm, except for panel H (50 µm). *cv:* central vein*; pv:* portal vein. *Arrows* indicate inflammatory infiltrate. Values are expressed as mean ± SEM (n=4-10 animals/group) in comparison to *a* control, *b* NAC, *c* $AgNO_3$, *d* AgNPs+NAC and *e* the AgNPs+GSH groups. Panel (**a**) ***p<0.001 for *a,b,c,e*; **p<0.01 for *d*; #p<0.05 for *a*; ##p<0.01 for *b,c,e*; Panel (**b,c**) **p<0.01 for *a,b,c,e*; *p<0.05 for *d*. One-way ANOVA plus Tukey post-comparison test.

3.3. NAC therapy for treatment of AgNPs toxicity

Having determined that thiol-containing antioxidants can reverse the hepatotoxic effects of AgNPs *in vivo*, we performed a more thorough assessment of the application of NAC as a potential antidote for AgNPs intoxication. Among the proposed thiol-compounds, NAC has the most favorable safety profile. This compound has been approved by the U.S. Food and Drug

Administration (FDA) since 1960 as a mucolytic agent and was later used as an antidote for the treatment of acetaminophen overdose intoxication (Rushworth and Megson, 2014). Besides the hepatotoxic effects, abnormal clinical signs and behaviors were also detected for the AgNPs-treated group. The animals exhibited abnormal gait and posture, akinesia, and a generalized decrease in spontaneous movements up to 5 h post-AgNPs i.v. injection. Immediately after injection, the hind paws exhibited a dark bluish color and, after NAC administration, this returned to its normal rose color (Supplementary information, Figure S2). Alterations in skin color as observed here are likely to be indicative of inadequate oxygenation of the blood.

Following the skin color alterations observed above, we assayed hematological parameters including red blood cells (RBCs) count, hemoglobin and hematocrit levels, along with platelet, and white blood cells (WBCs) counts (Table 1). Compared to the control group, the AgNPs group showed a decrease in many blood parameters such as RBCs (-11%, $p<0.05$), hemoglobin (-14%, $p<0.01$), hematocrit (-14%, $p<0.05$), and platelet count (-103%, $p<0.01$). These parameters were unaffected in rats treated with NAC and $AgNO_3$. Albeit $AgNO_3$ treatment had induced little or no effects, AgNPs treatment induced alterations in biochemical and hematological parameters in rats, including alterations in RBC, platelet count, WBC count, and AST, in agreement with another study (Qin et al., 2017). Such toxicity induced by AgNPs could be attributed to the direct interaction of the nanoparticles with RBCs or, more specifically, to the heme group of hemoglobin (Bhunia et al., 2017). This could result in membrane damage, hemagglutination, and subsequently hemolysis (Asharani et al., 2010; Chen et al., 2015). No alterations in hematological parameters were found in the animals treated with AgNPs+NAC, possibly related to partial restoration of intracellular thiol groups (Zhou et al., 2013).

Table 1. Effects of NAC therapy on hematological parameters of male Wistar rats.

	Unit	Control	NAC	$AgNO_3$	AgNPs	AgNPs + NAC
RBCs	$10^6/\mu l$	6.97 ± 0.07 *	6.76 ± 0.23	6.398 ± 0.14	6.27 ± 0.12 *	6.39 ± 0.17
Hb	g/dl	13.65 ± 0.09 #	13.07 ± 0.42	12.42 ± 0.25	11.95 ± 0.32 #	12.33 ± 0.43
Hct	%	44.33 ± 0.40 * ϕ	42.75 ± 1.40	38.40 ± 0.71 ϕ	38.83 ± 1.20 *	39.85 ± 1.73
PLTs	$10^3/\mu l$	804.4 ± 18.22 #	785.8 ± 54.27 ≠	660.4 ± 19.12	396.5 ± 75.93 #≠	503.8 ± 104.2
WBCs	$10^3/\mu l$	7.08 ± 0.42 *	7.12 ± 0.31 ϕ	6.21 ± 0.82 #	11.47 ± 1.02 * ϕ #	8.254 ± 0.740
Neutrophils	$10^3/\mu l$	11.86 ± 2.47 *	8.33 ± 7.28 #	10.13 ± 10.17≠	36.43 ± 5.63 *#≠	22.85 ± 7.85
Lymphocytes	$10^3/\mu l$	5.82 ± 6.51	6.09 ± 3.93	4.95 ± 7.10	7.36 ± 5.40	6.08 ± 4.67
Monocytes	$10^3/\mu l$	2.12 ± 4.16 *	1.72 ± 1.91 #	1.64 ± 2.47 ≠	6.07 ± 7.92 *#≠ϕ	2.68 ± 6.80 ϕ

RBCs red blood cells; *Hb* hemoglobin; *Hct* hematocrit; *PLTs* platelets; *WBCs* white blood cells. The same symbol in each line indicates a significant difference between groups. Data are shown as mean ± SEM, n = 4-10 animals in each group. *, □ $p<0.05$ and #, ≠$p<0.01$. One-way ANOVA plus Tukey post-comparison test.

The WBCs count was higher in the AgNPs group when compared to the control (+62%, $p < 0.05$), NAC (+61%, $p < 0.05$) and $AgNO_3$ (+85%, $p < 0.01$) groups. Normally, an increased number of WBCs is associated with inflammation, as shown at the liver portal system of AgNPs-treated animals. The inflammatory response is characterized by the rapid recruitment of neutrophils and monocytes to the site of injury to support Kupffer cells, the resident macrophages in the liver, for the rapid clearance of circulating xenobiotics. Nevertheless, to investigate the possibility of AgNPs triggering an inflammatory response, we examined the distribution of CD68-positive Kupffer cells.

As shown in Figure 2(a), the number of CD68 immunolabeled cells in the liver of AgNPs-treated animals was higher than that of the corresponding cells labeled in the control (+70 %, $p < 0.001$), NAC (+84 %, $p < 0.001$), and $AgNO_3$ (+91 %, $p < 0.001$) groups. Furthermore, the CD68-positive cells in the AgNPs group were hypertrophied, whereas this was not observed in the other groups (comparison of Figure 2(e) and (f) to 2 (b-d) and (g)). A major density of Kupffer cells was found nearby the portal area although this was possibly also found along the sinusoid capillaries running freely between hepatocyte plates. This agrees with

the finding of the recruited leukocytes, which were also confined to the portal area. In animals treated with AgNPs+NAC (Figure 2(g)), the population of CD68-positive cells was more rarefied, presented a normal size and were not confined to the portal area. These findings suggest that Kupffer cells mediate the hepatic response to AgNPs brought about by portal vein and hepatic artery tributaries reaching the portal space.

Considering the intrinsic differences in the toxicity profile of the AgNPs and $AgNO_3$ described above, the toxicity of AgNPs can be partially attributed to nanoparticles deposition in the tissues, which can result in ROS generation (Wang et al., 2015). Several *in vivo* and *in vitro* studies have demonstrated that AgNPs induced ROS increase (Kim and Ryu, 2013b), due to specific characteristics of AgNPs, not only due to the presence of silver ions. We found that the AgNPs injuries are reflected in the antioxidant defenses of the liver, and NAC treatment could restore the redox equilibrium due to its metal-chelating properties that increase AgNPs excretion, leading to reduced blood and tissue silver concentrations (Supplementary Information, Figure S3).

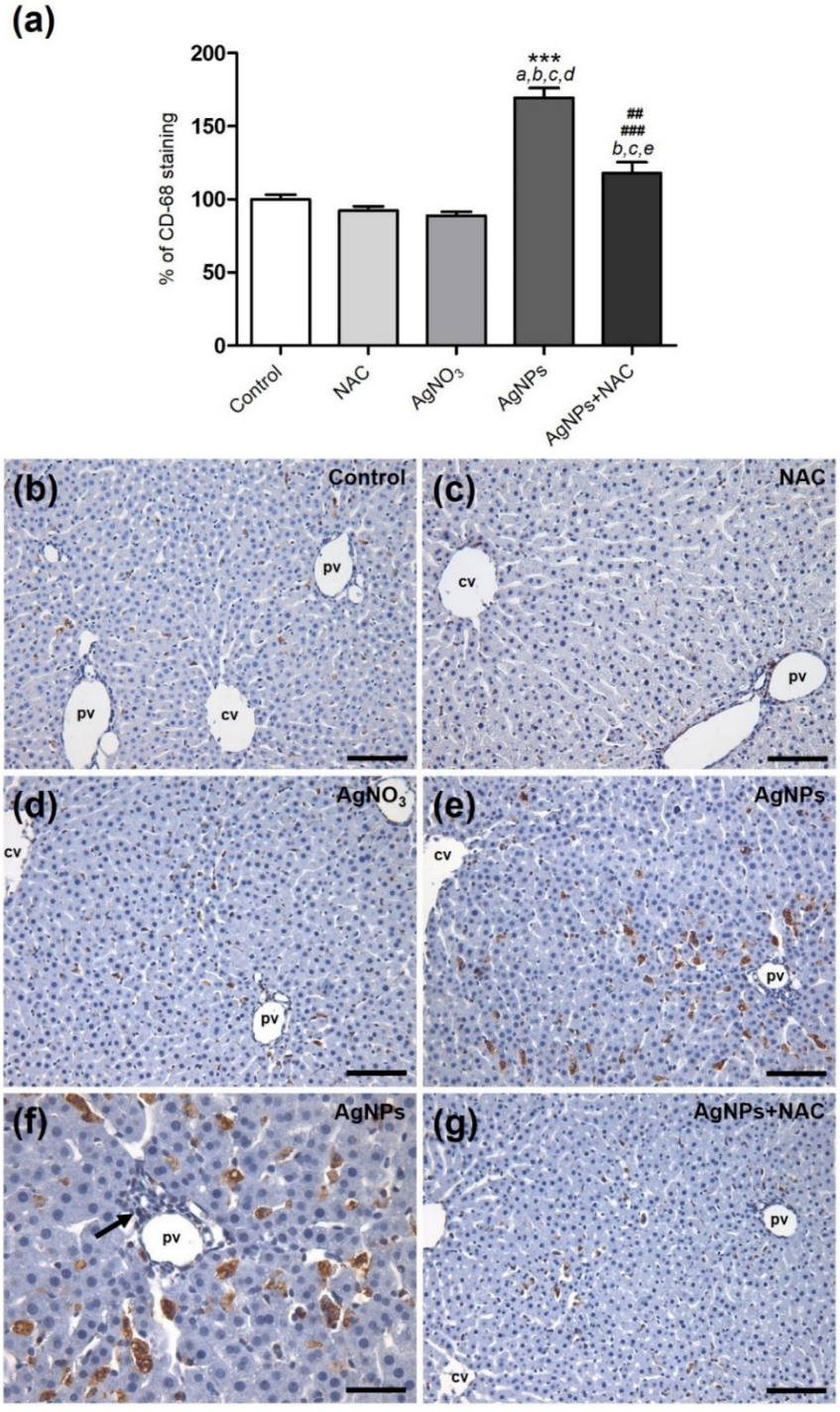

Figure 2. *Immunostaining of CD68+ Kupffer cells in rat liver sections*. **(a)** Percentage of pixels density of CD-68 labeled macrophages. **(b-g)** Representative photomicrographs of resident macrophages (brown) 24 h after administration of (**b**) 0.9% saline, (**c**) NAC, **(d)** $AgNO_3$, **(e,f)** AgNPs and **(g)** AgNPs+NAC. Bars: 100 µm (a-d, f), 50 µm (e). *cv* centrilobular vein*; pv* portal vein. The arrow indicates inflammatory cells encasing the portal triad. Values are expressed as mean ± SEM (n=3 animals/group) in comparison to *a* control, *b* NAC, *c* $AgNO_3$, *d* AgNPs+NAC and *e* the AgNPs groups. ***p<0.001 for *a,b,c,d*; ##p<0.01 for *b;* ###p<0.001 for *c,e.* One-way ANOVA plus Tukey post-comparison test.

3.4. NAC modifies the biodistribution and the clearance of AgNPs

After demonstrating that NAC could prevent specific AgNPs toxicities *in vivo*, we performed biodistribution experiments to further investigate the NAC mechanism of action. First, we quantified the silver concentration in important organs of the body 24 h after injection. We found the highest concentration in the liver and, in decreasing order, in the spleen, lung and kidney (Figure 3(a)). *In vivo* studies have demonstrated that nanoparticles usually accumulate in cells of the mononuclear phagocyte system (MPS), which is more prevalent in the liver, spleen, lung, and bone marrow than in the kidney. Once in present in these MPS-containing tissues, the nanoparticles remain there or have protracted elimination (Weaver et al., 2017). The treatment with a single injection of NAC led to an altered silver biodistribution. We found the highest concentration in the kidney and then, in decreasing order, in the spleen, liver and lung, thus indicating interference of NAC with the AgNPs biodistribution dynamics. The comparison of hepatic silver accumulation before and after NAC treatment (AgNPs *vs*. AgNPs+NAC) showed a 3.4-fold decrease (136 ± 11.14 *vs*. 40 ± 3.69 μg/kg, respectively). Consistent with the hepatic decrease in concentration, we found that the renal concentration of AgNPs+NAC-treated rats was about 10 times higher than in rats treated with AgNPs (248.2 ± 21.31 *vs.* 24.46 ± 1.04 μg/kg) 24 h after administration. Although the silver levels were higher in the kidneys of AgNPs+NAC-treated rats, there were no significant changes in markers of renal function such as BUN (Figure 3(b)) and creatinine (Figure 3(c)). Furthermore, histopathological evaluation of the kidney tissues revealed a normal pattern in all groups (Supplementary information, Figure S4). It is well known that changing nanoparticles topography, curvature, surface energy, and imposing immobilized steric barriers can decrease phagocytic recognition (Gustafson et al., 2015) and therefore alter the nanoparticles-cell interactions.

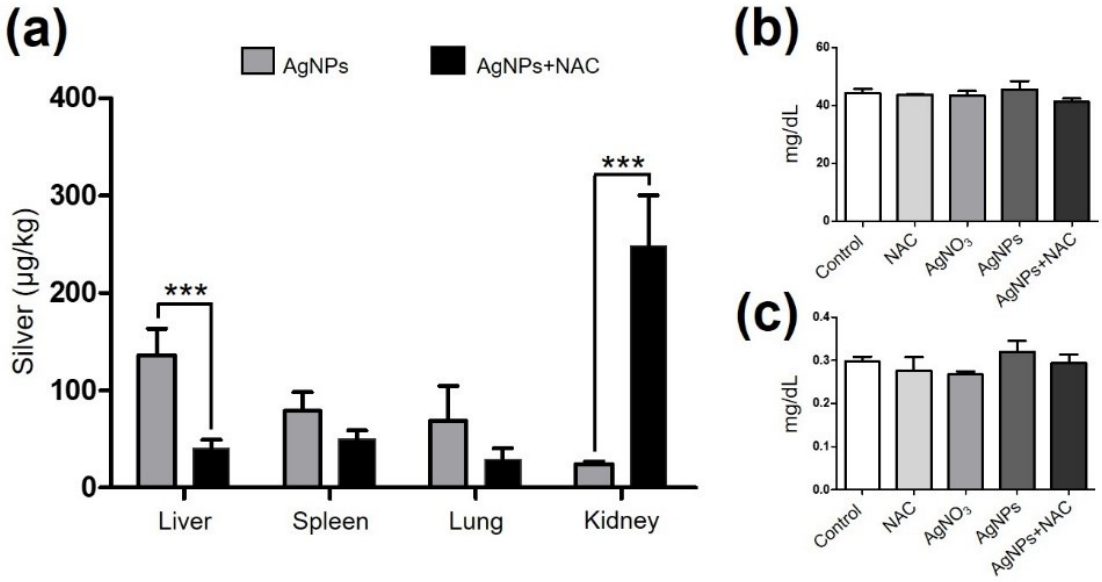

Figure 3. *Comparison of total silver content in rat organs between the AgNPs and AgNPs+NAC groups*. The animals received a single intravenous injection of AgNPs (5 mg/kg), and after 1 h the animals were treated intraperitoneally with NAC (1 g/kg) (Group AgNPs+NAC). Twenty-four hours post-treatment, animals were sacrificed, and organ tissues collected. (a) The silver content of lyophilized liver, spleen, lung, and kidney of AgNPs and AgNPs+NAC groups (n = 3-6 animals/group). (b,c) Serum concentration of renal injury markers (b) blood urea nitrogen and (c) creatinine. (n = 5-7 animals/group). ***p <0.001. Student's *t*-test.

We reasoned that the changes in AgNPs biodistribution induced by NAC treatment may have led to silver excretion through the renal route, preventing its reabsorption and further hepatotoxicity. To assess this possibility, we analyzed the silver concentration in feces and urine. Figure 4(a) presents the total of silver content in urine and feces after 24 h and 48 h of collection. In the AgNPs-treated group, the excretion of silver through urine was low compared to that in feces, suggesting that AgNPs were excreted from the liver through the biliary pathway. Excretion of silver through the fecal route has been confirmed in rodents and rabbits, following oral or intravenous AgNPs administration (Jiménez-Lamana et al., 2014; Lee et al., 2012; Yang et al., 2017). Renal clearance was observed in the animals treated with AgNPs+NAC, suggesting that the silver accumulated in the kidney was eliminated through urine. It has long

been acknowledged that sulfhydryl-containing compounds can chelate metals and that a hydrophilic chelator, such as NAC, can enhance renal excretion (Flora and Pachauri, 2010).

The observed differential NAC-dependent excretion routes may be related to differential bioaccumulation in the hepatic *versus* renal tissue, respectively. To confirm this hypothesis, we evaluated the density of silver accumulated in the liver and kidney after 24 h administration of AgNPs or AgNPs+NAC by AMG. The AMG staining method converts silver ions to a black color in tissue in the presence of an electron donator (Miller et al., 2016). AMG staining of control tissues exhibits no detectable silver deposition in the liver (Figure 4(b)) or kidney parenchyma (Figure 4(c)). However, silver was distributed through all parenchyma with preferential peri-portal accumulation in the AgNPs-treated rats. Peri-portal hepatocytes were also loaded with tiny silver particles. In these regions, Kupffer cells were intensely showed high staining, indicative of intense phagocytosis (Figure 4(d)). For the kidney, silver particle deposition was observed more in the interstices of proximal convoluted segments and also inside the cells of these segments (Figure 4(e)). In contrast, the hepatic deposition of silver was minimal following administration of NAC (Figure 4(f)). Instead, a broad distribution was observed inside the renal glomeruli and into the lumen of proximal tubules. Moreover, a silver deposition markedly occupied the interstices around collecting tubules in the renal medulla (Figure 4(g)) and close to the renal papilla. In agreement with GF-AAS results, the silver concentration was higher in the kidney than in the liver, corroborating its greater excretion in urine.

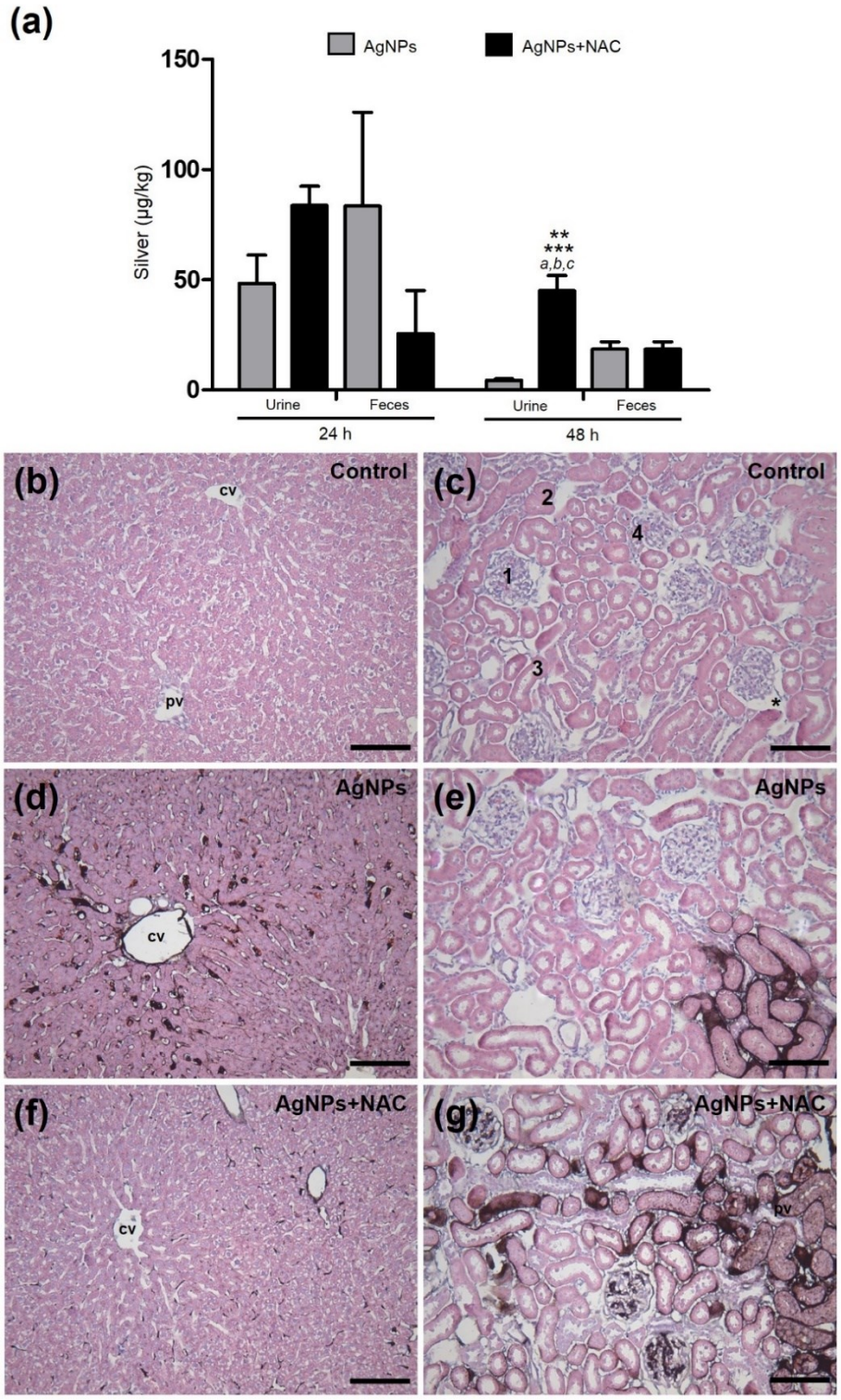

Figure 4. *Comparison of silver excretion after AgNPs and AgNPs+NAC administration*. (**a**) Amount of silver excreted in urine and feces within 24 h and 48 h post-AgNPs administration. (**b**) Representative images from silver-stained (black) sections of rat liver (left panels) and kidney (right panels) 24 h after administration of (**b,c**) 0.9% saline (control), (**d,e**) AgNPs and (**f,g**) AgNPs+NAC. Images were counterstained with Hematoxylin-eosin. Bars = 100 µm. *cv* central vein; *pv* portal vein. *1* Renal glomeruli; *2* proximal tubule; *3* distal tubule; *4* collecting

tubule;*Bowman's space of the renal corpuscle. Values are expressed as mean ± SEM (n=3 animals/group). *a* compared to urine AgNPs 48 h (***p<0.001); *b* compared to feces AgNPs 48 h (**p<0.01); *c* compared to feces AgNPs+NAC 48 h (**p<0.01). One-way ANOVA plus Tukey post-comparison test.

4. Conclusions

Overall, we conclude that thiol-antioxidants, such as NAC, reversed toxic effects of AgNPs, suggesting that NAC could be a potential candidate for early intervention in cases of AgNPs intoxication. Our study also provides insight into the mechanism of AgNPs clearance, demonstrating that NAC treatment led to elimination through renal excretion. We hope that this work will encourage other similar studies towards nanotoxicity antidotes, since the use of nanomaterials is growing exponentially and there are no established treatment protocols in cases of intoxication.

5. Supplementary Information

To confirm the metal-chelating properties of NAC, we performed surface plasmon resonance (SPR) analysis. NAC was added to an AgNPs formulation containing 5% serum bovine albumin (BSA) as a representative protein for assessing interactions with blood proteins.

The SPR peak obtained for AgNPs varies from 410-440 nm (Figure S1(a)). The addition of NAC to the AgNP formulation tends to shift this to smaller peak at a longer wavelength, which indicates aggregation of AgNPs. The aggregation was further confirmed by NTA. The AgNPs were smallest in size with average of 81.0 ± 29.6 nm, when compared to a of size 114.0 ± 52.5 nm in the presence of 10 mM of NAC (Figure S1(b)).

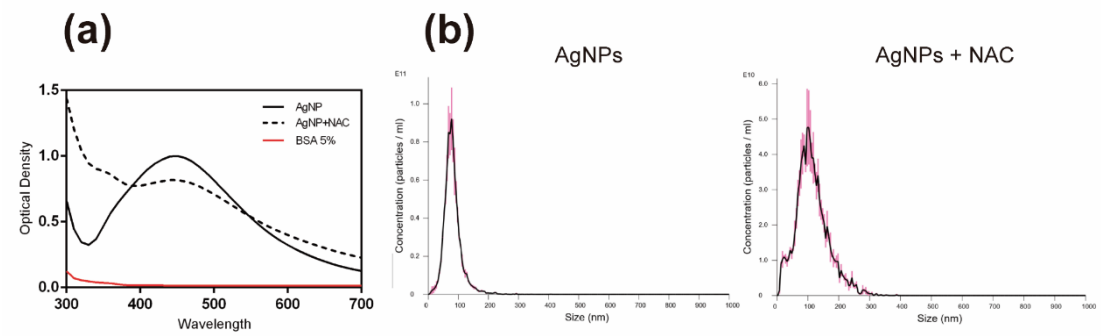

Figure S1. *Effects of N-acetylcysteine (NAC) on physicochemical properties of silver nanoparticles (AgNPs).* (a) Absorption spectra showing the effect of NAC (10 mM) on surface plasmon resonance peak of AgNPs. (b) Size distribution histograms of AgNPs and AgNPs+NAC from NTA.

AgNPs treatment trend to increase both the expression of SOD-1 (Figure S3(a)) and catalase (Figure S3(b)) in liver homogenates while the levels of these enzymes remained undistinguishable from the basal levels for the control, NAC, and $AgNO_3$ groups. Considering the caveat that protein expression levels do not necessarily translate to levels of protein activity, we also measured activities of total SODs, catalase, and GSH in liver homogenates and serum samples, in addition to the concentration of TBARS, as an indicator of lipid peroxidation. Unexpectedly, AgNPs administration resulted in a decrease in SOD ($p<0.05$), catalase ($p<0.01$), and GSH ($p<0.05$) activities in serum compared to the levels of these activities in the controls (Figure S3(c) to S3(e)), whereas an increase was observed in catalase ($p<0.05$) and GSH ($p<0.01$) activities in liver samples (Figure S3(f) to S3(h)). The TBARS were increased in serum (Figure S3(i)) and liver (Figure S3(j)). NAC alone did not affect the activity of the antioxidant enzymes, but this reversed the SOD, catalase, and GSH activities that had been decreased by a single injection of AgNPs one hour before. Alterations in the SOD, catalase and GSH levels of AgNPs-injected rats indicate an adaptive response against the production of ROS and corroborate the upregulation of the proteins seen by immunoblotting. Since the liver is the main producer of such enzymes, we believe that the increased activity of catalase, as well as the GSH content in the AgNPs group, reflects the coping mechanisms of the organism in

fighting the redox dysfunction when insulted by certain ROS reactions. However, the serum showed lower levels of SOD and catalase activity as well as lower GSH levels, which reflected the oxidative stress of the whole system, causing lipid peroxidation in the cells.

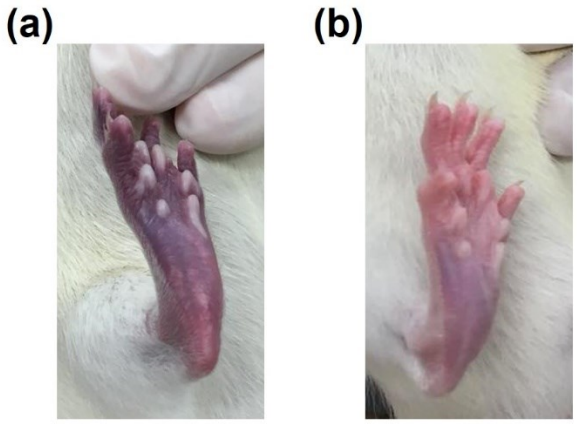

Figure S2. *Gross view of the hind paws after AgNPs administration*. Representative photographs of hind paws from (**a**) AgNPs-treated rat 30 min after i.v. injection. (5 mg/kg) and (**b**) AgNPs+NAC-treated rat 2 h after NAC i.p. injection (1 g/kg).

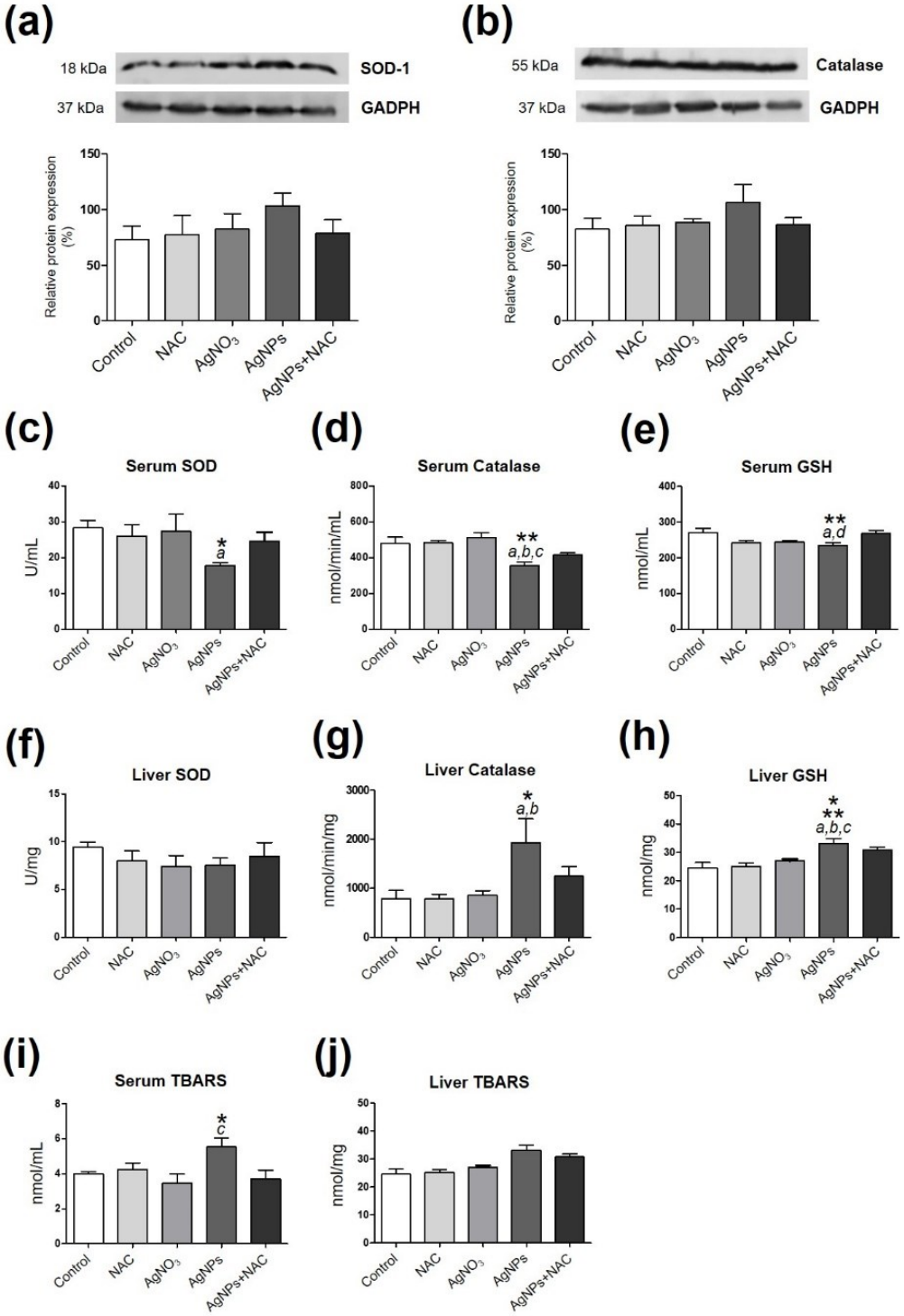

Figure S3. *Markers of oxidative stress and lipid peroxidation in the liver and serum.* Immunoblots of (**a**) superoxide dismutase (SOD-1) and (**b**) catalase in liver tissue lysates. Rats were treated intravenously with 0.9% saline (control), NAC, silver nitrate ($AgNO_3$) and silver nanoparticles (AgNPs) (5 mg/kg). After 1 h, animals treated with AgNPs received an intraperitoneal injection of NAC (1 g/kg). All animals were euthanized 24 h post-treatments. GAPDH was used as loading control. Densitometric values were expressed as a percentage of control (100%) and represent mean ± SEM (n = 4-5 rats/group). Antioxidant enzyme activity

in (**c-e**) serum and (**g-h**) liver samples. Lipid peroxidation measured using thiobarbituric acid-reactive substances (TBARS) in (**i**) serum and (**j**) liver. Values are expressed as mean ± SEM (n=5-8 animals/group) in comparison to *a* control, *b* NAC, *c* $AgNO_3$, *d* AgNPs+NAC, *e* AgNPs+GSH groups. Panel (**c**) *p<0.05 for *a*; Panel (*d*) **p<0.01 for *a,b,c*; Panel (**e**) **p<0.01 for *a,b,d*; Panel (**g**) *p<0.05 for *a,b*; Panel (**h**) **p<0.01 for *a,b*;*p<0.05 for *c*; Panel (**i**) *p<0.05 for *c*. One-way ANOVA plus Tukey post-comparison test.

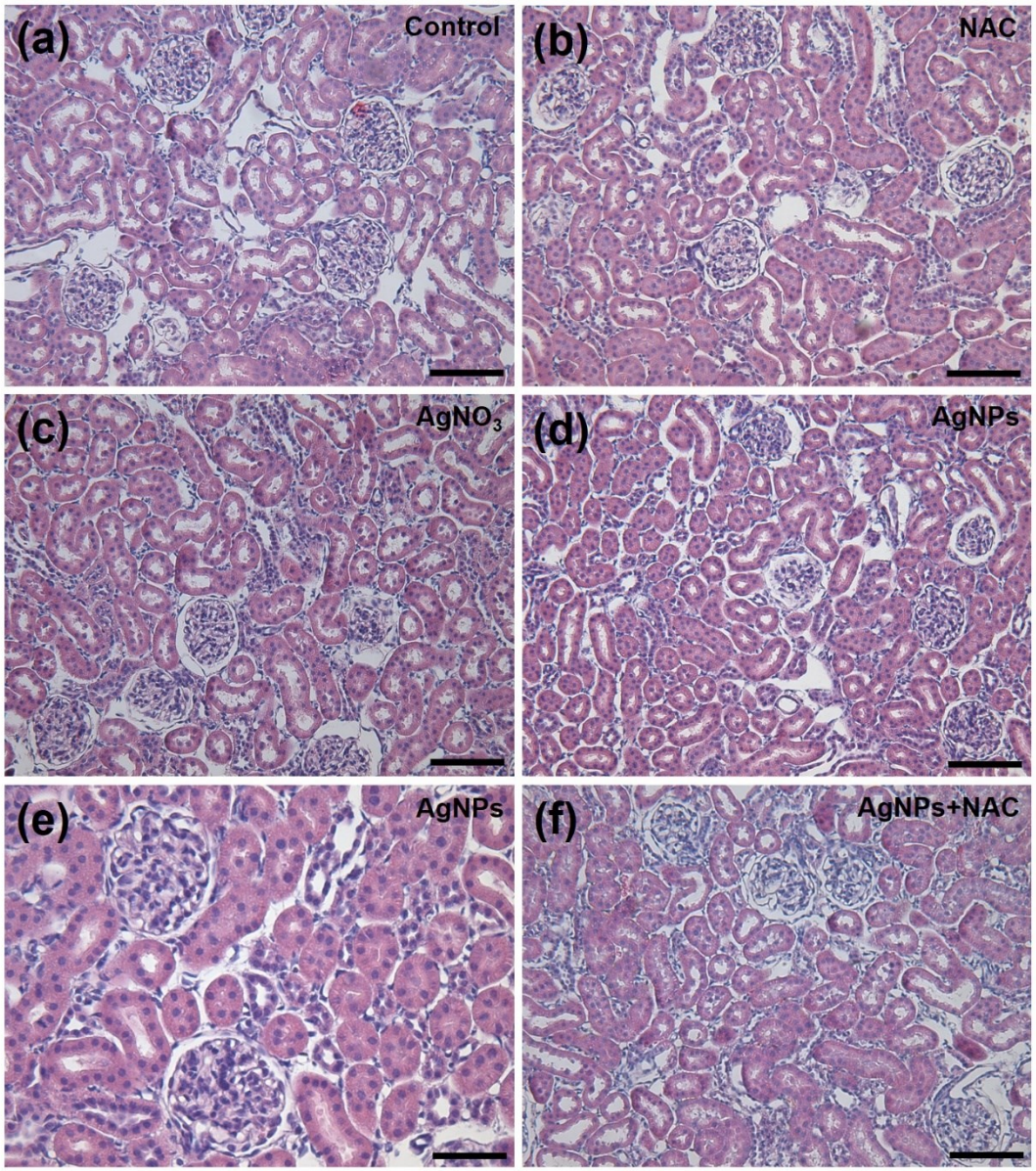

Figure S4. *Histopathological evaluation of AgNPs and NAC treatment of rats.* Representative photomicrographs of the renal parenchyma stained with hematoxylin-eosin after administration of (**a**) 0.9% saline, (**b**) NAC, (**c**) $AgNO_3$, (**d,e**) AgNPs, and (**f**) AgNPs+NAC. Bars = 100 µm for all panels, except for panel (**e**) (50 µm).

CÁPITULO 4 - Aplicação das nanopartículas de prata biossintéticas no tratamento contra o câncer de bexiga

Silver nanoparticles trigger apoptosis in bladder carcinoma cells 5637 and antitumor activity in non-muscle invasive bladder cancer

Luiz Alberto Bandeira Ferreira[1], Fernanda Garcia Fóssa[1], Allan Radaic[1], Nelson Duran[234], Wagner J. Fávaro[3,4], Marcelo Bispo de Jesus[1]

[1]*Nano-cell Interactions Lab.; Department Biochemistry & Tissue Biology, Biology Institute, University of Campinas, Campinas, SP, Brazil* [2]NanoBioss, Institute of Chemistry, University of Campinas, Campinas, SP, Brazil, [3]Institute of Chemistry, BiolChemLab., University of Campinas, Campinas, SP, Brazil, [4]Brazilian National Nanotechnology Laboratory (LNNANO-CNPEM), Campinas, SP, Brazil. [5]Laboratory of Urogenital Carcinogenesis and Immunotherapy, Department of Structural and Functional Biology, University of Campinas, Campinas, SP, Brazil.

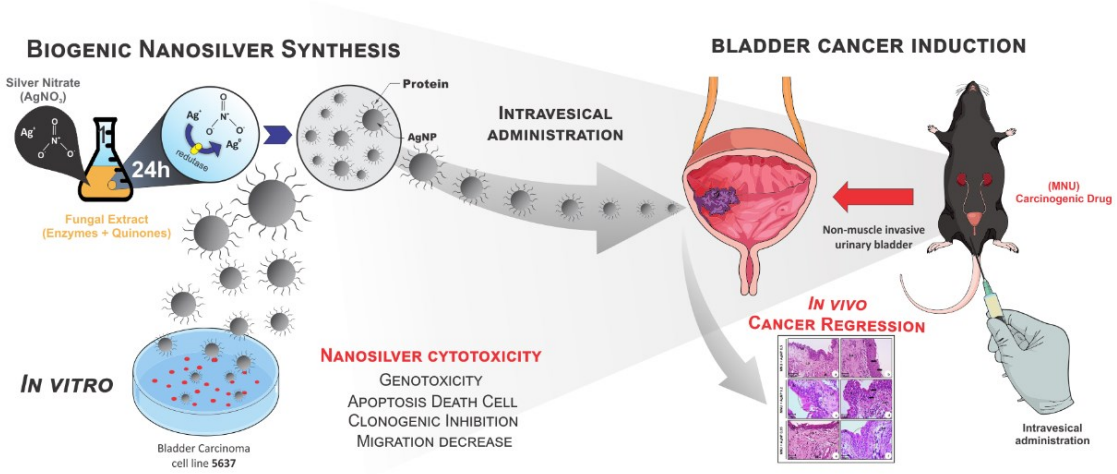

Abstract

Bladder cancer is the fifth most common form of malignancy in the United States, and the treatment and outcomes for patients have not changed in the last decades. An alternative source of therapeutics is the nanomedicine that aims to provide tools to target chemotherapies selectively to cancer cells and enhance their therapeutic efficacy. In this scenario, silver nanoparticles (AgNP) have been used in the treatment of various cancer, mainly because of the antineoplastic activity; however, their use and the molecular mechanisms towards blatter cancer still unexplored. Therefore, this work aims to evaluate in vitro and in vivo the antitumoral mechanisms of biogenic silver nanoparticles synthesized from Fusarium sp. Initially, we determined the cytotoxic profile and cell death molecular mechanism in human bladder carcinoma 5637 cells. The results showed that AgNP induced cytotoxicity in a dose-time dependent manner, and detailed analysis demonstrated the induction of cell death via apoptosis, inhibition in cell migration and proliferation. Next, we evaluated the antitumoral activity of AgNP against non-muscle invasive bladder cancer (NMIBC). Bladder cancer was chemically induced with N-methyl-N-nitrosourea (MNU) on C57BL/6Junib female mice and treated by intravesical route with AgNP concentrations of 0.5, 0.2, and 0.05 mg/mL. The histopathological analyzes showed the treated with AgNP 0.5 group presented 50% of pTa and 50% of pTis, indicating that this treatment was not effective in regressing the neoplastic lesions. MNU + AgNP 0.2 group showed 50% of tumor regression, and 50% of the animals presented flat hyperplasia. Finally, treatment with 0.05 AgNP led to 100% tumor regression, with 50% of the animals showing normal urothelium and 50% showing flat hyperplasia, considering a benign lesion. Overall, these findings demonstrated that AgNP might be a cost-effective alternative and promising candidate for the treatment of bladder cancer.

Keywords: *Biogenic silver nanoparticle, bladder cancer, DNA damage, antitumor activity.*

1. Introduction

Bladder cancer (BC) in the USA is the fourth most incidence tumor in men and the ninth in women, showing high morbidity and mortality rates, potentially lethal disease requiring aggressive treatment, and if left untreated, less than 15% of patients survive within two years. The European Association of Urology considers BC as the eleventh most common cancer diagnosed worldwide and the American Cancer Society reported on 2019 that 80,470 new cases of BC (about 61,700 in men and 18,770 in women) and with 17,670 deaths (American Cancer Society's, 2019; Babjuk et al., 2017). More than 70% of BC is superficial, non-muscle invasive bladder cancer: pTis (flat carcinoma in situ) stage, pTa (papillary carcinoma non-invasive) stage and pT1 (tumor invading mucosa or submucosa of the bladder wall) stage. Unfortunately, despite the prognosis associated with NMIBC (no muscle invasive bladder cancer), almost 50% of patients will experience a recurrence of their disease within 4 years of their initial diagnosis, and 11% will progress to muscle-invasive bladder cancer (MIBC). It is known that the primary treatment for high-grade NMIBC is based on surgery by transurethral resection of bladder tumor (TURBT), followed by intravesical immunotherapy with Bacillus Calmette–Guerin (BCG) (Askeland et al., 2012).

The limited pharmacological and therapeutic options for the treatment of BC together with the high mortality creates a scenario that demands the development of new tools for the BC treatment. Thus, nanotechnology presents a very innovative initiative for the development of such tools, aiming to achieve more efficient and less toxic therapies. Among the most used nanoparticles appears Silver Nanoparticles (AgNP), extensively incorporated in several industrial products due to its broad antimicrobial spectrum. Lately, AgNP has been used for the treatment of various cancers, mainly because of the antineoplastic activity that can induce cancer cell death similar to conventional chemotherapy (Egorova et al., 2016; Ibrahim M, 2015; Lim et al., 2017; Ong et al., 2013). The mechanisms of AgNP antitumor activity is claimed to

be related to the releasing of metallic silver (Ag^0) and silver ions (Ag^+), which can trigger oxidative stress, DNA damage, mitochondrial damage, membrane damage, genotoxicity, resulting in cell death by necrosis or apoptosis (Ishida, 2017; Ong et al., 2013; Satapathy et al., 2013).

An alternative for improving and increasing nanoparticle the cytotoxicity action and coloidal stability is biosynthesis, which uses bacteria, fungi and plants for podruction of nanoparticles (Durán et al., 2005; Kowshik et al., 2003, Sintubin et al., 2009, Krishnaraj et al., 2010). The method consists of the chemical reduction by inorganic or organic reducing agents. Biosynthesis has the advantages of producing unique characteristic particles with proteins present on the surface. These proteins act similarly as surfactants, preventing the collision between particles, reducing aggregation and precipitation (Durán et al., 2016, 2005). In addition, proteins on the surface of silver nanoparticles may bring about mechanisms of toxicity of the diversified particles, altering pathways of endocytosis or specific mechanisms of cell death, or even acting as immunomodulators, favoring recognition by defense cells (Durán et al., 2015).

Therefore, this study establishes the use of biosynthetic AgNP *in vitro* and *in vivo* against bladder cancer. The activity antitumor of nanoparticles obtained through silver biomass of the *Fusarium oxysporum* was evaluated in bladder carcinoma cell line 5637, regarding the cytotoxicity, molecular mechanism of cell death, and inhibition of cell migration and proliferation. After the *in vitro* mechanisms being elucidated, this study evaluated the efficacy of AgNP *in vivo* against the NMIBC chemically induced in female mice of the C57BL/6 lineage by intravesical administration.

2. Materials and Methods

2.1. Nanoparticle synthesis

Biosynthesis of AgNP was obtained from the reaction with reductases enzymes and quinones contained in *Fusarium oxysporum* filtrate. The fungal prove ESALQ-USP Genetic and Molecular Biology Laboratory Piracicaba, S.P., Brazil, were incubated at 28°C in Petri dishes with a medium containing malt extract 2% and yeast extract 0.5% for seven days. After the fungus growth, approximated 10 g of biomass was taken in a conical flask containing 100 mL of distilled water, kept for 72 h at 28 ºC and then filtration separated the aqueous solution components. In fungal filtrated was added $AgNO_3$ (10^{-3} M) and kept for several hours at 28 °C. Metallic silver production (Ag^o) was followed by absorption measured in a UV-Vis at 300-700 nm using microplate reader Cytation 5 (Biotek Instruments, USA). Silver concentrations were measured by inductively coupled plasma mass spectrometry (ICP-MS) using Optima 5300DV (PerkinElmer, USA) (Andrade et al., 2017; Durán et al., 2016, 2005).

2.2. Cell Culture

Homo sapiens urinary bladder grade II (5637, BCRJ code: 0026) were obtained from Cell Bank of Rio de Janeiro (BCRJ, Brazil) and cultured as a monolayer in RPMI-1640 medium modified to contain 2 mM L-glutamine, 10 mM HEPES, 1 mM sodium pyruvate, fetal bovine serum to a final concentration of 10% and 1% penicillin and streptomycin. The cell line was cultured in a humidified incubator with 5% CO_2 at 37 °C. The most experiments were performed in the cells were plated at the density of 1.5 x 10^4 cell/well for 96-well plate and 1.0 x 10^5 cell/well for 12-well plate and incubated overnight. All experiments were conducted in 1-10 cell passage number.

2.3. MTT assay

5637 cells were seeded into 96-well plates at a density of 1.5 x 10^4 cells per well in 100 µL and kept under 5% CO2 at 37 °C overnight. Next day, cells were treated with increasing concentrations of AgNP (1-50 µM) diluted in serum-free medium at 37 °C. After 24 h, the medium was replaced by 100 µL of 0.5 mg/mL (3-(4,5-dimethylthiazol-2-yl)-2,5-diphenyltetrazolium bromide) tetrazolium (MTT) solution (Sigma-Aldrich, USA) diluted in serum-free RMPI medium. After 2 hours of incubation at 37 °C, the medium was replaced with 100 µL of DMSO to dissolve the formazan crystals. Finally, the plates were shaken for 10 minutes and the absorbance was determined by the microplate reader Cytation 5 (Biotek Instruments, USA) at λ = 570 nm.

2.4. Calcein/Hoechst/PI cell viability assay

5637 cells were seeded into 96-well plates at a density of 1.5 x 10^4 cells per well in 100 µL and kept under 5% CO_2 at 37 °C overnight. Cells were treated with increasing concentrations of AgNP (1-50 µM) diluted in serum-free RMPI medium at 37 °C. After 24 h, the medium was replaced with 100 µL of FluoroBrite DMEM Media (Thermo Fisher Scientific, USA) containing Calcein-AM (1 µM, Thermo Fisher Scientific, USA), Hoechst 33342 (1 µM, Sigma-Aldrich, USA), and Propidium Iodide (PI) (1 µM, Abcam, UK). After 30 minutes of incubation at 37 °C, images were acquired under GFP, DAPI, and PI filters with the objective of 10x using the image multi-mode reader of Cytation 5 (Biotek Instruments, USA). Hoechst-nuclei were used to calculate the total cells, Calcein-positive cells were used to calculate viable cells, and PI-nuclei were used to calculate dead cells. Cells were counted using the Gen5 software (Biotek, Winooski, VT, USA). Finally, viability was estimated using Calcein fluorescence (ex/em ~492/517 nm). Cell viability was normalized to untreated control and used for the construction of concentration-response curves.

2.5. TUNNEL immunostaining

5637 cells were seeded onto 18-mm sterile glass coverslips in 24-well plates at a density of 100 cells/well in 0.5 mL and kept under 5% CO_2 at 37 °C overnight. Next day, cells were treated with AgNP (IC_{50}) for 3h, 6h, and 24h. After treatment, cells were washed twice times with PBS and fixed with 4% paraformaldehyde for 30 min. Next, cells were permeabilized with 0.2% Triton-X-100 in PBS for 10 min. The Terminal deoxynucleotidyltransferase end immunostaining (TUNEL) was performed following the manufacturer's instructions, using the Click-iT TUNEL Alexa Fluor Imaging Assay kit (Molecular Probes, Invitrogen). Cell nuclei were stained with 1 µg/ml Hoechst 33258 in PBS for 30 min at room temperature. Images were acquired using Cytation™ Cell Imaging (BioTek Instruments, Inc., Winooski, VT, USA) with Olympus objective of 10x under GFP and DAPI filters. Total GFP fluorescence was measured by Gen5 software (Biotek, Winooski, VT, USA). Doxorubicin-treated (3.5 µM for 24h) cells were used as a positive control.

2.6. Caspase-3 Confocal Microscopy

5637 cells were seeded onto 13-mm sterile glass coverslips in 12-well plates at a density of 1.0 x 10^5 cells/well in 2 mL and kept under 5% CO_2 at 37 °C overnight. Next day, cells were treated with AgNP (IC_{50}) for 3h, 6h, and 24h. After treatment, cells were washed twice times with PBS and fixed with 4% paraformaldehyde for 30 min. Next, cells were permeabilized with 0.2% Triton-X/PBS for 2 minutes and blocked with 10% FBS/PBS. Next, cells were stained with primary antibody Cleaved Caspase-3 (Asp175) (5A1E) Rabbit mAb (Cell Signaling Technology) at dilution 1:100 in 10% FBS/PBS for 60 minutes. Finally, the cells were stained with secondary antibody Alexa 488 anti-Rabbit (Molecular Probes) and nuclei were counterstained with DRAQ-5 1:1000 (BioStatus Limited) for 30 minutes. The coverslips were mounted on glass slides using a drop of Dako mounting medium (Agilent

Dako). Confocal fluorescence microscopy was performed with confocal laser scanning microscopy (Leica, Solms, Germany) in the objective of ×20 and the images analyzed using FIJI (FIJI version 1.52k, http://fiji.sc).

2.7. Electrophoresis

Aliquots of 1 µg of pEGFP-N1 plasmid (Clonetech, Palo Alto) was exposed to 1 to 40µg/mL of bio-AgNP for 1 hour in TE buffer solution. Then, the solution was transferred to agarose gel (1.3%) stained with ethidium bromide and run at 50 V for 1 h. The gel was fotodocumented using the Gel Doc XR+ gel documentation system (Bio-Rad, USA) and analyzed using Fiji software.

2.8. Plasmid Integrity Assay

The pDNA integrity upon the incubation with AgNP was assessed by agarose gel assay. The reaction mixture, containing 1 µg of pEGFP-N1 plasmid (Clonetech, Palo Alto), was exposed to increasing concentrations of AgNP (1 to 40µg/mL) for 1 hour in TE buffer solution. Then, the mixture was transferred to 1.3% (w/v) agarose gel, stained with ethidium bromide and run at 50 V for 1 h. The gel was fotodocumented using the Gel Doc XR+ gel documentation system (Bio-Rad, USA) and analyzed using ImageJ software.

2.9. DNA damage: γ-H2AX phosphorylation

5637 cells were seeded onto 18-mm sterile glass coverslips in 12-well plates at a density of 10^5 cells/well in 1 mL and kept under 5% CO2 at 37 °C overnight. Next day, complete RPMI 1640 medium was replaced by incomplete medium for fetal bovine serum (FBS) starvation. After 24h, the cells were treated with AgNP (IC_{50}) during 1h, 3h, 6h, and 24h. For DNA damage positive control, cells were treated with hydrogen peroxide (Amresco) at 100 µM for 1h. After treatment, cells were fixed with 4% paraformaldehyde (Sigma-Aldrich),

permeabilized with 0.1% Triton-X/PBS and blocked with 10% FBS/PBS. Next, cells were stained with conjugated primary antibody Alexa Fluor® 488 Mouse anti-H2AX (pS139) (BD Biosciences) at dilution 1:200 in 10% FBS/PBS and the nuclei were counterstained with DAPI 1:1000 (Cell Biolabs, ref# 112002). The coverslips were mounted on glass slides using a drop of Dako mounting medium (Agilent Dako). Images were acquired using a CytationTM Cell Imaging Multi-Mode Reader (BioTek Instruments, Inc., Winooski, VT, USA) with Olympus 10x/0.3 phase objective Plan Fluorite, using a digital camera with associated software Gen 5.03.

The analysis of γ-H2AX was performed using CellProfiler 2.2.0 (Kalyanaraman et al., 2012). The DAPI (for nuclei) and GFP (for γ-H2AX) images were acquired with 5 images per treatment, around 150 cells per image. Data were analyzed creating a mask from the nucleus using an intensity threshold strategy. Then, the mean intensity of the pixels in the image of γ-H2AX was measured only from areas enclosed by the nuclei object.

2.10. Migration arrest in the presence of AgNP

5637 cells were seeded into 12-well plates at a density of 1 x 10^5 per well in 1 mL and kept under 5% CO2 at 37 °C overnight. Next day, complete RPMI 1640 medium was replaced by incomplete medium for FBS starvation for 24h. Serum-starved cells were treated with AgNP (IC25) for 6h. After the treatment, the scratch was made with a pipette tip (p200) and washed with PBS to remove floating cells. Then, complete RPMI 1640 medium was added, and phase contrast images were acquired every 15 minutes for 16 h using CytationTM Cell Imaging Multi-Mode Reader (BioTek Instruments, Inc., Winooski, VT, USA) with Olympus 10x/0.3 phase objective Plan Fluorite, using a digital camera with associated software Gen 5.03.

2.11. Clonogenic survival assay

Confluent T25 flasks containing 5637 cells were treated with AgNP (IC_{25} and IC_{50}) and incubated for 24 hours. Next day, cells were trypsinized and the viable cells (counted by trypan blue) plated on 6 well (10^3 cells/well). Cells were incubated in normal conditions of

culture. After 14 days, colonies were fixed with 4% paraformaldehyde (Sigma-Aldrich) and stained with 0.5% crystal violet (Sigma-Aldrich). Images were acquired using a Cytation™ Cell Imaging Multi-Mode Reader (BioTek Instruments, Inc., Winooski, VT, USA) with Olympus 4x objective imaging the entire 6 wells in a 14x19 montage. The area of the colonies was measured by BioTek Gen 5.03 Software and normalized to the untreated control:

Normalized area = (area of colonies in AgNP-pretreatment/area of colonies untreated cells) × 100.

2.12. NMIBC Induction Protocol and Treatment

Twenty-five female C57BL/6 mice, all 7 weeks old, were obtained from the Multidisciplinary Center for Biological Investigation at the University of Campinas (CEMIB-UNICAMP). They were housed in a temperature-controlled room under a regular 12 h light/dark cycle (22 ± 2 °C) with ad libitum water and food (Nuvital, Curitiba, PR, Brazil) (n=5 animals/plastic cage). After one week of acclimatization, animals were randomly allocated into the following groups (n= 5/group): (i) Control (0.9 % saline solution), (ii) Cancer (N-methyl-N-nitrosourea (MNU)), (iii) Cancer + 0.5 mg/mL AgNP, (iv) Cancer + 0.2 mg/mL AgNP and (v) Cancer + 0.05 mg/mL AgNP.

Prior to intravesical catheterisation with a 22-gauge angiocatheter, the rats were anesthetized with 10% ketamine (60mg/kg, i.m.; Vibra®, Roseira, SP, Brazil) and 2% xylazine (5mg/kg, i.m.; Vibra®, Roseira, SP, Brazil). The animals remained anesthetized for approximately 45 min after catheterization to prevent spontaneous micturition. Thus, the NMIBC was carried out in 20 mices that received N-methyl-N-nitrosourea (MNU, 1.5 mg of MNU dissolved in 0.3 mL of 1 M Sodium citrate (pH 6.0) (Sigma-Aldrich, St. Louis, MO, USA)) intravesically every other weeks, totaling 3 doses (Garcia et al., 2016). Two weeks after the last dose of MNU, the respective groups were treated weekly with intravesical instillation

of AgNP (0.05, 0.2 and 0.5 mg/mL) during 4 consecutive weeks. After the treatment period, the animals were euthanized through anesthesia followed by cervical dislocation, and the urinary bladders were collected and submitted to histopathological analyzes.

All procedures followed the Brazilian National Council to Control Animal Experimentation (CONCEA) and were approved by the Institutional Committee for Ethics in Animal Use (CEUA/UNICAMP, protocol no. 4017-1).

2.13. NMIBC: Histopathological Analysis

Samples of urinary bladders (n = 5 per group) were processed as previously described. Subsequently, 5-µm thick sections were cut on a rotary microtome (Slee CUT5062 RM 2165; Slee Mainz, Mainz, Germany), stained with hematoxylin-eosin and photographed with a Leica DM2500 photomicroscope (Leica, Munich, Germany). A senior uropathologist analyzed the urinary bladder lesions based on the criteria of the Health/World International Society of Urological Pathology Organization (Epstein et al., 1998). In the present work, malignant lesions were found and divided as follow: High-grade intraurothelial neoplasia – flat carcinoma in situ (pTis), Low-grade papillary carcinoma in situ (pTa), High-grade pTa, Tumor invading mucosa or submucosa of the bladder wall (pT1).

3. Results and Discussion

3.1. AgNP cytotoxicity is time and concentration dependent in 5637 cells

To evaluate the antitumor activity of AgNP, first, we determined the half-maximal inhibitory concentration (IC_{50}) and the incubation time used next to investigate the molecular mechanisms of cell death in 5637 cells. For determining the IC_{50}, it was used two approaches MTT assay and Calcein/Hoechst/PI assay. These methods are based on different underlying mechanisms, which together with the appropriate controls, increases the robustness and reduce artifacts during the experiments (Azhdarzadeh et al., 2015; de Jesus and Kapila, 2014; Rösslein

et al., 2015). Figure 1(a) shows that both cytotoxicity assays reported similar dose–response relationship and IC_{50} values: 10.57 μM for MTT, 9.79 μM for Calcein, and 13.72 μM for PI. Next, it was evaluated the cytotoxicity of AgNP within 24 h (Figure 1-B); and no difference was found between 6 h and 24 h of treatment (24 h vs. 6 h *p>0.05). In addition, the influence of AgNP treatment on cell morphology is illustrated in Figure 1-C. The representative images of Calcein/Hoechst/PI assay show that control cells are mostly attached and depicted a cuboidal epithelial-like morphology; upon AgNP treatment, the cell number was reduced and it was observe detached and morphologically altered cells (cell shrinkage and rounding). It was also observed that calcein-negative cells, indicating no viable cells, and nuclei positive for PI, indicating cell death. Therefore, AgNP cytotoxicity is dose and time-dependent under the conditions tested and cell death was significantly observed during the experiments.

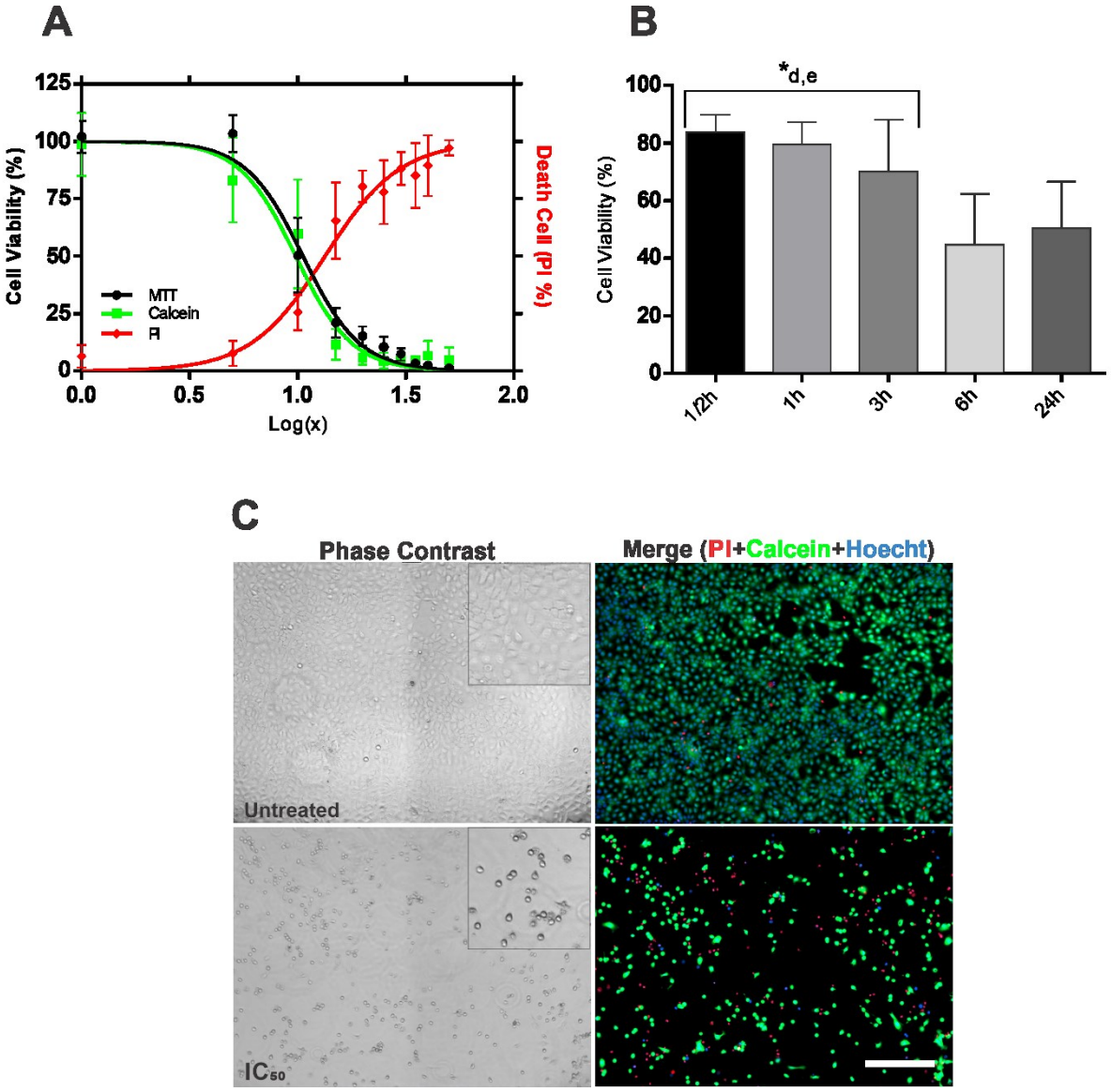

Figure 1. *Biogenic AgNP cytotoxicity in urinary bladder carcinoma 5636 cell.* (A) Cells were incubated with increasing concentrations of AgNP (1-50 µM) for 24 h. Cell viability was assessed by MTT formazan absorbance (ex. 570 nm) and Calcein fluorescence (ex/em ~492/517nm). Cytotoxicity evaluation was obtained by dividing the number of PI-positive nuclei by the total nuclei labeled with Hoechst 33342. (B) Cytotoxicity of the AgNP evaluated within 24 h; cells were treated with AgNP IC50 for 1 h, 3 h, 6h, and 24 h. The results were normalized to the untreated group (100% viable cells). Each value represents the mean ± S.D. of 3 independent experiments. For statistical tests, $p < 0.05$ for ANOVA was used, followed by Tukey's test (24 h vs. 30 min, 1 h, 3 h, 6 h). (C) Representative images of cells untreated and treated with IC50, acquired in phase contrast, PI (in red), Calcein (in green), and Hoechst (in blue). Scale bar: 200 µm

3.2. Biogenic AgNP trigger apoptosis in 5637 cells

Next, we decide to investigate the underlying mechanisms of AgNP cell death induction in 5637 cells. Part of the cytotoxicity is determined by the physicochemical characteristics of nanoparticles (*i.e.,* size, shape, and surface properties such as corona protein) (de Lima et al., 2012; Petros and DeSimone, 2010). A large number of studies describes apoptosis as the main pathway of cell death by silver nanoparticles (Cheng et al., 2013; Hsin et al., 2008; Locht et al., 2011). A large However, biogenic nanoparticles may have particular cytotoxicity mechanisms, as the protein corona from the production process may affect the cell internalization and by itself play some cytotoxicity effects (Durán et al., 2015; Mirshafiee et al., 2013; Safi et al., 2011). Hence, we started evaluating DNA fragmentation by TUNEL analysis, which is an apoptosis hallmark (Figure 2). The results showed in Figure 2A – II successfully report 5637 cells labeled with fluorescein dUTP after 24h incubation with apoptosis-inducing agent doxorubicin, used as a positive control. Cells treated for 6h (figure 2A - IV) and 24h (figure 2A - V) with AgNP also reported a significant increase of dUTP fluorescence, meaning the induction of DNA fragmentation (* $p < 0.05$, Figure 2B).

In addition to TUNEL assay, we confirmed the apoptosis through the evaluation of caspase-3 activation by immunostaining of Cleaved Caspase-3. Figure 2-C show the representative images of Cleaved Caspase-3 evaluation by confocal microscopy. Positive control, treated with Doxorubicin, showed a significant increase in Cleaved Caspase-3 levels compared to untreated cells. Cells treated with AgNP displayed a gradual increase in the cleaved caspase-3 levels in 1h, 3h, and 6h. Activation of caspase- 3 results in the cleavage of ICAD (inhibitor of caspase-activated DNAse) and translocation of CAD (caspase-activated DNAse) to the nucleus ultimately resulting in DNA fragmentation (Arora et al., 2008; Wolf et al., 1999).

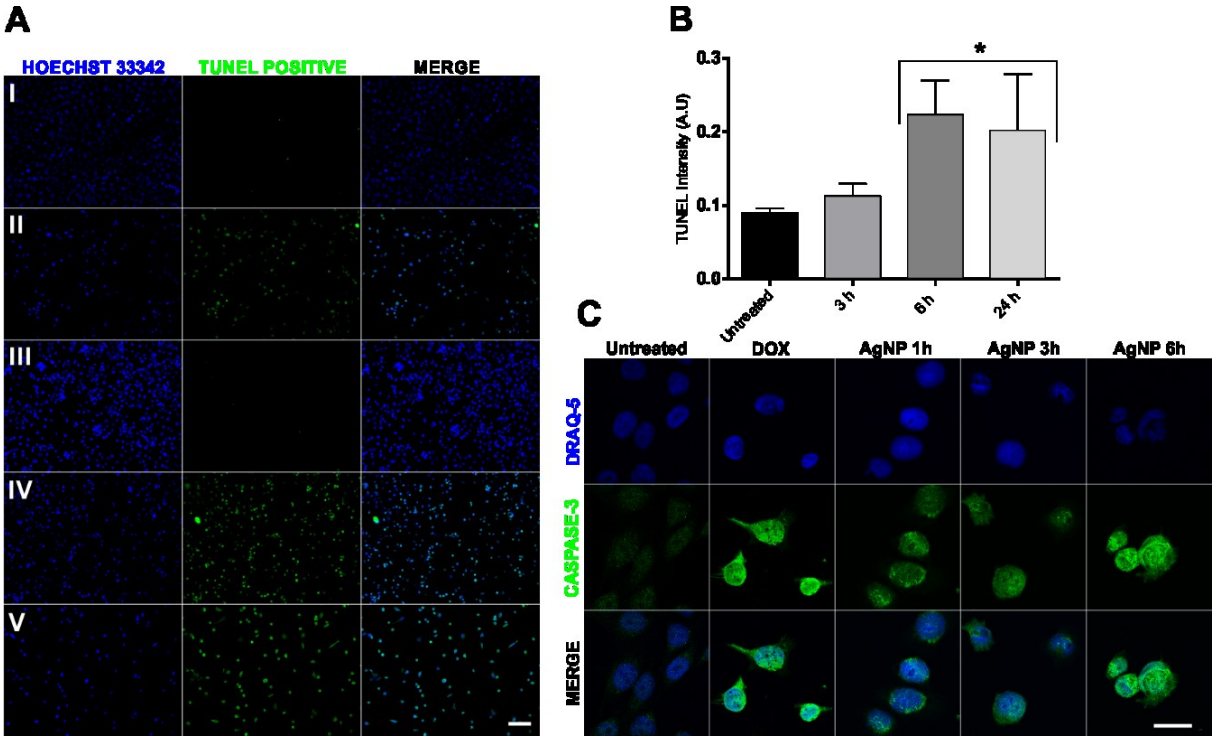

Figure 2. *Apoptosis induction by bio-AgNP in time dependent.* **A –** Cells were exposed to IC_{50} AgNP for 3, 6, and 24 hours. Cells containing the terminal deoxynucleotidyl transferase dUTP nick end-labeling were labeled with Click-iT TUNEL Alexa Fluor Imaging Assay kit (Molecular Probes, Invitrogen) following the manufacturer's instructions. **(A)** Hoechst 33342 (blue) and TUNEL (green) double-positive cells are shown. Groups: Untreated; Doxorubicin; AgNP 3 h; AgNP 6h; AgNP 24h. The images were obtained with fluorescence microscopy (Cytation 5) in the objective of ×10, scale bar of 50 µm. **(B) –** Fluorescence intensity (A.U.) of images labeled with Click-iT TUNEL Alexa Fluor 488 was quantitated by BioTek software Gen5 (Cytation 5). For statistical tests, $p < 0.05$ for ANOVA was used, followed by Tukey's test (untreated vs. 3 h, 6 h, and 24 h). **(C)** – Activation of Caspase-3 in 5637 cells in response to AgNP exposure. Cells were treated for 1 h, 3 h, 6 h with AgNP IC_{50} and for 24 h with Doxorubicin (apoptosis positive control). After the treatment, cells were fixed with PFA 4%, immunostained with primary antibody cleaved Caspase-3 (Asp175) in green, and counterstained with DRAQ5 (nuclei, blue). Confocal images were obtained in the objective of ×63 with and AIRY fixed in 1. Scale bar of 25 µm.

3.3. AgNP treatment induces DNA damage and γ-H2AX responsein 5637 cells

Genotoxicity is one mechanism described for AgNP inducing apoptosis. The DNA damage could lead to p53 protein response, triggering cell cycle arrest to provide time for the damage to be repaired (Ahamed et al., 2008; Eom and Choi, 2010; Hackenberg et al., 2011). To investigate the possibility of AgNP-induced DNA damage, we evaluated the response to DNA Double-Strand Breaks (DBS) by phosphorylation of the histone γ-H2AX. The analyze of

γ-H2AX response show substantially increase in mean intensity occurs with 6 and 24 hours of treatment that is comparable to the positive control for DNA damage ($p < 0.05$ no difference from Control H_2O_2) (Figure 3, A and B). As previously reported, other types of AgNP (polyvinyl alcohol capped AgNP) can induce phosphorylation of γ-H2AX in cell lines like breast cancer MCF-7 cells (Lim et al., 2017). In vitro experiments showed that when AgNPs are internalized by cells, Ag ions induce formation of ROS (Reactive Oxygen Species), generating damage molecules that leads to DSB (Zhao et al., 2016). Upon DSB induction, γ-H2AX is activated, and function as a monitor do DNA damage (Ivashkevich et al., 2012). The ROS has been accounted for great part of the toxic effect of AgNP; thus, much less attention has been was devoted to the direct effect of the AgNP.

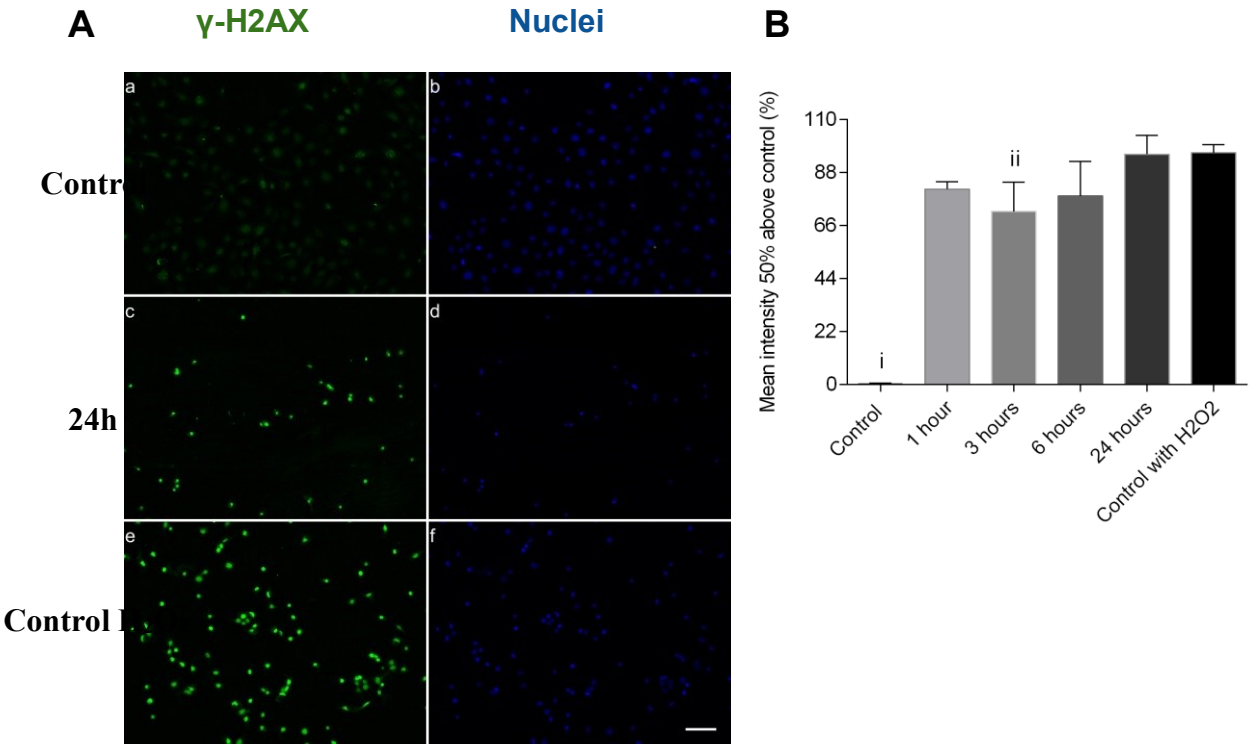

Figure 3. *Intensity of γ-H2AX in the nucleus of 5637 cells during AgNP treatment*. After serum starvation for 24 h for cell cycle synchronization, cells were treated with AgNP IC_{50} during 1 h, 3 h, 6 h and 24 h. After the treatment, cells were fixed with PFA 4% and labeled with anti-H2AX (pS139) Alexa Fluor® 488 (phosphorylated γ-H2AX, in green) and DAPI (nuclei, in blue). **(A)** Representative images of phosphorylated γ-H2AX in the nucleus of control cells (a and b), 24 hours before treatment (c and d) and positive control with 100 µM of H2O2 (e and f). Scale bar: 200 µM. **(B)** Mean Intensity of pixels of phosphorylated γ-H2AX located in the

nucleus of treated cells after 1 h, 3 h, 6 h and 24 h. The value of mean intensity is 50% above the mean intensity of control cells. Each value represents average ± S.D. of two independent experiments (n = 2), couting around 1500 cells per treatment. i = Control vs 1, 3, 6, 24 hours and Control H_2O_2; ii = Control H2O2 vs 3 hours. $p < 0.05$ significative difference by ANOVA followed by Tukey's test

After detecting γ-H2AX phosphorylation in early stages (within 6h) of treatment with AgNP, we reasoned that the DNA damage could be mediated by direct interaction with AgNP or Ag^+ ions. To assess such possibility, we incubated 1 µg of pEGFP-N1 plasmid with increasing concentrations of AgNP for 1 hour. After that, we evaluated the plasmid integrity in an agarose gel, the significant amount of DNA detected decreased upon incubation with AgNP above 5 µg/mL. Surprisingly, even low concentrations of AgNP compared with the IC_{50} (10 µM, approximated ~1µg/mL of Ag) was sufficient to degrade DNA within 1 hour of incubation (Figure 4). In summary, our results confirm the DNA double strand breakage and direct DNA degradation in human bladder carcinoma cells that suggesting cell death by apoptosis. We show here that a biogenic AgNP can induce DNA damage in human bladder carcinoma cells.

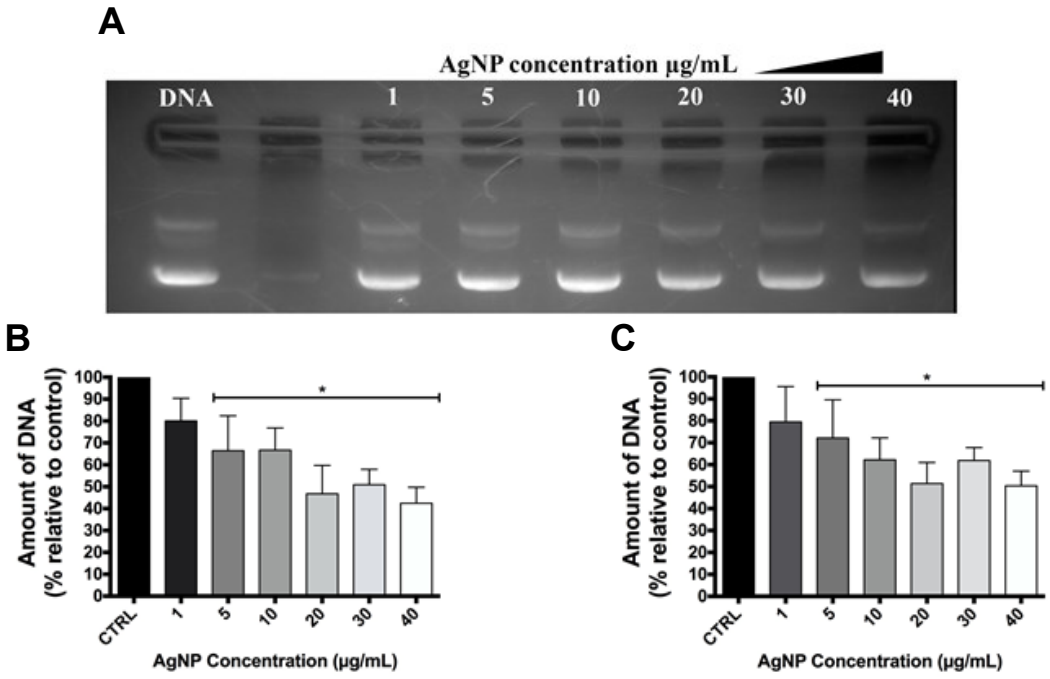

Figure 4. *DNA degradation upon exposure to AgNP.* **(A)** Representative image of the agarose gel obtained; **(B)** semi-quantification of the nicked DNA bands (upper band) and **C**) semi-quantification of the supercoiled DNA Bands (bottom band), both percentages are relative to each control. *means significative difference ($p<0.05$) between the sample and control (CTRL).

3.4. In vitro antitumoral activity of AgNP

After shedding light on the molecular mechanisms of the AgNP cell death in 5637 cells, we decided to investigate the therapeutic usefulness of the AgNP for bladder cancer treatment. Two cellular events are closely related to tumor aggressiveness, the capacity of the cell migration, and proliferation ability. Hence, we performed the cell migration assay and the clonogenic survival assay (Figure 5). Cell migration assay showed that non-treated cells close the gap within 16 h (Figure 5, A and B), while AgNP-treated (IC_{25}) cells were significantly slower; moreover, treated cells were not capable of closing the gap during the experiment (16 h). In addition, clonogenic survival assay was performed using cells pre-treated with AgNP and replated onto the dishes, without nanoparticles, to evaluate the effect of this exposure on colony formation (Figure 5, C and D). The results show that pre-incubation with the IC_{50} significantly decreased clonogenic survival; in contrast, IC_{25} pre-incubation had little effect on clonogenic survival (Figure 5D). These results support the biogenic AgNP anticancer activity by mitigating the potential of individual cells to form a colony.

Altogether, these results show that AgNP delay tumor progression, the lasting effects observed on clonogenic survival assay could be linked with the DNA damaged demonstrated above. Genotoxicity is crucial in the decay of tumor cell proliferation, as observed in other AgNP dose-dependent studies with Sub-G1 formation, increased DNA degradation by comet assay and chromosomal damage (Bendale et al., 2017; Nymark et al., 2013; Souza et al., 2016). DNA damage directly influences the cellular division and, consequently, the reduction of clonogenesis. As previously mentioned, AgNP damage is often related to the action of oxidative stress on nucleic acids. However, another hypothesis would be the binding of Ag + with nitrogenous bases such as Guanine and Cytosine, which could interfere in the process of transcription and cellular division (Kain et al., 2012; Rai et al., 2012; Swasey et al., 2015).

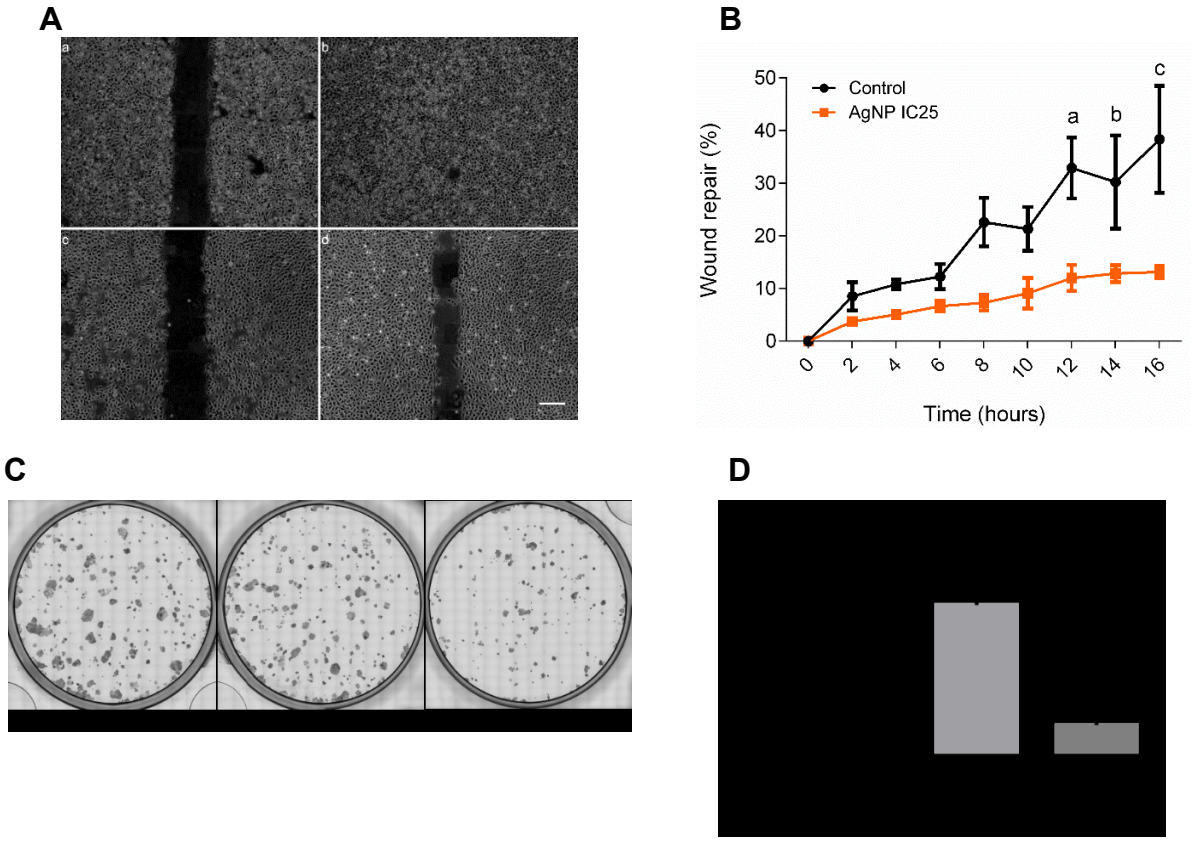

Figure 5. *Effects of AgNP on tumor progression evaluated in 5637 cells. Migration assay:* After 24 hours of serum starvation, cells were treated with AgNP (IC_{25}) for 6 h. Next, the gap was created with p200 tip and cells were imaged every 15 minutes using Cytation™ 5. **(A)** Representative images of the migration assay. Non-treated cells at time 0h (a) and 16h (b); AgNP-treated cells at time 0h (c) and 16h (d). Scale bar = 200 µm **(B)** was normalized by the area without cells at time zero. Each value represents the average ± S.D of three independents experiments (n = 2) **a** = 12h Control vs 12h IC_{25}, **b** = 14h Control vs 14h IC_{25} and **c** = 16h Control vs 16h IC_{25}. **a, b and c** = $p < 0,05$ significant difference by ANOVA followed by Tukey's test. **(C)** Reduction of colonies formation by AgNP. *Clonogenic survival assay*: Bladder cells cancer was incubated with silver nanoparticles for 24 h. After this, 10^3 the lives cells (counted by trypan blue) was incubated for 14 days, and the colonies formations were analyzed. The images of wells were obtained with objective 4x (14 x 19 images), and the area of colonies was measured by BioTek Gen5 Software. **(D)** Normalized colony area. Area of cell colonies labeled by crystal violet was quantitated by BioTek software Gen5 (Cytation 5). For statistical tests, $p < 0.05$ for ANOVA was used, followed by Tukey's test (untreated vs. IC_{25} and IC_{50}).

3.5. In vivo antitumor activity

Many clinical trials have been conducted to improve therapeutic efficacy, most of them aiming to improve the life quality of patients suffering from high-grade NMIBC. From a therapeutic perspective, little is known about the use of biogenic silver nanoparticles for bladder cancer treatment. The promising results found in the anti-tumor activity studies on cultures of

bladders cells 5637; *i.e.*, DNA degradation that resulted in the inhibition of migration and anti-proliferative activity by decreased colony formation, prompted us to investigate the antitumor activity of biogenic *in vivo*.

Our results demonstrated that the urinary tract of the animals from the Control group did not present microscopic changes (Supplementary Material S1, Table 1). The most frequent neoplastic lesions in the NMIBC + AgNP 0.5 group were pTa (Figure 7a), pTis (Figure 7b) and pT1 in 42.85%, 28.57%, and 28.57% of the animals, respectively (Table 1), indicating that this treatment did not reduce neoplastic lesions. The pTis carcinoma was characterized by a disordered proliferation of urothelial cells (hyperplasia) in a flat urothelium, with marked cellular atypia characterized by bulky nuclei, reduced cytoplasm, and multiple and prominent nucleoli.

Histopathological examination in animals of the NMIBC + AgNP 0.2 Group showed 28.57% of tumor regression, which showed flat hyperplasia (Figure 6c; Table 1). pTis represents the majority related to neoplastic lesions (57.15%), followed by pTa (14.28%), Figure 7d and Table 1. Thickening of the urothelium and absence of cytological atypia were characteristics of flat hyperplasia. Treatment with AgNP 0.05 presented 57.15% tumor regression (Table 1), with 14.28% of the animals showing normal urothelium (Figure 6e) and 42.85% presenting flat hyperplasia (Figure 6f), which is considered a benign lesion.

Table 1. Histopathological changes (%) of mice's urinary bladder from different experimental groups.

	Groups				
Histopatology	**Control** (***n*=7**)	**NMIBC (Cancer)** (***n*=7**)	**NMIBC+AgNP 0.05 mg/mL** ***(n=7)***	**NMIBC+AgNP 0.2 mg/mL** (***n*=7**)	**NMIBC+AgNP 0.5 mg/mL** (***n*=7**)
Normal	7(100%)*	-	1(14.28%)	-	-
Flat hyperplasia	-	-	3(42.85%)*	2(28.57%)	-
Flat Carcinoma *in situ* (pTis)	-	-	2(28.57%)	4(57.15%)*	2(28.57%)
Papillary Urothelial Carcinoma (pTa)	-	3(42.85%)*	1(14.28%)	1(14.28%)	3(42.85%)*
High-grade urothelial cancer invading the lamina propria (pT1)	-	4(57.15%)*	-	-	2(28.57%)

Benign Lesions: Flat hyperplasia; Malignant lesions: pTis; pTa; pT1.
The histopathological alterations were normalized by the number of mice (n) examined in each group.
*$P<0.0001$ (proportions test).

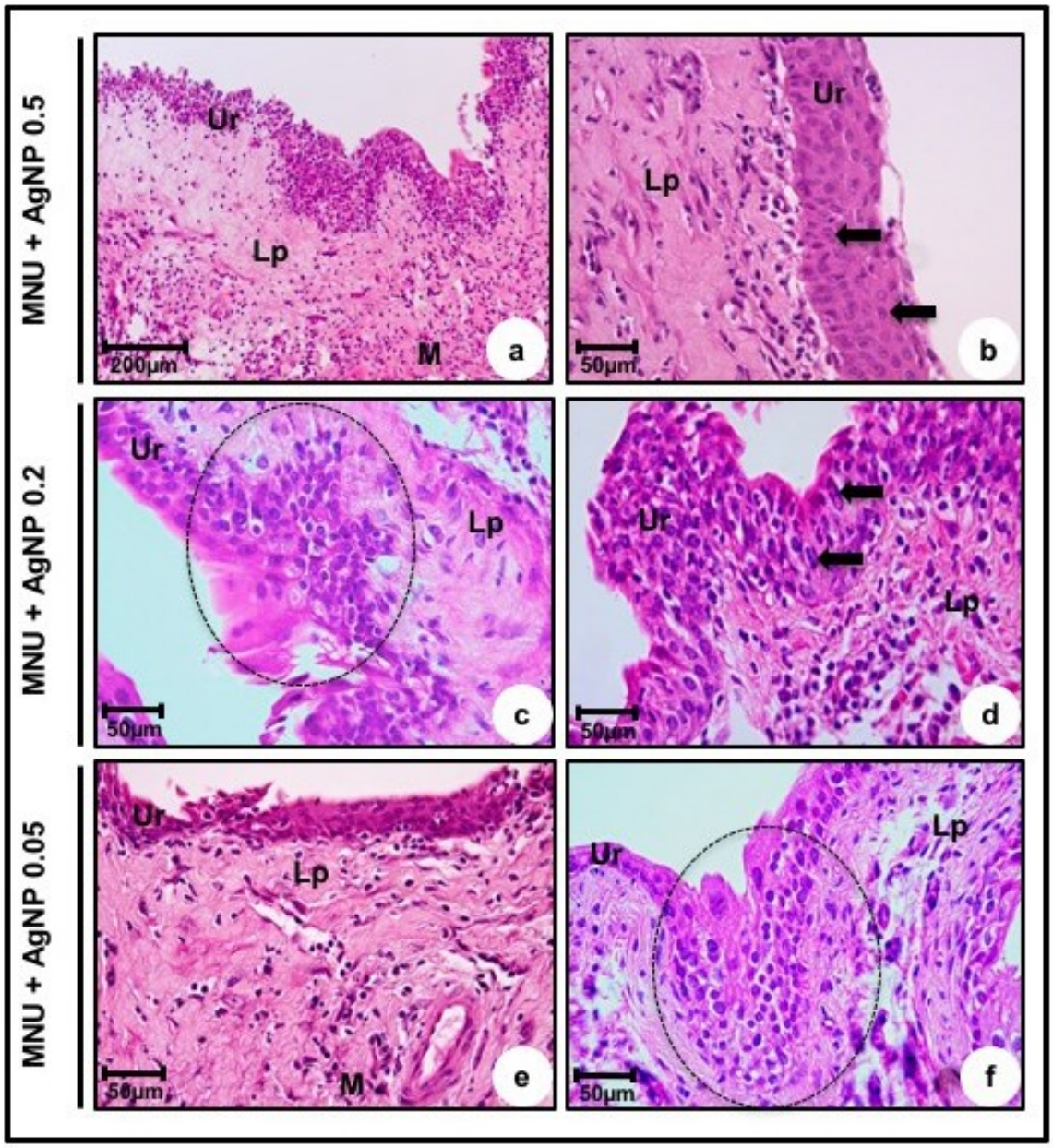

Figure 6. *Photomicrographs of urinary bladder treated with biogenic AgNP.* MNU + AgNP 0.5 (a, b), MNU + AgNP 0.2 (c, d) and MNU + AgNP 0.05 (e, f) groups. (a) pTa tumor characterized by extensive papillary lesions, urothelial cells with disordered arrangement and loss of polarity, intense cellular pleomorphism and numerous mitosis figures. (b), (d) pTis tumor characterized by cellular atypia: bulky nuclei with reduced cytoplasm and prominent nucleoli (arrows). (c), (f) Flat hyperplasia (circle) characterized by thickening of the urothelium and absence of cytological atypia. (e) Normal urothelium composed of 2-3 layers: a layer of basal cells, an intermediate layer of cells, and a superficial or apical layer composed of cells in umbrella. **a - f: Lp -** lamina propria, **M -** muscular layer, **Ur -** urothelium.

4. Conclusion

Collectively, our results demonstrated that the biogenic AgNPs is a promising tool against bladder cancer *in vitro* and *in vivo*. In bladder carcinoma cells, AgNP induced DNA damage and triggered apoptosis, reducing migration and cell proliferation. The promising results obtained *in vitro* were reflected in the *in vivo* assays against NMIBC, where substantial tumor reduction was observed. Thus, these findings suggest that AgNP may be a cost-effective alternative and candidate for the treatment of bladder cancer. Intravesical administration (directly in the tumor) is a critical factor for the potency of the treatment, since it reduces possible toxicity, avoiding the systemic route of administration and interactions with plasma proteins. Biogenic AgNP should be investigated from a new angle for its therapeutical potential for treating high-grade NMIBC treatment, including a new alternative for the treatment of BCG-refractory or relapsed patients.

5. Supplementary material

The normal urothelium was composed of 2-3 layers, being: a layer of basal cells, an intermediate cell layer, and a superficial or apical layer formed of cells in an umbrella (Figures S1a, S1b). In contrast, the NMIBC urinary tract presented drastic histopathological changes, such as: pT1 (Figures S1c, S1d) and pTa (Figures S1e, S1f) tumors in 57.15% and 42.85% of the animals, respectively (Table 1). The pT1 carcinoma was characterized by neoplastic cells grouped into small groups or cords invading the lamina propria, pleomorphic cells with enlarged nuclei, and numerous mitotic figures. The pTa carcinoma was characterized by papillary lesions, loss of polarity, and urothelial cells with a disordered arrangement, intense cellular pleomorphism, and numerous mitosis figures.

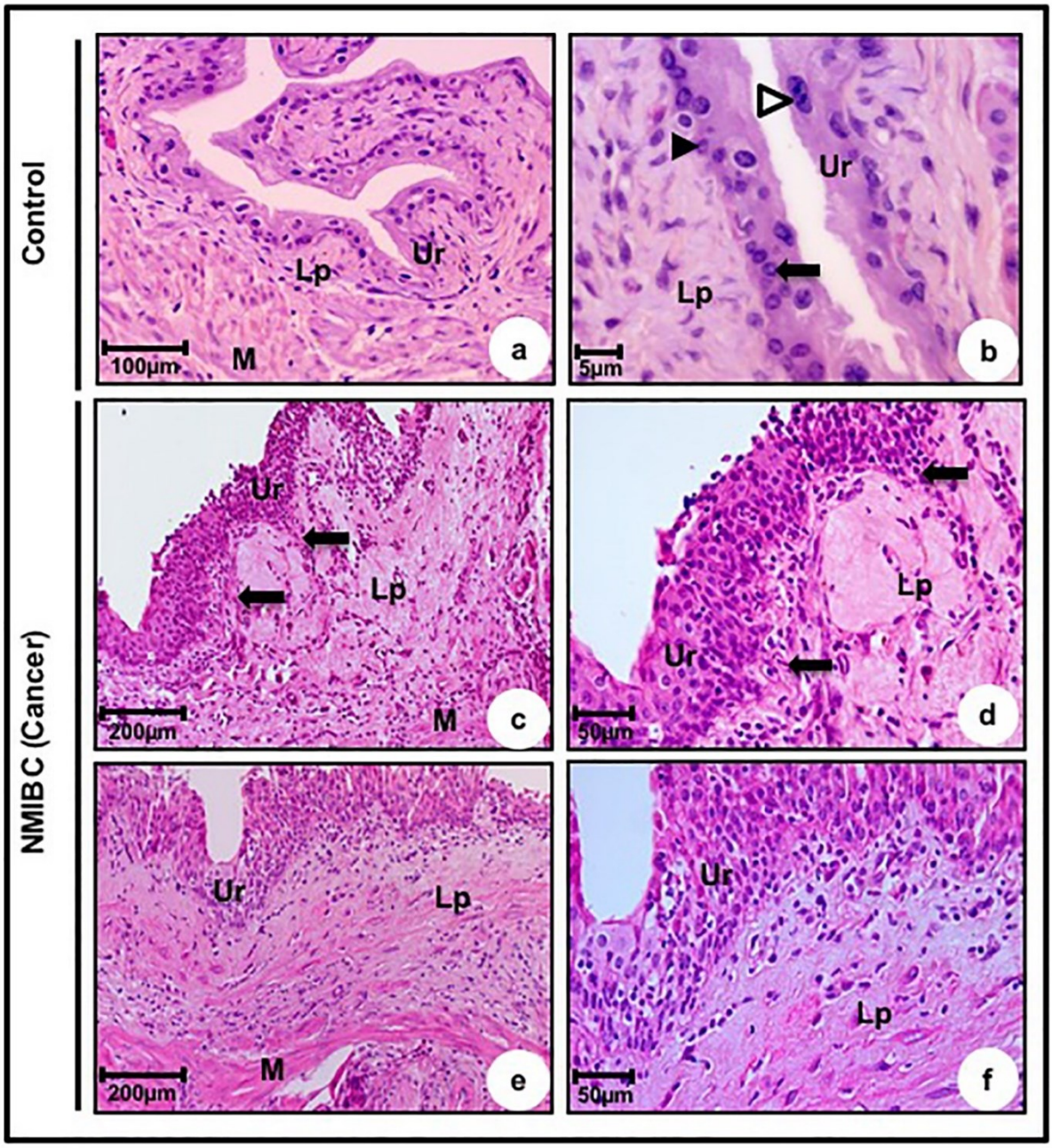

Figure S1. *Photomicrographs of the urinary bladder induction. Control (a, b) and NMIBC (c, d, e, f) groups.* (a), (b) Normal urothelium composed of 2-3 layers: a layer of basal cells (closed arrowhead), an intermediate layer of cells (arrow), and a superficial or apical layer composed of umbrella cells (open arrowhead). (c), (d) pT1 tumor: neoplastic cells arranged in small groups (arrows) invading the lamina propria. (e), (f) pTa tumor characterized by extensive papillary lesions, urothelial cells with a disordered arrangement and loss of polarity, intense cellular pleomorphism, and numerous mitosis figures. a - f: Lp - lamina propria, M - muscular layer, Ur – urothelium.

CAPÍTULO 5 - Discussão

Devido à expressiva incorporação em diversos produtos industrias, atual preocupação sobre a bioacumilação e toxicidade, por fim, a relevância científica com novas aplicações na área de biociência e nanomedicina, as AgNP sintetizadas através dos princípios da Química Verde (do inglês, *Green Chemistry*) foram o objeto de estudo desta tese de doutorado. Desta forma, o primeiro objetivo desta tese foi avaliar a toxicidade das nanopartículas de prata biossíntéticas e correlacionar com os achados encontrados em literatura, principalmente em relação as nanopartículas de síntese química, ainda, explorar mecanismos moleculares de toxicidade não encontrados anteriormente, pois muitas vezes os estudos com AgNP divergem em relação ao mecanismo de citotoxicidade. São descritos que as nanopartículas podem induzir danos em membrana celular via peroxidação lipídica, genotoxicidade, interagir com diferentes proteínas inferindo em vias de sinalização e síntese de proteínas, estimular o fluxo autofágico e desencadear morte celular e o por necrose e/ou apoptose (Hsin et al. 2008, Foldbjerg et al. 2009, de Lima et al. 2012, Ong et al. 2013, Satapathy et al. 2013, Zhornik et al. 2014, Ishida 2017). Muitos destes eventos citados anteriormente são frequentemente correlacionados com o estresse oxidativo, sendo portanto, descrito como o principal fator causador da citotoxicidade em diferentes linhagens celulares e mais citados em trabalhos científicos (Kim and Ryu 2013; Figura 1).

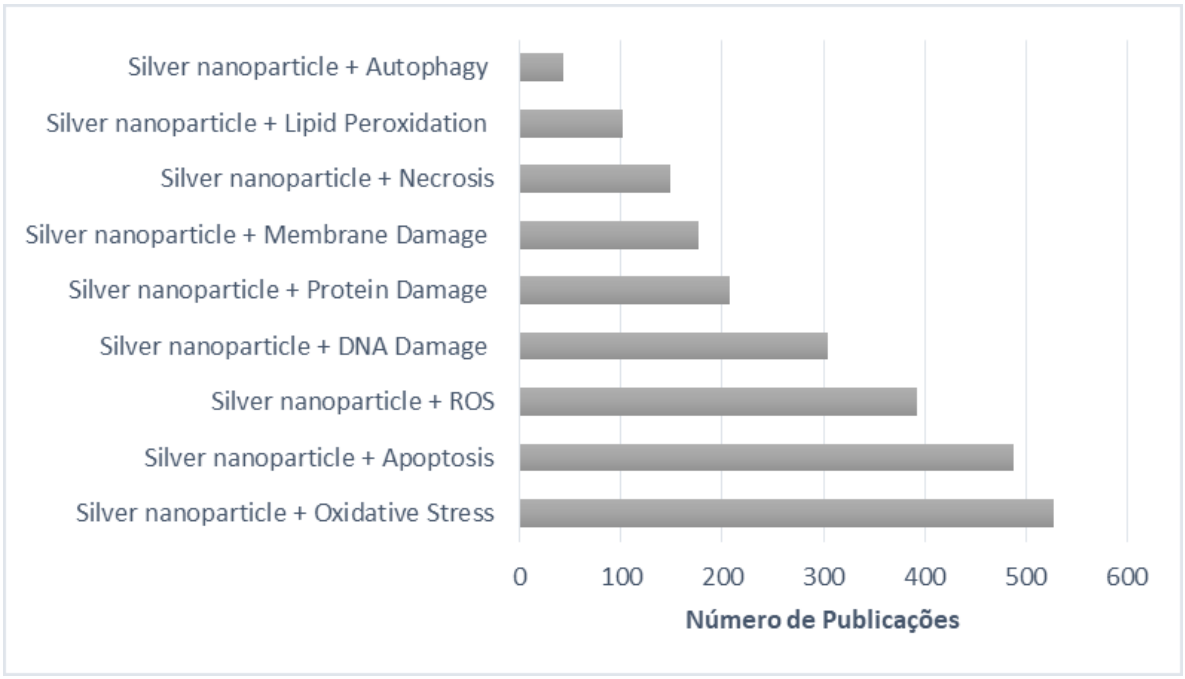

Figura 1. *Resultado da busca de trabalhos na plataforma PubMed*. Pesquisa realizada no dia 01/07/2019 com as palavras-chave*: Silver nanoparticle + Autophagy; Silver nanoparticle +Lipid Peroxidation; Silver nanoparticle +Necrosis; Silver nanoparticle +Membrane Damage; Silver nanoparticle + Protein Damage; Silver nanoparticle + DNA Damage; Silver nanoparticle + ROS; Silver nanoparticle + Apoptosis; Silver nanoparticle + Oxidative Stress.*

Durante a avaliação dos mecanismos moleculares de citotoxicidade das AgNP biossintéticas em cultura de células hepatocarcinoma (Huh-7), observamos o aumento do estresse oxidativo, corroborando com os achados em literatura. Contudo, a reversão da toxicidade pelos tióis-antioxidantes está muito mais associada ao efeito quelante sobre a prata, do que em relação a redução dos níveis de citoplasmáticos de ROS. Um exemplo disso são os resultados encontrados com TLX, onde observou-se a redução dos níveis de ROS, entretanto não obtivemos o aumento da viabilidade. Esses achados convergem com os estudos do Prof. Harald Schmidt e colaboradores, no qual reforçam que o estresse oxidativo seria um evento secundário, relacionado mais como consequência do que a causa de doenças. Logo, a teoria da utilização de antioxidantes no aumento do estresse oxidativo se mostra uma forma habitual e pouco fundamentada de solucionar a citotoxicidade e outros problemas. Está teoria pode se tornar falha, um vez que o tratamento com antioxidantes não mostram evidências suficiente

para serem incorporados em diretrizes, aprovados por agências reguladoras, pois muitas vezes são ineficientes na cura de doenças em que o aumento do estresse oxidativo é observado (Ghezzi et al. 2017, Elbatreek et al. 2019). Outro importante resultado que reforça a influência da complexação dos tios-antioxidantes no estudo da citotoxicidade é a redução dos níveis de internalização das AgNP, o que diretamente impossibilitou com que o nobre nanomaterial causasse danos intracelulares.

Uma vez encontrado que o efeito do antioxidante era uma interação direta com a partícula, o Capítulo 2 teve o intuito de alertar a sociedade científica em relação a presença de "artefatos" no estudo do estresse oxidativo e AgNP, o que poderia criar falsas interpretações sobre os mecanismos moleculares de toxicidade. Em vista disso, este trabalho também nos trouxe o *insight* de direcionarmos para uma nova aplicação. O Capítulo 3 "Como um artefato pode se transformar em um antídoto" abordou a ação do tiol-antioxidante NAC na reversão dos efeitos tóxicos causados pelas AgNP. Devido ao aumento da produção, uso generalizado e documentação de casos reais de intoxicação terapêutica, ocupacional ou acidental com prata (Durán et al. 2018, Mendonça et al. 2018). Nosso estudo expôs ratos Wistar a uma dose subletal intravenosa de AgNP para avaliação da toxicidade sistêmica. Posteriormente, avaliamos se a terapia intraperitoneal, 1 h da administração das nanopartículas, com tiol-antioxidantes neutralizaria a nanotoxicidade, conforme observado nos experimentos *in vitro*.

Nossos resultados mostraram que após 24 horas as AgNP induziram hepatotoxicidade aguda, através do aumento níveis séricos de transaminases hepáticas (AST, ALT), alteração morfológica, presença infiltrado inflamatório (aumento de células de Kupffer), aumento do estresse oxidativo, eventualmente correlacionados com o aumento da concentração e afinidade das AgNP neste tecido. Em contrapartida, os tióis-antioxidantes NAC e GSH previniram a toxicidade hepática, diferentemente da vitamina C, onde não se observou significativa redução. Além disso, a quantificação da prata tecidual revelou o favorecimento da excreção do

nanomaterial em estudo, reduzindo os níveis de prata no fígado, consequentemente aumentando os níveis de prata nos rins e urina. Este resultado explica o efeito preventivo da hepatotoxicidade e confirma a nossa hipótese de que a complexação das AgNP com os tióis-antioxidantes teria aplicações terapêuticas.

Portanto, o capítulo 3 deste trabalho propõe uma inovadora terapia para NAC contra intoxicações por AgNP, principalmente em casos de acidentes ocupacionais e/ou exposições crônicas, diferentemente das terapias convencionais do NAC contra intoxicação por acetaminofeno e atividade mucolítica. E ainda, nós sugerimos não se limitar apenas intoxicação relacionadas ao elemento prata, mas sim abranger para diferentes tipos de nanomateriais metálicos, como por exemplo cobre, chumbo, ferro, platina, entre outros; hipótese essa que ainda precisa ser testada. Esperamos que este trabalho encoraje outros estudos semelhantes em relação a antídotos para nanotoxicidade, uma vez que o uso de nanomateriais está crescendo exponencialmente e não existem protocolos de tratamento estabelecidos em casos de intoxicação.

Por fim, o Capítulo 4 desta tese direcionou os achados sobre a citotoxicidade das AgNP biossintéticas para uma nova aplicação terapêutica. O câncer de bexida é um dos tumores de maior incidência mundial, potencialmente letal, muitas vezes negligenciado, que exige tratamento muitas vezes agressivo. Sendo assim, nós avaliamos os efeitos citotóxicos das AgNP biossintéticas no combate contra câncer de bexiga, especificamente modelo não musculo invasivo. Os promissores resultados obtidos em células tumorais de bexiga 5637 de danos em DNA (genotoxicidade), regressão da proliferação e migração celular, refletiram nos resultados contra o modelo *in vivo* de câncer de bexiga não músculo invasivo (NMIBC), em que relevante regressão tumoral foi observada nos ensaios histológicos. Portanto, consideramos que as AgNP seriam um importante candidato a fármaco no tratamento do câncer de bexiga.

As AgNP apresentam infinidades oportunidades para o uso em aplicações farmacêuticas e médicas, em vista disso a compreensão da toxicidade *in vivo* se faz necessária. A caracterização mais criteriosa sobre a nanotoxicidade é um desfio para aplicações mais seguras de nanomateriais.

CAPÍTULO 6 - Conclusão

Através dos estudos preconizados nesta tese de doutorado, concluímos que a mitigação da citotoxicidade na presença de tiol-antioxidantes foi resultado da ligação direta do radical SH com a Ag^0, ao invés da inibição das EROs como amplamente descrito em literatura. Ainda, os tióis-antioxidantes são capazes de reduzir significativamente a internalização das nanopartículas, prevenindo possíveis danos intracelulares. Estes resultados nos levou a compreensão de direcionarmos fármacos tiol-antioxidantes (NAC, L-Cys e GSH) para o tratamento de intoxicações relacionadas ao AgNP, uma vez que elas poderiam neutralizar os efeitos toxicos. Sendo assim, observamos que a nossa hipótese estava correta. Nossos achados mostraram que o antioxidante NAC é capaz de prevenir de forma significativa os efeitos tóxicos causados AgNPs (hepatotoxicidade, nefrotoxicidade, etc.), demonstrando ser um potencial candidato para intervenção precoce em casos de intoxicação por AgNPs. Além disso, nosso estudo também forneceu informações sobre o mecanismo de depuração de AgNPs, demonstrando que o tratamento com NAC estimular eliminação por excreção renal. Por fim, esperamos que este trabalho fomente estudos semelhantes em relação a antídotos contra a nanotoxicidade, uma vez que o uso de nanomateriais está crescendo exponencialmente e não existem protocolos de tratamento estabelecidos em casos de intoxicação.

Após investigações da nanotoxicidade promovidas por AgNPs, nós avaliamos seus efeitos citotóxicos para estudos contra câncer de bexiga. Os nossos promissores resultados obtidos *in vitro* de genotoxicidade, diminuição da proliferação e migração celular, refletiram nos resultados *in vivo* contra NMIBC, em que relevante regressão tumoral foi observada nos ensaios histológicos. Desta maneira, consideramos que as AgNPs seriam um importante candidato a fármaco, ou ainda adjuvante, no tratamento do câncer de bexiga. Além disso, sugerimos também a associação desta terapia com campos magnéticos para obtenção de

sinergismo citotóxicos, pois além de possuir a atividade antitumoral intrínseca, o campo magnético geraria o superaquecimento das nanopartículas e consequentemente a destruição das células tumorais.

AGRADECIMENTO

O presente trabalho foi realizado com apoio da Coordenação de Aperfeiçoamento de Pessoal de Nível Superior - Brasil (CAPES) - Código de Financiamento 001.

CAPÍTULO 7 - Referências

Capitulo 1 - Introdução

Abbasi, E., Milani, M., Aval, S.F., Kouhi, M., Akbarzadeh, A., Nasrabadi, H.T., Nikasa, P., Joo, S.W., Hanifehpour, Y., Nejati-Koshki, K., Samiei, M., 2016. Silver nanoparticles: Synthesis methods, bio-applications and properties. Crit. Rev. Microbiol. 42, 173–180. https://doi.org/10.3109/1040841X.2014.912200

Caro, C., M., P., Klippstein, R., Pozo, D., P., A., 2010. Silver Nanoparticles: Sensing and Imaging Applications, in: Pozo, D. (Ed.), Silver Nanoparticles. InTech. https://doi.org/10.5772/8513

Chakraborty, B., Pal, R., Ali, M., Singh, L.M., Shahidur Rahman, D., Kumar Ghosh, S., Sengupta, M., 2016. Immunomodulatory properties of silver nanoparticles contribute to anticancer strategy for murine fibrosarcoma. Cell. Mol. Immunol. 13, 191–205. https://doi.org/10.1038/cmi.2015.05

Dhillon, G.S., Brar, S.K., Kaur, S., Verma, M., 2011. Green approach for nanoparticle biosynthesis by fungi: current trends and applications. Crit. Rev. Biotechnol. 32, 49–73. https://doi.org/10.3109/07388551.2010.550568

Durán, N., Marcato, P.D., Alves, O.L., Souza, G.I.D., Esposito, E., 2005. Mechanistic aspects of biosynthesis of silver nanoparticles by several Fusarium oxysporum strains. J. Nanobiotechnology 3, 8. https://doi.org/10.1186/1477-3155-3-8

Durán, N., Marcato, P.D., De Conti, R., Alves, O.L., Costa, F.T., Brocchi, M., 2010. Potential use of silver nanoparticles on pathogenic bacteria, their toxicity and possible mechanisms of action. J Braz Chem Soc 21, 949–959.

Durán, N., Marcato, P.D., De Souza, G.I.H., Alves, O.L., Esposito, E., 2007. Antibacterial Effect of Silver Nanoparticles Produced by Fungal Process on Textile Fabrics and Their Effluent Treatment. J. Biomed. Nanotechnol. 3, 203–208. https://doi.org/10.1166/jbn.2007.022

Durán, N., Nakazato, G., Seabra, A.B., 2016. Antimicrobial activity of biogenic silver nanoparticles, and silver chloride nanoparticles: an overview and comments. Appl. Microbiol. Biotechnol. 100, 6555–6570. https://doi.org/10.1007/s00253-016-7657-7

Durán, N., Silveira, C.P., Durán, M., Martinez, D.S.T., 2015. Silver nanoparticle protein corona and toxicity: a mini-review. J. Nanobiotechnology 13. https://doi.org/10.1186/s12951-015-0114-4

Kowshik, M., Ashtaputre, S., Kharrazi, S., Vogel, W., Urban, J., Kulkarni, S.K., Paknikar, K.M., 2003. Extracellular synthesis of silver nanoparticles by a silver-tolerant yeast strain MKY3. Nanotechnology 14, 95. https://doi.org/10.1088/0957-4484/14/1/321

Krishnaraj, C., Jagan, E.G., Rajasekar, S., Selvakumar, P., Kalaichelvan, P.T., Mohan, N., 2010. Synthesis of silver nanoparticles using Acalypha indica leaf extracts and its antibacterial activity against water borne pathogens. Colloids Surf. B Biointerfaces 76, 50–56. https://doi.org/10.1016/j.colsurfb.2009.10.008

Mohanpuria, P., Rana, N.K., Yadav, S.K., 2008. Biosynthesis of nanoparticles: technological concepts and future applications. J. Nanoparticle Res. 10, 507–517. https://doi.org/10.1007/s11051-007-9275-x

Mytych, J., Zebrowski, J., Lewinska, A., Wnuk, M., 2017. Prolonged Effects of Silver Nanoparticles on p53/p21 Pathway-Mediated Proliferation, DNA Damage Response, and Methylation Parameters in HT22 Hippocampal Neuronal Cells. Mol. Neurobiol. 54, 1285–1300. https://doi.org/10.1007/s12035-016-9688-6

Nanda, A., Saravanan, M., 2009. Biosynthesis of silver nanoparticles from Staphylococcus aureus and its antimicrobial activity against MRSA and MRSE. Nanomedicine Nanotechnol. Biol. Med. 5, 452–456. https://doi.org/10.1016/j.nano.2009.01.012

Sintubin, L., De Windt, W., Dick, J., Mast, J., van der Ha, D., Verstraete, W., Boon, N., 2009. Lactic acid bacteria as reducing and capping agent for the fast and efficient production of silver nanoparticles. Appl. Microbiol. Biotechnol. 84, 741–749. https://doi.org/10.1007/s00253-009-2032-6

Capítulo 2 - A influência de tióis-antioxidantes na avaliação da citotoxicidade por nanopartículas de prata

Andersson Lars-Olov, 2003. Study of some silver-thiol complexes and polymers: Stoichiometry and optical effects. J. Polym. Sci. [A1] 10, 1963–1973. https://doi.org/10.1002/pol.1972.150100707

Andrade, P.F., Nakazato, G., Durán, N., 2017. Additive interaction of carbon dots extracted from soluble coffee and biogenic silver nanoparticles against bacteria. J. Phys. Conf. Ser. 838, 012028. https://doi.org/10.1088/1742-6596/838/1/012028

Azhdarzadeh, M., Saei, A.A., Sharifi, S., Hajipour, M.J., Alkilany, A.M., Sharifzadeh, M., Ramazani, F., Laurent, S., Mashaghi, A., Mahmoudi, M., 2015. Nanotoxicology: advances and pitfalls in research methodology. Nanomed. 10, 2931–2952. https://doi.org/10.2217/nnm.15.130

Chen, X., Schluesener, H.J., 2008. Nanosilver: A nanoproduct in medical application. Toxicol. Lett. 176, 1–12. https://doi.org/10.1016/j.toxlet.2007.10.004

Choi, O., Clevenger, T.E., Deng, B., Surampalli, R.Y., Ross Jr., L., Hu, Z., 2009. Role of sulfide and ligand strength in controlling nanosilver toxicity. Water Res. 43, 1879–1886. https://doi.org/10.1016/j.watres.2009.01.029

de Jesus, M.B., Kapila, Y.L., 2014. Cellular Mechanisms in Nanomaterial Internalization, Intracellular Trafficking, and Toxicity, in: Durán, N., Guterres, S.S., Alves, O.L. (Eds.), Nanotoxicology, Nanomedicine and Nanotoxicology. Springer New York, pp. 201–227.

de Lima, R., Seabra, A.B., Durán, N., 2012. Silver nanoparticles: a brief review of cytotoxicity and genotoxicity of chemically and biogenically synthesized nanoparticles. J. Appl. Toxicol. 32, 867–879. https://doi.org/10.1002/jat.2780

Durán, N., Marcato, P.D., Alves, O.L., Souza, G.I.D., Esposito, E., 2005. Mechanistic aspects of biosynthesis of silver nanoparticles by several Fusarium oxysporum strains. J. Nanobiotechnology 3, 8. https://doi.org/10.1186/1477-3155-3-8

Durán, N., Nakazato, G., Seabra, A.B., 2016. Antimicrobial activity of biogenic silver nanoparticles, and silver chloride nanoparticles: an overview and comments. Appl. Microbiol. Biotechnol. 100, 6555–6570. https://doi.org/10.1007/s00253-016-7657-7

Foldbjerg, R., Olesen, P., Hougaard, M., Dang, D.A., Hoffmann, H.J., Autrup, H., 2009. PVP-coated silver nanoparticles and silver ions induce reactive oxygen species, apoptosis and necrosis in THP-1 monocytes. Toxicol. Lett. 190, 156–162. https://doi.org/10.1016/j.toxlet.2009.07.009

Galiano, K., Pleifer, C., Engelhardt, K., Brössner, G., Lackner, P., Huck, C., Lass-Flörl, C., Obwegeser, A., 2008. Silver segregation and bacterial growth of intraventricular catheters impregnated with silver nanoparticles in cerebrospinal fluid drainages. Neurol. Res. 30, 285–287. https://doi.org/10.1179/016164107X229902

Ge, L., Li, Q., Wang, M., Ouyang, J., Li, X., Xing, M.M., 2014. Nanosilver particles in medical applications: synthesis, performance, and toxicity. Int. J. Nanomedicine 9, 2399–2407. https://doi.org/10.2147/IJN.S55015

Gromadzka-Ostrowska, J., Dziendzikowska, K., Lankoff, A., Dobrzyńska, M., Instanes, C., Brunborg, G., Gajowik, A., Radzikowska, J., Wojewódzka, M., Kruszewski, M., 2012. Silver nanoparticles effects on epididymal sperm in rats. Toxicol. Lett. 214, 251–258. https://doi.org/10.1016/j.toxlet.2012.08.028

Hsin, Y.-H., Chen, C.-F., Huang, S., Shih, T.-S., Lai, P.-S., Chueh, P.J., 2008. The apoptotic effect of nanosilver is mediated by a ROS- and JNK-dependent mechanism involving the mitochondrial pathway in NIH3T3 cells. Toxicol. Lett. 179, 130–139. https://doi.org/10.1016/j.toxlet.2008.04.015

Issels, R.D., Nagele, A., Eckert, K.-G., Wllmanns, W., 1988. Promotion of cystine uptake and its utilization for glutathione biosynthesis induced by cysteamine and N-acetylcysteine. Biochem. Pharmacol. 37, 881–888. https://doi.org/10.1016/0006-2952(88)90176-1

Kim, S., Choi, J.E., Choi, J., Chung, K.-H., Park, K., Yi, J., Ryu, D.-Y., 2009. Oxidative stress-dependent toxicity of silver nanoparticles in human hepatoma cells. Toxicol. In Vitro 23, 1076–1084. https://doi.org/10.1016/j.tiv.2009.06.001

Kim, S., Ryu, D.-Y., 2013. Silver nanoparticle-induced oxidative stress, genotoxicity and apoptosis in cultured cells and animal tissues: Silver nanoparticle-induced toxicity. J. Appl. Toxicol. 33, 78–89. https://doi.org/10.1002/jat.2792

Lee, K.-C., Lin, S.-J., Lin, C.-H., Tsai, C.-S., Lu, Y.-J., 2008. Size effect of Ag nanoparticles on surface plasmon resonance. Surf. Coat. Technol. 202, 5339–5342. https://doi.org/10.1016/j.surfcoat.2008.06.080

Levard, C., Hotze, E.M., Colman, B.P., Dale, A.L., Truong, L., Yang, X.Y., Bone, A.J., Brown, G.E., Tanguay, R.L., Di Giulio, R.T., Bernhardt, E.S., Meyer, J.N., Wiesner, M.R., Lowry, G.V., 2013. Sulfidation of Silver Nanoparticles: Natural Antidote to Their Toxicity. Environ. Sci. Technol. 47, 13440–13448. https://doi.org/10.1021/es403527n

Li, X., Lenhart, J.J., 2012. Aggregation and Dissolution of Silver Nanoparticles in Natural Surface Water. Environ. Sci. Technol. 46, 5378–5386. https://doi.org/10.1021/es204531y

Li, Y., Qin, T., Ingle, T., Yan, J., He, W., Yin, J.-J., Chen, T., 2017. Differential genotoxicity mechanisms of silver nanoparticles and silver ions. Arch. Toxicol. 91, 509–519. https://doi.org/10.1007/s00204-016-1730-y

Lima, R., Feitosa, L.O., Ballottin, D., Marcato, P.D., Tasic, L., Durán, N., 2013. Cytotoxicity and genotoxicity of biogenic silver nanoparticles. J. Phys. Conf. Ser. 429, 012020. https://doi.org/10.1088/1742-6596/429/1/012020

Mendonça, M.C.P., Ferreira, L.B., Rizoli, C., Batista, Â.G., Maróstica Júnior, M.R., da Silva, E. do N., Cadore, S., Durán, N., Cruz-Höfling, M.A. da, de Jesus, M.B., 2018. N-Acetylcysteine reverses silver nanoparticle intoxication in rats. Nanotoxicology 1–13. https://doi.org/10.1080/17435390.2018.1544302

Moore, K., 2006. A new silver dressing for wounds with delayed healing. WOUNDS UK 2, 70.

Rösslein, M., Elliott, J.T., Salit, M., Petersen, E.J., Hirsch, C., Krug, H.F., Wick, P., 2015. Use of Cause-and-Effect Analysis to Design a High-Quality Nanocytotoxicology Assay. Chem. Res. Toxicol. 28, 21–30. https://doi.org/10.1021/tx500327y

Samuni, Y., Goldstein, S., Dean, O.M., Berk, M., 2013. The chemistry and biological activities of N-acetylcysteine. Biochim. Biophys. Acta BBA - Gen. Subj. 1830, 4117–4129. https://doi.org/10.1016/j.bbagen.2013.04.016

Shi, J., Sun, X., Lin, Y., Zou, X., Li, Z., Liao, Y., Du, M., Zhang, H., 2014. Endothelial cell injury and dysfunction induced by silver nanoparticles through oxidative stress via

IKK/NF-κB pathways. Biomaterials 35, 6657–6666. https://doi.org/10.1016/j.biomaterials.2014.04.093

Xiao, H., Wu, M., Shao, F., Guan, G., Huang, B., Tan, B., Yin, Y., 2016. N-Acetyl-L-cysteine Protects the Enterocyte against Oxidative Damage by Modulation of Mitochondrial Function. Mediators Inflamm. 2016, e8364279. https://doi.org/10.1155/2016/8364279

Yang, E.-J., Kim, S., Kim, J.S., Choi, I.-H., 2012. Inflammasome formation and IL-1β release by human blood monocytes in response to silver nanoparticles. Biomaterials 33, 6858–6867. https://doi.org/10.1016/j.biomaterials.2012.06.016

Zhornik, E.V., Baranova, L.A., Drozd, E.S., Sudas, M.S., Chau, N.H., Buu, N.Q., Dung, T.T.N., Chizhik, S.A., Volotovski, I.D., 2014. Silver nanoparticles induce lipid peroxidation and morphological changes in human lymphocytes surface. Biophysics 59, 380–386. https://doi.org/10.1134/S0006350914030282

Zhou, W., Ma, Y., Yang, H., Ding, Y., Luo, X., 2011. A label-free biosensor based on silver nanoparticles array for clinical detection of serum p53 in head and neck squamous cell carcinoma. Int. J. Nanomedicine 6, 381–386. https://doi.org/10.2147/IJN.S13249

Informaçao Suplementar

Durán, N., Marcato, P.D., Alves, O.L., Souza, G.I.D., Esposito, E., 2005. Mechanistic aspects of biosynthesis of silver nanoparticles by several Fusarium oxysporum strains. J. Nanobiotechnology 3, 8. https://doi.org/10.1186/1477-3155-3-8

Lee, K.-C., Lin, S.-J., Lin, C.-H., Tsai, C.-S., Lu, Y.-J., 2008. Size effect of Ag nanoparticles on surface plasmon resonance. Surf. Coat. Technol. 202, 5339–5342. https://doi.org/10.1016/j.surfcoat.2008.06.080

Marcato, P.D., De Paula, L.B., Melo, P.S., Ferreira, I.R., Almeida, A.B.A., Torsoni, A.S., Alves, O.L., 2015. In Vivo Evaluation of Complex Biogenic Silver Nanoparticle and Enoxaparin in Wound Healing. J. Nanomater. 2015, e439820. https://doi.org/10.1155/2015/439820

Capítulo 3 - Como um artefato pode se transformar um antídoto

Andersson Lars-Olov, 2003. Study of some silver-thiol complexes and polymers: Stoichiometry and optical effects. J. Polym. Sci. [A1] 10, 1963–1973. https://doi.org/10.1002/pol.1972.150100707

Andrade, P.F., Nakazato, G., Durán, N., 2017. Additive interaction of carbon dots extracted from soluble coffee and biogenic silver nanoparticles against bacteria. J. Phys. Conf. Ser. 838, 012028. https://doi.org/10.1088/1742-6596/838/1/012028

Asharani, P. V., Sethu, S., Vadukumpully, S., Zhong, S., Lim, C.T., Hande, M.P., Valiyaveettil, S., 2010. Investigations on the structural damage in human erythrocytes exposed to silver, gold, and platinum nanoparticles. Adv. Funct. Mater. 20, 1233–1242. https://doi.org/10.1002/adfm.200901846

Azhdarzadeh, M., Saei, A.A., Sharifi, S., Hajipour, M.J., Alkilany, A.M., Sharifzadeh, M., Ramazani, F., Laurent, S., Mashaghi, A., Mahmoudi, M., 2015. Nanotoxicology:

advances and pitfalls in research methodology. Nanomed. 10, 2931–2952. https://doi.org/10.2217/nnm.15.130

Batista, Â.G., Lenquiste, S.A., Cazarin, C.B.B., da Silva, J.K., Luiz-Ferreira, A., Bogusz, S., Wang Hantao, L., de Souza, R.N., Augusto, F., Prado, M.A., Maróstica, M.R., 2014. Intake of jaboticaba peel attenuates oxidative stress in tissues and reduces circulating saturated lipids of rats with high-fat diet-induced obesity. J. Funct. Foods 6, 450–461. https://doi.org/10.1016/j.jff.2013.11.011

Behra, R., Sigg, L., Clift, M.J.D., Herzog, F., Minghetti, M., Johnston, B., Petri-Fink, A., Rothen-Rutishauser, B., 2013. Bioavailability of silver nanoparticles and ions: from a chemical and biochemical perspective. J. R. Soc. Interface 10, 20130396–20130396. https://doi.org/10.1098/rsif.2013.0396

Bell, R., Kramer, J.R., 1999. Structural chemistry and geochemistry of silver-sulfur compounds: Critical review. Environ. Toxicol. Chem. 18, 9–22. https://doi.org/10.1002/etc.5620180103

Bhunia, A.K., Kamilya, T., Saha, S., 2017. Silver nanoparticle-human hemoglobin interface: time evolution of the corona formation and interaction phenomenon. Nano Converg. 4, 28. https://doi.org/10.1186/s40580-017-0122-1

Bostan, H.B., Rezaee, R., Valokala, M.G., Tsarouhas, K., Golokhvast, K., Tsatsakis, A.M., Karimi, G., 2016. Cardiotoxicity of nano-particles. Life Sci. 165, 91–99. https://doi.org/10.1016/j.lfs.2016.09.017

Chen, L.Q., Fang, L., Ling, J., Ding, C.Z., Kang, B., Huang, C.Z., 2015. Nanotoxicity of silver nanoparticles to red blood cells: Size dependent adsorption, uptake, and hemolytic activity. Chem. Res. Toxicol. 28, 501–509. https://doi.org/10.1021/tx500479m

Chen, X., Schluesener, H.J., 2008. Nanosilver: A nanoproduct in medical application. Toxicol. Lett. 176, 1–12. https://doi.org/10.1016/j.toxlet.2007.10.004

Choi, O., Clevenger, T.E., Deng, B., Surampalli, R.Y., Ross Jr., L., Hu, Z., 2009. Role of sulfide and ligand strength in controlling nanosilver toxicity. Water Res. 43, 1879–1886. https://doi.org/10.1016/j.watres.2009.01.029

Dayyoub, E., Frant, M., Pinnapireddy, S.R., Liefeith, K., Bakowsky, U., 2017. Antibacterial and anti-encrustation biodegradable polymer coating for urinary catheter. Int. J. Pharm. 531, 205–214. https://doi.org/10.1016/j.ijpharm.2017.08.072

de Jesus, M.B., Kapila, Y.L., 2014. Cellular Mechanisms in Nanomaterial Internalization, Intracellular Trafficking, and Toxicity, in: Durán, N., Guterres, S.S., Alves, O.L. (Eds.), Nanotoxicology, Nanomedicine and Nanotoxicology. Springer New York, pp. 201–227.

de Lima, R., Seabra, A.B., Durán, N., 2012. Silver nanoparticles: a brief review of cytotoxicity and genotoxicity of chemically and biogenically synthesized nanoparticles. J. Appl. Toxicol. 32, 867–879. https://doi.org/10.1002/jat.2780

Drake, P.L., Hazelwood, K.J., 2005. Exposure-related health effects of silver and silver compounds: A review. Ann. Occup. Hyg. 49, 575–585. https://doi.org/10.1093/annhyg/mei019

Durán, Nelson., Durán, M., de Jesus, M.B., Seabra, A.B., Fávaro, W.J., Nakazato, G., 2016. Silver nanoparticles: A new view on mechanistic aspects on antimicrobial activity. Nanomedicine Nanotechnol. Biol. Med. 12, 789–799. https://doi.org/10.1016/j.nano.2015.11.016

Durán, N., Marcato, P.D., Alves, O.L., De Souza, G.I., Esposito, E., 2005a. Mechanistic aspects of biosynthesis of silver nanoparticles by several Fusarium oxysporum strains. J. Nanobiotechnology 3, 8. https://doi.org/10.1186/1477-3155-3-8

Durán, N., Marcato, P.D., Alves, O.L., Souza, G.I.D., Esposito, E., 2005b. Mechanistic aspects of biosynthesis of silver nanoparticles by several Fusarium oxysporum strains. J. Nanobiotechnology 3, 8. https://doi.org/10.1186/1477-3155-3-8

Durán, Nelson, Nakazato, G., Seabra, A.B., 2016a. Antimicrobial activity of biogenic silver nanoparticles, and silver chloride nanoparticles: an overview and comments. Appl. Microbiol. Biotechnol. 100, 6555–6570. https://doi.org/10.1007/s00253-016-7657-7

Durán, Nelson, Nakazato, G., Seabra, A.B., 2016b. Antimicrobial activity of biogenic silver nanoparticles, and silver chloride nanoparticles: an overview and comments. Appl. Microbiol. Biotechnol. 100, 6555–6570. https://doi.org/10.1007/s00253-016-7657-7

Dziendzikowska, K., Gromadzka-Ostrowska, J., Lankoff, A., Oczkowski, M., Krawczyńska, A., Chwastowska, J., Sadowska-Bratek, M., Chajduk, E., Wojewódzka, M., Dušinská, M., Kruszewski, M., 2012. Time-dependent biodistribution and excretion of silver nanoparticles in male Wistar rats. J. Appl. Toxicol. 32, 920–928. https://doi.org/10.1002/jat.2758

Fanti, J.R., Tomiotto-Pellissier, F., Miranda-Sapla, M.M., Cataneo, A.H.D., Andrade, C.G.T. de J., Panis, C., Rodrigues, J.H. da S., Wowk, P.F., Kuczera, D., Costa, I.N., Nakamura, C.V., Nakazato, G., Durán, N., Pavanelli, W.R., Conchon-Costa, I., 2018. Biogenic silver nanoparticles inducing Leishmania amazonensis promastigote and amastigote death in vitro. Acta Trop. 178, 46–54. https://doi.org/10.1016/j.actatropica.2017.10.027

Ferreira, L.A.B., Bernardes, J.S., Durán, N.C., B., de J.M., 2018. Thiol antioxidants interfere with assessing silver nanoparticle cytotoxicity. Submitted.

Flora, S.J.S., Pachauri, V., 2010. Chelation in metal intoxication. Int. J. Environ. Res. Public. Health 7, 2745–2788. https://doi.org/10.3390/ijerph7072745

Foldbjerg, R., Olesen, P., Hougaard, M., Dang, D.A., Hoffmann, H.J., Autrup, H., 2009. PVP-coated silver nanoparticles and silver ions induce reactive oxygen species, apoptosis and necrosis in THP-1 monocytes. Toxicol. Lett. 190, 156–162. https://doi.org/10.1016/j.toxlet.2009.07.009

Franci, G., Falanga, A., Galdiero, S., Palomba, L., Rai, M., Morelli, G., Galdiero, M., 2015. Silver nanoparticles as potential antibacterial agents. Molecules 20, 8856–8874. https://doi.org/10.3390/molecules20058856

Galiano, K., Pleifer, C., Engelhardt, K., Brössner, G., Lackner, P., Huck, C., Lass-Flörl, C., Obwegeser, A., 2008. Silver segregation and bacterial growth of intraventricular catheters impregnated with silver nanoparticles in cerebrospinal fluid drainages. Neurol. Res. 30, 285–287. https://doi.org/10.1179/016164107X229902

Ge, L., Li, Q., Wang, M., Ouyang, J., Li, X., Xing, M.M., 2014. Nanosilver particles in medical applications: synthesis, performance, and toxicity. Int. J. Nanomedicine 9, 2399–2407. https://doi.org/10.2147/IJN.S55015

Gondikas, A.P., Morris, A., Reinsch, B.C., Marinakos, S.M., Lowry, G. V., Hsu-Kim, H., 2012. Cysteine-induced modifications of zero-valent silver nanomaterials: Implications for particle surface chemistry, aggregation, dissolution, and silver speciation. Environ. Sci. Technol. 46, 7037–7045. https://doi.org/10.1021/es3001757

Gromadzka-Ostrowska, J., Dziendzikowska, K., Lankoff, A., Dobrzyńska, M., Instanes, C., Brunborg, G., Gajowik, A., Radzikowska, J., Wojewódzka, M., Kruszewski, M., 2012. Silver nanoparticles effects on epididymal sperm in rats. Toxicol. Lett. 214, 251–258. https://doi.org/10.1016/j.toxlet.2012.08.028

Guo, H., Zhang, J., Boudreau, M., Meng, J., Yin, J. jie, Liu, J., Xu, H., 2016. Intravenous administration of silver nanoparticles causes organ toxicity through intracellular ros-related loss of interendothelial junction. Part. Fibre Toxicol. 13, 1–13. https://doi.org/10.1186/s12989-016-0133-9

Gustafson, H.H., Holt-Casper, D., Grainger, D.W., Ghandehari, H., 2015. Nanoparticle uptake: The phagocyte problem. Nano Today 10, 487–510. https://doi.org/10.1016/j.nantod.2015.06.006

Hadrup, N., Lam, H.R., 2014. Oral toxicity of silver ions, silver nanoparticles and colloidal silver – A review. Regul. Toxicol. Pharmacol. 68, 1–7. https://doi.org/10.1016/j.yrtph.2013.11.002

Hadrup, N., Sharma, A.K., Loeschner, K., 2018. Toxicity of silver ions, metallic silver, and silver nanoparticle materials after in vivo dermal and mucosal surface exposure: A review. Regul. Toxicol. Pharmacol. 98, 257–267. https://doi.org/10.1016/j.yrtph.2018.08.007

Hsin, Y.-H., Chen, C.-F., Huang, S., Shih, T.-S., Lai, P.-S., Chueh, P.J., 2008. The apoptotic effect of nanosilver is mediated by a ROS- and JNK-dependent mechanism involving the mitochondrial pathway in NIH3T3 cells. Toxicol. Lett. 179, 130–139. https://doi.org/10.1016/j.toxlet.2008.04.015

Issels, R.D., Nagele, A., Eckert, K.-G., Wllmanns, W., 1988. Promotion of cystine uptake and its utilization for glutathione biosynthesis induced by cysteamine and N-acetylcysteine. Biochem. Pharmacol. 37, 881–888. https://doi.org/10.1016/0006-2952(88)90176-1

Jiménez-Lamana, J., Laborda, F., Bolea, E., Abad-Álvaro, I., Castillo, J.R., Bianga, J., He, M., Bierla, K., Mounicou, S., Ouerdane, L., Gaillet, S., Rouanet, J.-M., Szpunar, J., 2014. An insight into silver nanoparticles bioavailability in rats. Metallomics 6, 2242–2249. https://doi.org/10.1039/C4MT00200H

Jung, I., Joo, E.-J., Suh, B. seong, Ham, C.-B., Han, J.-M., Kim, Y.-G., Yeom, J.-S., Choi, J.-Y., Park, J.-H., 2017. A case of generalized argyria presenting with muscle weakness. Ann. Occup. Environ. Med. 29, 45. https://doi.org/10.1186/s40557-017-0201-0

Kim, J.S., Kuk, E., Yu, K.N., Kim, J.-H., Park, S.J., Lee, H.J., Kim, S.H., Park, Y.K., Park, Y.H., Hwang, C.-Y., Kim, Y.-K., Lee, Y.-S., Jeong, D.H., Cho, M.-H., 2007. Antimicrobial effects of silver nanoparticles. Nanomedicine Nanotechnol. Biol. Med. 3, 95–101. https://doi.org/10.1016/j.nano.2006.12.001

Kim, S., Choi, J.E., Choi, J., Chung, K.-H., Park, K., Yi, J., Ryu, D.-Y., 2009. Oxidative stress-dependent toxicity of silver nanoparticles in human hepatoma cells. Toxicol. In Vitro 23, 1076–1084. https://doi.org/10.1016/j.tiv.2009.06.001

Kim, S., Ryu, D.-Y., 2013a. Silver nanoparticle-induced oxidative stress, genotoxicity and apoptosis in cultured cells and animal tissues: Silver nanoparticle-induced toxicity. J. Appl. Toxicol. 33, 78–89. https://doi.org/10.1002/jat.2792

Kim, S., Ryu, D.-Y., 2013b. Silver nanoparticle-induced oxidative stress, genotoxicity and apoptosis in cultured cells and animal tissues. J. Appl. Toxicol. 33, 78–89. https://doi.org/10.1002/jat.2792

Kokura, S., Handa, O., Takagi, T., Ishikawa, T., Naito, Y., Yoshikawa, T., 2010. Silver nanoparticles as a safe preservative for use in cosmetics. Nanomedicine Nanotechnol. Biol. Med. 6, 570–574. https://doi.org/10.1016/j.nano.2009.12.002

Kondakçı, G., Aydın, A.F., Doğru-Abbasoğlu, S., Uysal, M., 2017. The effect of N-acetylcysteine supplementation on serum homocysteine levels and hepatic and renal oxidative stress in homocysteine thiolactone-treated rats. Arch. Physiol. Biochem. 123, 128–133. https://doi.org/10.1080/13813455.2016.1273365

Lee, K.-C., Lin, S.-J., Lin, C.-H., Tsai, C.-S., Lu, Y.-J., 2008. Size effect of Ag nanoparticles on surface plasmon resonance. Surf. Coat. Technol. 202, 5339–5342. https://doi.org/10.1016/j.surfcoat.2008.06.080

Lee, Y., Kim, P., Yoon, J., Lee, B., Choi, K., Kil, K.-H., Park, K., 2012. Serum kinetics, distribution and excretion of silver in rabbits following 28 days after a single

intravenous injection of silver nanoparticles. Nanotoxicology 7, 1120–1130. https://doi.org/10.3109/17435390.2012.710660

Levard, C., Hotze, E.M., Colman, B.P., Dale, A.L., Truong, L., Yang, X.Y., Bone, A.J., Brown, G.E., Tanguay, R.L., Di Giulio, R.T., Bernhardt, E.S., Meyer, J.N., Wiesner, M.R., Lowry, G.V., 2013. Sulfidation of Silver Nanoparticles: Natural Antidote to Their Toxicity. Environ. Sci. Technol. 47, 13440–13448. https://doi.org/10.1021/es403527n

Li, X., Lenhart, J.J., 2012. Aggregation and Dissolution of Silver Nanoparticles in Natural Surface Water. Environ. Sci. Technol. 46, 5378–5386. https://doi.org/10.1021/es204531y

Li, Y., Qin, T., Ingle, T., Yan, J., He, W., Yin, J.-J., Chen, T., 2017. Differential genotoxicity mechanisms of silver nanoparticles and silver ions. Arch. Toxicol. 91, 509–519. https://doi.org/10.1007/s00204-016-1730-y

Lima, R., Feitosa, L.O., Ballottin, D., Marcato, P.D., Tasic, L., Durán, N., 2013. Cytotoxicity and genotoxicity of biogenic silver nanoparticles. J. Phys. Conf. Ser. 429, 012020. https://doi.org/10.1088/1742-6596/429/1/012020

Mansour, H.H., Hafez, H.F., Fahmy, N.M., Hanafi, N., 2008. Protective effect of N-acetylcysteine against radiation induced DNA damage and hepatic toxicity in rats. Biochem. Pharmacol. 75, 773–780. https://doi.org/10.1016/j.bcp.2007.09.018

Mao, B.-H., Tsai, J.-C., Chen, C.-W., Yan, S.-J., Wang, Y.-J., 2016. Mechanisms of silver nanoparticle-induced toxicity and important role of autophagy. Nanotoxicology 10, 1021–1040. https://doi.org/10.1080/17435390.2016.1189614

Marcato, P.D., De Paula, L.B., Melo, P.S., Ferreira, I.R., Almeida, A.B.A., Torsoni, A.S., Alves, O.L., 2015. In Vivo Evaluation of Complex Biogenic Silver Nanoparticle and Enoxaparin in Wound Healing. J. Nanomater. 2015, e439820. https://doi.org/10.1155/2015/439820

Marin, S., Vlasceanu, G., Tiplea, R., Bucur, I., Lemnaru, M., Marin, M., Grumezescu, A., 2015. Applications and toxicity of silver nanoparticles: A recent review. Curr. Top. Med. Chem. 15, 1596–1604. https://doi.org/10.2174/1568026615666150414142209

McShan, D., Ray, P.C., Yu, H., 2014. Molecular toxicity mechanism of nanosilver. J. Food Drug Anal. 22, 116–127. https://doi.org/10.1016/j.jfda.2014.01.010

Miller, D.L., Yu, I.J., Genter, M.B., 2016. Use of autometallography in studies of nanosilver distribution and toxicity. Int. J. Toxicol. 35, 47–51. https://doi.org/10.1177/1091581815616602

Moore, K., 2006. A new silver dressing for wounds with delayed healing. WOUNDS UK 2, 70.

Peters, R.J.B., Bouwmeester, H., Gottardo, S., Amenta, V., Arena, M., Brandhoff, P., Marvin, H.J.P., Mech, A., Moniz, F.B., Pesudo, L.Q., Rauscher, H., Schoonjans, R., Undas, A.K., Vettori, M.V., Weigel, S., Aschberger, K., 2016. Nanomaterials for products and application in agriculture, feed and food. Trends Food Sci. Technol. 54, 155–164. https://doi.org/10.1016/j.tifs.2016.06.008

Qin, G., Tang, S., Li, S., Lu, H., Wang, Y., Zhao, P., Li, B., Zhang, J., Peng, L., 2017. Toxicological evaluation of silver nanoparticles and silver nitrate in rats following 28 days of repeated oral exposure. Environ. Toxicol. 32, 609–618. https://doi.org/10.1002/tox.22263

Ramadi, K.B., Mohamed, Y.A., Al-Sbiei, A., Almarzooqi, S., Bashir, G., Al Dhanhani, A., Sarawathiamma, D., Qadri, S., Yasin, J., Nemmar, A., Fernandez-Cabezudo, M.J., Haik, Y., Al-Ramadi, B.K., 2016. Acute systemic exposure to silver-based nanoparticles induces hepatotoxicity and NLRP3-dependent inflammation. Nanotoxicology 10, 1061–1074. https://doi.org/10.3109/17435390.2016.1163743

Recordati, C., De Maglie, M., Bianchessi, S., Argentiere, S., Cella, C., Mattiello, S., Cubadda, F., Aureli, F., D'Amato, M., Raggi, A., Lenardi, C., Milani, P., Scanziani, E., 2015. Tissue distribution and acute toxicity of silver after single intravenous administration in mice: nano-specific and size-dependent effects. Part. Fibre Toxicol. 13, 12. https://doi.org/10.1186/s12989-016-0124-x

Rhim, J.-W., Park, H.-M., Ha, C.-S., 2013. Bio-nanocomposites for food packaging applications. Prog. Polym. Sci. 38, 1629–1652. https://doi.org/10.1016/j.progpolymsci.2013.05.008

Rösslein, M., Elliott, J.T., Salit, M., Petersen, E.J., Hirsch, C., Krug, H.F., Wick, P., 2015. Use of Cause-and-Effect Analysis to Design a High-Quality Nanocytotoxicology Assay. Chem. Res. Toxicol. 28, 21–30. https://doi.org/10.1021/tx500327y

Rushworth, G.F., Megson, I.L., 2014. Existing and potential therapeutic uses for N-acetylcysteine: The need for conversion to intracellular glutathione for antioxidant benefits. Pharmacol. Ther. 141, 150–159. https://doi.org/10.1016/j.pharmthera.2013.09.006

Samuni, Y., Goldstein, S., Dean, O.M., Berk, M., 2013. The chemistry and biological activities of N-acetylcysteine. Biochim. Biophys. Acta BBA - Gen. Subj. 1830, 4117–4129. https://doi.org/10.1016/j.bbagen.2013.04.016

Savery, L.C., Viñas, R., Nagy, A.M., Pradeep, P., Merrill, S.J., Hood, A.M., Malghan, S.G., Goering, P.L., Brown, R.P., 2017. Deriving a provisional tolerable intake for intravenous exposure to silver nanoparticles released from medical devices. Regul. Toxicol. Pharmacol. 85, 108–118. https://doi.org/10.1016/j.yrtph.2017.01.007

Shi, J., Sun, X., Lin, Y., Zou, X., Li, Z., Liao, Y., Du, M., Zhang, H., 2014. Endothelial cell injury and dysfunction induced by silver nanoparticles through oxidative stress via IKK/NF-κB pathways. Biomaterials 35, 6657–6666. https://doi.org/10.1016/j.biomaterials.2014.04.093

Shrestha, A., Kishen, A., 2016. Antibacterial nanoparticles in endodontics: A review. J. Endod. 42, 1417–1426. https://doi.org/10.1016/j.joen.2016.05.021

Statista, 2018. Global mine production of silver from 2005 to 2017 (in metric tons) [WWW Document]. Stat. Doss. Silver.

Trop, M., Novak, M., Rodl, S., Hellbom, B., Kroell, W., Goessler, W., 2006. Silver-coated dressing Acticoat caused raised liver enzymes and argyria-like symptoms in burn patient. J. Trauma Inj. Infect. Crit. Care 60, 648–652. https://doi.org/10.1097/01.ta.0000208126.22089.b6

Vance, M.E., Kuiken, T., Vejerano, E.P., McGinnis, S.P., Hochella, M.F., Rejeski, D., Hull, M.S., 2015. Nanotechnology in the real world: Redeveloping the nanomaterial consumer products inventory. Beilstein J. Nanotechnol. 6, 1769–1780. https://doi.org/10.3762/bjnano.6.181

Wang, Z., Xia, T., Liu, S., 2015. Mechanisms of nanosilver-induced toxicological effects: more attention should be paid to its sublethal effects. Nanoscale 7, 7470–7481. https://doi.org/10.1039/C5NR01133G

Weaver, J.L., Tobin, G.A., Ingle, T., Bancos, S., Stevens, D., Rouse, R., Howard, K.E., Goodwin, D., Knapton, A., Li, X., Shea, K., Stewart, S., Xu, L., Goering, P.L., Zhang, Q., Howard, P.C., Collins, J., Khan, S., Sung, K., Tyner, K.M., 2017. Evaluating the potential of gold, silver, and silica nanoparticles to saturate mononuclear phagocytic system tissues under repeat dosing conditions. Part. Fibre Toxicol. 14, 25. https://doi.org/10.1186/s12989-017-0206-4

Weldon, B.A., M. Faustman, E., Oberdörster, G., Workman, T., Griffith, W.C., Kneuer, C., Yu, I.J., 2016. Occupational exposure limit for silver nanoparticles: considerations on the

derivation of a general health-based value. Nanotoxicology 5390, 1–13. https://doi.org/10.3109/17435390.2016.1148793

Wijnhoven, S.W.P., Peijnenburg, W.J.G.M., Herberts, C.A., Hagens, W.I., Oomen, A.G., Heugens, E.H.W., Roszek, B., Bisschops, J., Gosens, I., Van De Meent, D., Dekkers, S., De Jong, W.H., Van Zijverden, M., Sips, A.J.A.M., Geertsma, R.E., 2009. Nano-silver - A review of available data and knowledge gaps in human and environmental risk assessment. Nanotoxicology 3, 109–138. https://doi.org/10.1080/17435390902725914

Windler, L., Height, M., Nowack, B., 2013. Comparative evaluation of antimicrobials for textile applications. Environ. Int. 53, 62–73. https://doi.org/10.1016/j.envint.2012.12.010

Xiao, H., Wu, M., Shao, F., Guan, G., Huang, B., Tan, B., Yin, Y., 2016. N-Acetyl-L-cysteine Protects the Enterocyte against Oxidative Damage by Modulation of Mitochondrial Function. Mediators Inflamm. 2016, e8364279. https://doi.org/10.1155/2016/8364279

Yang, E.-J., Kim, S., Kim, J.S., Choi, I.-H., 2012. Inflammasome formation and IL-1β release by human blood monocytes in response to silver nanoparticles. Biomaterials 33, 6858–6867. https://doi.org/10.1016/j.biomaterials.2012.06.016

Yang, L., Kuang, H., Zhang, W., Aguilar, Z.P., Wei, H., Xu, H., 2017. Comparisons of the biodistribution and toxicological examinations after repeated intravenous administration of silver and gold nanoparticles in mice. Sci. Rep. 7, 3303. https://doi.org/10.1038/s41598-017-03015-1

Zhang, X.-F., Liu, Z.-G., Shen, W., Gurunathan, S., 2016. Silver Nanoparticles: Synthesis, Characterization, Properties, Applications, and Therapeutic Approaches. Int. J. Mol. Sci. 17, 1534. https://doi.org/10.3390/ijms17091534

Zhornik, E.V., Baranova, L.A., Drozd, E.S., Sudas, M.S., Chau, N.H., Buu, N.Q., Dung, T.T.N., Chizhik, S.A., Volotovski, I.D., 2014. Silver nanoparticles induce lipid peroxidation and morphological changes in human lymphocytes surface. Biophysics 59, 380–386. https://doi.org/10.1134/S0006350914030282

Zhou, W., Ma, Y., Yang, H., Ding, Y., Luo, X., 2011. A label-free biosensor based on silver nanoparticles array for clinical detection of serum p53 in head and neck squamous cell carcinoma. Int. J. Nanomedicine 6, 381–386. https://doi.org/10.2147/IJN.S13249

Zhou, Y.-T., He, W., Lo, Y.M., Hu, X., Wu, X., Yin, J.-J., 2013. Effect of silver nanomaterials on the activity of thiol-containing antioxidants. J. Agric. Food Chem. 61, 7855–7862. https://doi.org/10.1021/jf402146s

Capítulo 4 - Aplicação das nanopartículas de prata biossintéticas no tratamento contra o câncer de bexiga

Ahamed, M., Karns, M., Goodson, M., Rowe, J., Hussain, S.M., Schlager, J.J., Hong, Y., 2008. DNA damage response to different surface chemistry of silver nanoparticles in mammalian cells. Toxicol. Appl. Pharmacol. 233, 404–410. https://doi.org/10.1016/j.taap.2008.09.015

American Cancer Society's, 2019. Key Statistics for Bladder Cancer [WWW Document]. URL https://www.cancer.org/cancer/bladder-cancer/about/key-statistics.html

Andrade, P.F., Nakazato, G., Durán, N., 2017. Additive interaction of carbon dots extracted from soluble coffee and biogenic silver nanoparticles against bacteria. J. Phys. Conf. Ser. 838, 012028. https://doi.org/10.1088/1742-6596/838/1/012028

Arora, S., Jain, J., Rajwade, J.M., Paknikar, K.M., 2008. Cellular responses induced by silver nanoparticles: In vitro studies. Toxicol. Lett. 179, 93–100. https://doi.org/10.1016/j.toxlet.2008.04.009

Askeland, E.J., Newton, M.R., O'Donnell, M.A., Luo, Y., 2012. Bladder Cancer Immunotherapy: BCG and Beyond [WWW Document]. Adv. Urol. https://doi.org/10.1155/2012/181987

Azhdarzadeh, M., Saei, A.A., Sharifi, S., Hajipour, M.J., Alkilany, A.M., Sharifzadeh, M., Ramazani, F., Laurent, S., Mashaghi, A., Mahmoudi, M., 2015. Nanotoxicology: advances and pitfalls in research methodology. Nanomed. 10, 2931–2952. https://doi.org/10.2217/nnm.15.130

Babjuk, M., Böhle, A., Burger, M., Capoun, O., Cohen, D., Compérat, E.M., Hernández, V., Kaasinen, E., Palou, J., Rouprêt, M., van Rhijn, B.W.G., Shariat, S.F., Soukup, V., Sylvester, R.J., Zigeuner, R., 2017. EAU Guidelines on Non–Muscle-invasive Urothelial Carcinoma of the Bladder: Update 2016. Eur. Urol. 71, 447–461. https://doi.org/10.1016/j.eururo.2016.05.041

Bendale, Y., Bendale, V., Paul, S., 2017. Evaluation of cytotoxic activity of platinum nanoparticles against normal and cancer cells and its anticancer potential through induction of apoptosis. Integr. Med. Res. 6, 141–148. https://doi.org/10.1016/j.imr.2017.01.006

Cheng, X., Zhang, W., Ji, Y., Meng, J., Guo, H., Liu, J., Wu, X., Xu, H., 2013. Revealing silver cytotoxicity using Au nanorods/Ag shell nanostructures: disrupting cell membrane and causing apoptosis through oxidative damage. RSC Adv. 3, 2296–2305. https://doi.org/10.1039/C2RA23131J

de Jesus, M.B., Kapila, Y.L., 2014. Cellular Mechanisms in Nanomaterial Internalization, Intracellular Trafficking, and Toxicity, in: Durán, N., Guterres, S.S., Alves, O.L. (Eds.), Nanotoxicology, Nanomedicine and Nanotoxicology. Springer New York, pp. 201–227.

de Lima, R., Seabra, A.B., Durán, N., 2012. Silver nanoparticles: a brief review of cytotoxicity and genotoxicity of chemically and biogenically synthesized nanoparticles. J. Appl. Toxicol. 32, 867–879. https://doi.org/10.1002/jat.2780

Durán, N., Marcato, P.D., Alves, O.L., Souza, G.I.D., Esposito, E., 2005. Mechanistic aspects of biosynthesis of silver nanoparticles by several Fusarium oxysporum strains. J. Nanobiotechnology 3, 8. https://doi.org/10.1186/1477-3155-3-8

Durán, N., Nakazato, G., Seabra, A.B., 2016. Antimicrobial activity of biogenic silver nanoparticles, and silver chloride nanoparticles: an overview and comments. Appl. Microbiol. Biotechnol. 100, 6555–6570. https://doi.org/10.1007/s00253-016-7657-7

Durán, N., Silveira, C.P., Durán, M., Martinez, D.S.T., 2015. Silver nanoparticle protein corona and toxicity: a mini-review. J. Nanobiotechnology 13. https://doi.org/10.1186/s12951-015-0114-4

Egorova, E.M., Kaba, S.I., Kubatiev, A.A., 2016. Toxicity of silver nanoparticles obtained by bioreduction as studied on malignant cells, in: Nanobiomaterials in Cancer Therapy. Elsevier, pp. 505–542. https://doi.org/10.1016/B978-0-323-42863-7.00015-3

Eom, H.-J., Choi, J., 2010. p38 MAPK Activation, DNA Damage, Cell Cycle Arrest and Apoptosis As Mechanisms of Toxicity of Silver Nanoparticles in Jurkat T Cells. Environ. Sci. Technol. 44, 8337–8342. https://doi.org/10.1021/es1020668

Garcia, P.V., Seiva, F.R.F., Carniato, A.P., de Mello Júnior, W., Duran, N., Macedo, A.M., de Oliveira, A.G., Romih, R., Nunes, I. da S., Nunes, O. da S., Fávaro, W.J., 2016. Increased toll-like receptors and p53 levels regulate apoptosis and angiogenesis in non-muscle invasive bladder cancer: mechanism of action of P-MAPA biological response modifier. BMC Cancer 16. https://doi.org/10.1186/s12885-016-2474-z

Hackenberg, S., Scherzed, A., Kessler, M., Hummel, S., Technau, A., Froelich, K., Ginzkey, C., Koehler, C., Hagen, R., Kleinsasser, N., 2011. Silver nanoparticles: Evaluation of DNA damage, toxicity and functional impairment in human mesenchymal stem cells. Toxicol. Lett. 201, 27–33. https://doi.org/10.1016/j.toxlet.2010.12.001

Hsin, Y.-H., Chen, C.-F., Huang, S., Shih, T.-S., Lai, P.-S., Chueh, P.J., 2008. The apoptotic effect of nanosilver is mediated by a ROS- and JNK-dependent mechanism involving the mitochondrial pathway in NIH3T3 cells. Toxicol. Lett. 179, 130–139. https://doi.org/10.1016/j.toxlet.2008.04.015

Ibrahim M, N.M.E.D., 2015. Novel Trend in Colon Cancer Therapy Using Silver Nanoparticles Synthesized by Honey Bee. J. Nanomedicine Nanotechnol. 06. https://doi.org/10.4172/2157-7439.1000265

Ishida, T., 2017. Anticancer activities of silver ions in cancer and tumor cells and DNA damages by Ag+ - DNA base-pairs reactions. MOJ Tumor Res. 1, 1–0. https://doi.org/10.15406/mojtr.2017.01.00003

Ivashkevich, A., Redon, C.E., Nakamura, A.J., Martin, R.F., Martin, O.A., 2012. Use of the γ-H2AX assay to monitor DNA damage and repair in translational cancer research. Cancer Lett. 327, 123–133. https://doi.org/10.1016/j.canlet.2011.12.025

Kain, J., Karlsson, H.L., Möller, L., 2012. DNA damage induced by micro- and nanoparticles—interaction with FPG influences the detection of DNA oxidation in the comet assay. Mutagenesis 27, 491–500. https://doi.org/10.1093/mutage/ges010

Kalyanaraman, B., Darley-Usmar, V., Davies, K.J.A., Dennery, P.A., Forman, H.J., Grisham, M.B., Mann, G.E., Moore, K., Roberts, L.J., Ischiropoulos, H., 2012. Measuring reactive oxygen and nitrogen species with fluorescent probes: challenges and limitations. Free Radic. Biol. Med. 52, 1–6. https://doi.org/10.1016/j.freeradbiomed.2011.09.030

Kowshik, M., Ashtaputre, S., Kharrazi, S., Vogel, W., Urban, J., Kulkarni, S.K., Paknikar, K.M., 2003. Extracellular synthesis of silver nanoparticles by a silver-tolerant yeast strain MKY3. Nanotechnology 14, 95. https://doi.org/10.1088/0957-4484/14/1/321

Krishnaraj, C., Jagan, E.G., Rajasekar, S., Selvakumar, P., Kalaichelvan, P.T., Mohan, N., 2010. Synthesis of silver nanoparticles using Acalypha indica leaf extracts and its antibacterial activity against water borne pathogens. Colloids Surf. B Biointerfaces 76, 50–56. https://doi.org/10.1016/j.colsurfb.2009.10.008

Lim, H.K., Gurung, R.L., Hande, M.P., 2017. DNA-dependent protein kinase modulates the anti-cancer properties of silver nanoparticles in human cancer cells. Mutat. Res. Toxicol. Environ. Mutagen. 824, 32–41. https://doi.org/10.1016/j.mrgentox.2017.10.001

Locht, L.J., Smidt, K., Rungby, J., Stoltenberg, M., Larsen, A., 2011. Uptake of silver from metallic silver surfaces induces cell death and a pro-inflammatory response in cultured J774 macrophages. Histol. Histopathol. 26, 689–697.

Mirshafiee, V., Mahmoudi, M., Lou, K., Cheng, J., Kraft, M.L., 2013. Protein corona significantly reduces active targeting yield. Chem. Commun. 49, 2557. https://doi.org/10.1039/c3cc37307j

Nymark, P., Catalán, J., Suhonen, S., Järventaus, H., Birkedal, R., Clausen, P.A., Jensen, K.A., Vippola, M., Savolainen, K., Norppa, H., 2013. Genotoxicity of polyvinylpyrrolidone-coated silver nanoparticles in BEAS 2B cells. Toxicology, Nanotoxicology 313, 38–48. https://doi.org/10.1016/j.tox.2012.09.014

Ong, C., Lim, J.Z.Z., Ng, C.-T., Li, J.J., Yung, L.-Y.L., Bay, B.-H., 2013. Silver Nanoparticles in Cancer: Therapeutic Efficacy and Toxicity 10.

Petros, R.A., DeSimone, J.M., 2010. Strategies in the design of nanoparticles for therapeutic applications. Nat. Rev. Drug Discov. 9, 615–627. https://doi.org/10.1038/nrd2591

Rai, M. k., Deshmukh, S. d., Ingle, A. p., Gade, A. k., 2012. Silver nanoparticles: the powerful nanoweapon against multidrug-resistant bacteria. J. Appl. Microbiol. 112, 841–852. https://doi.org/10.1111/j.1365-2672.2012.05253.x

Rösslein, M., Elliott, J.T., Salit, M., Petersen, E.J., Hirsch, C., Krug, H.F., Wick, P., 2015. Use of Cause-and-Effect Analysis to Design a High-Quality Nanocytotoxicology Assay. Chem. Res. Toxicol. 28, 21–30. https://doi.org/10.1021/tx500327y

Safi, M., Courtois, J., Seigneuret, M., Conjeaud, H., Berret, J.-F., 2011. The effects of aggregation and protein corona on the cellular internalization of iron oxide nanoparticles. Biomaterials 32, 9353–9363. https://doi.org/10.1016/j.biomaterials.2011.08.048

Satapathy, S.R., Mohapatra, P., Preet, R., Das, D., Sarkar, B., Choudhuri, T., Wyatt, M.D., Kundu, C.N., 2013. Silver-based nanoparticles induce apoptosis in human colon cancer cells mediated through p53. Nanomed. 8, 1307–1322. https://doi.org/10.2217/nnm.12.176

Sintubin, L., De Windt, W., Dick, J., Mast, J., van der Ha, D., Verstraete, W., Boon, N., 2009. Lactic acid bacteria as reducing and capping agent for the fast and efficient production of silver nanoparticles. Appl. Microbiol. Biotechnol. 84, 741–749. https://doi.org/10.1007/s00253-009-2032-6

Souza, T.A.J., Franchi, L.P., Rosa, L.R., da Veiga, M.A.M.S., Takahashi, C.S., 2016. Cytotoxicity and genotoxicity of silver nanoparticles of different sizes in CHO-K1 and CHO-XRS5 cell lines. Mutat. Res. Toxicol. Environ. Mutagen. 795, 70–83. https://doi.org/10.1016/j.mrgentox.2015.11.002

Swasey, S.M., Leal, L.E., Lopez-Acevedo, O., Pavlovich, J., Gwinn, E.G., 2015. Silver (I) as DNA glue: Ag+-mediated guanine pairing revealed by removing Watson-Crick constraints. Sci. Rep. 5, 10163. https://doi.org/10.1038/srep10163

Wolf, B.B., Schuler, M., Echeverri, F., Green, D.R., 1999. Caspase-3 Is the Primary Activator of Apoptotic DNA Fragmentation via DNA Fragmentation Factor-45/Inhibitor of Caspase-activated DNase Inactivation. J. Biol. Chem. 274, 30651–30656. https://doi.org/10.1074/jbc.274.43.30651

Zhao, X., Takabayashi, F., Ibuki, Y., 2016. Coexposure to silver nanoparticles and ultraviolet A synergistically enhances the phosphorylation of histone H2AX. J. Photochem. Photobiol. B 162, 213–222. https://doi.org/10.1016/j.jphotobiol.2016.06.046.

Capítulo 5 - Discussão

Durán, N., Rolim, W., Durán, M., Fávaro, W., and Seabra, A., 2018. Nanotoxicologia de nanopartículas de prata: toxicidade em animais e humanos. Química Nova, 42 (2), 206–213.

Elbatreek, M.H., Pachado, M.P., Cuadrado, A., Jandeleit-Dahm, K., and Schmidt, H.H.H.W., 2019. Reactive Oxygen Comes of Age: Mechanism-Based Therapy of Diabetic End-Organ Damage. Trends in Endocrinology & Metabolism, 30 (5), 312–327.

Foldbjerg, R., Olesen, P., Hougaard, M., Dang, D.A., Hoffmann, H.J., and Autrup, H., 2009. PVP-coated silver nanoparticles and silver ions induce reactive oxygen species, apoptosis and necrosis in THP-1 monocytes. Toxicology Letters, 190 (2), 156–162.

Ghezzi, P., Jaquet, V., Marcucci, F., and Schmidt, H.H.H.W., 2017. The oxidative stress theory of disease: levels of evidence and epistemological aspects. British Journal of Pharmacology, 174 (12), 1784–1796.

Hsin, Y.-H., Chen, C.-F., Huang, S., Shih, T.-S., Lai, P.-S., and Chueh, P.J., 2008. The apoptotic effect of nanosilver is mediated by a ROS- and JNK-dependent mechanism involving the mitochondrial pathway in NIH3T3 cells. Toxicology Letters, 179 (3), 130–139.

Ishida, T., 2017. Anticancer activities of silver ions in cancer and tumor cells and DNA damages by Ag+ - DNA base-pairs reactions. MOJ Tumor Research, 1 (1), 1–0.

Kim, S. and Ryu, D.-Y., 2013. Silver nanoparticle-induced oxidative stress, genotoxicity and apoptosis in cultured cells and animal tissues: Silver nanoparticle-induced toxicity. Journal of Applied Toxicology, 33 (2), 78–89.

de Lima, R., Seabra, A.B., and Durán, N., 2012. Silver nanoparticles: a brief review of cytotoxicity and genotoxicity of chemically and biogenically synthesized nanoparticles. Journal of Applied Toxicology, 32 (11), 867–879.

Mendonça, M.C.P., Ferreira, L.B., Rizoli, C., Batista, Â.G., Maróstica Júnior, M.R., da Silva, E. do N., Cadore, S., Durán, N., Cruz-Höfling, M.A. da, and de Jesus, M.B., 2018. N-Acetylcysteine reverses silver nanoparticle intoxication in rats. Nanotoxicology, 1–13.

Ong, C., Lim, J.Z.Z., Ng, C.-T., Li, J.J., Yung, L.-Y.L., and Bay, B.-H., 2013. Silver Nanoparticles in Cancer: Therapeutic Efficacy and Toxicity, 10.

Satapathy, S.R., Mohapatra, P., Preet, R., Das, D., Sarkar, B., Choudhuri, T., Wyatt, M.D., and Kundu, C.N., 2013. Silver-based nanoparticles induce apoptosis in human colon cancer cells mediated through p53. Nanomedicine, 8 (8), 1307–1322.

Zhornik, E.V., Baranova, L.A., Drozd, E.S., Sudas, M.S., Chau, N.H., Buu, N.Q., Dung, T.T.N., Chizhik, S.A., and Volotovski, I.D., 2014. Silver nanoparticles induce lipid peroxidation and morphological changes in human lymphocytes surface. Biophysics, 59 (3), 380–386.

CAPÍTULO 8 - Apêndices

1. Artigos publicados em revistas científicas

1.1. Effects of intravesical therapy with platelet-rich plasma (PRP) and Bacillus Calmette-Guérin (BCG) in non-muscle invasive bladder cancer

Tissue and Cell 52 (2018) 17–27

Contents lists available at ScienceDirect

Tissue and Cell

journal homepage: www.elsevier.com/locate/tice

Effects of intravesical therapy with platelet-rich plasma (PRP) and *Bacillus Calmette-Guérin* (BCG) in non-muscle invasive bladder cancer

Lara Paro Dias[a], Ângela C. Malheiros Luzo[b], Bruno B. Volpe[b], Marcela Durán[a], Sofia E.M. Galdames[c], Luiz A.B. Ferreira[d], Nelson Durán[c,f], Wagner J. Fávaro[a,c,*]

[a] Laboratory of Urogenital Carcinogenesis and Immunotherapy, Department of Structural and Functional Biology, University of Campinas (UNICAMP), Campinas, SP, Brazil
[b] Public Umbilical Cord Blood Bank, Haematology Hemotherapy Center/INCT do Sangue, University of Campinas (UNICAMP), Campinas, Brazil
[c] Department of Engineering of Materials and Bioprocesses, School of Chemical Engineering, University of Campinas (UNICAMP), Campinas, SP, Brazil
[d] Department of Biochemistry and Tissue Biology, Institute of Biology, University of Campinas (UNICAMP), Campinas, SP, Brazil
[e] NanoBioss, Institute of Chemistry, University of Campinas (UNICAMP), Campinas, SP, Brazil
[f] Nanomedicine Research Unit (Nanomed), Federal University of ABC (UFABC), Santo André, Brazil

ARTICLE INFO

Keywords:
Platelet-rich plasma
Bladder cancer
Immunotherapy
Bacillus Calmette-Guerin

ABSTRACT

This study describes the effects of a promising therapeutic alternative for non-muscle invasive bladder cancer (NMIBC) based on *Bacillus Calmette-Guerin* (BCG) intravesical immunotherapy combined with Platelet-rich plasma (PRP) in an animal model. Furthermore, this study describes the possible mechanisms of this therapeutic combination involving Toll-like Receptors (TLRs) 2 and 4 signaling pathways. NMIBC was induced by treating female Fischer 344 rats with *N-methyl-N-nitrosourea* (MNU). After treatment with MNU, the animals were distributed into four experimental groups: Control (without MNU) group, MNU (cancer) group, MNU + PRP group, MNU + BCG group and MNU + PRP + BCG group. Our results demonstrated that PRP treatment alone or associated with BCG triggered significant cytotoxicity in bladder carcinoma cells (HTB-9). Animals treated with PRP associated to BCG clearly showed better histopathological recovery from the cancer state and decrease of urothelial neoplastic lesions progression in 70% of animals when compared to groups that received the same therapies administered singly. In addition, this therapeutic association led to distinct activation of immune system TLRs 2 and 4-mediated, resulting in increased MyD88, TRIF, IRF3, IFN-γ immunoreactivities. Taken together, the data obtained suggest that interferon signaling pathway activation by PRP treatment in combination with BCG immunotherapy may provide novel therapeutic approaches for non-muscle invasive bladder cancer.

1.2. N-Acetylcysteine reverses silver nanoparticle intoxication in rats

NANOTOXICOLOGY
https://doi.org/10.1080/17435390.2018.1544302

N-Acetylcysteine reverses silver nanoparticle intoxication in rats

Monique Culturato Padilha Mendonça[a*], Luiz Bandeira Ferreira[a*], Cintia Rizoli[a], Ângela Giovana Batista[b], Mário Roberto Maróstica Júnior[b], Emanueli do Nascimento da Silva[c], Solange Cadore[c], Nelson Durán[c,d], Maria Alice da Cruz-Höfling[a] and Marcelo Bispo de Jesus[a]

[a]Department of Biochemistry and Tissue Biology, Institute of Biology, University of Campinas, São Paulo, Brazil; [b]Department of Food and Nutrition, University of Campinas, São Paulo, Brazil; [c]Institute of Chemistry, University of Campinas, São Paulo, Brazil; [d]Nanomedine Units, Federal University of ABC (UFABC), São Paulo, Brazil

ABSTRACT

The increasing use of silver nanoparticles (AgNPs) in consumer products raises the risk of human toxicity. Currently, there are no therapeutic options or established treatment protocols in cases of AgNPs intoxication. We demonstrated previously that thiol antioxidants compounds can reverse the cytotoxicity induced by AgNPs in Huh-7 hepatocarcinoma cells. Here, we investigated the use of N-acetylcysteine (NAC) against the systemic toxic effects of AgNPs (79.3 nm) in rats. Biochemical, histopathological, hematological, and oxidative parameters showed that a single intravenous injection of AgNPs (5 mg/kg b.w.) induced deleterious effects such as hepatotoxicity, potentially as a result of AgNPs accumulation in the liver. Treatment with a single intraperitoneal injection of NAC (1 g/kg b.w.) one hour after AgNPs exposure significantly attenuated all toxic effects evaluated and altered the bioaccumulation and release patterns of AgNPs in rats. The findings show that NAC may be a promising candidate for clinical management of AgNPs intoxication.

ARTICLE HISTORY
Received 17 July 2018
Accepted 31 October 2018

KEYWORDS
Nanotoxicology; metallic nanoparticles; thiol compounds; glutathione; ascorbic acid

2. Depósitos de patentes nacionais

2.1. BR102017004724-5

Favaro, W. J. ; Souza, J. G. ; Dini, A. X. P. ; Muniz, M. S. ; Matsumoto, M. Y. ; **Ferreira, L. A. B.** ; de Jesus, M. B. ; Duran, N. *Processo de obtenção e funcionalização de carreador lipídico nanoestruturado à base de lipídios vegetais, carreador lipídico nanoestruturado e usos*. Instituto Nacional da Propriedade Industrial (INPI); 09/03/2017.

DESTAQUE INOVA 2017

2.2. BR102017018129-4

Favaro, W. J. ; **Ferreira, L. A. B.** ; Garcia, P. V. ; de Jesus, M. B. ; Duran, N. *Processo de obtenção de nanopartículas biossintéticas de prata, nanopartículas biossintéticas de prata obtidas e seu uso*. Instituto Nacional da Propriedade Industrial (INPI); 24/08/2017.

DESTAQUE INOVA 2017

República Federativa do Brasil
Ministério da Economia
Instituto Nacional da Propriedade Industrial

(21) BR 102017018129-4 A2

(22) Data do Depósito: 24/08/2017

(43) Data da Publicação Nacional: 26/03/2019

(54) Título: PROCESSO DE OBTENÇÃO DE NANOPARTÍCULAS BIOSSINTÉTICAS DE PRATA, NANOPARTÍCULAS BIOSSINTÉTICAS DE PRATA OBTIDAS E SEU USO

(51) Int. Cl.: C12P 3/00; C12P 1/02; C12R 1/77; C22B 11/00; B82B 3/00; (...).

(71) Depositante(es): UNIVERSIDADE ESTADUAL DE CAMPINAS - UNICAMP.

(72) Inventor(es): WAGNER JOSÉ FÁVARO; LUIZ ALBERTO BANDEIRA FERREIRA; PATRICK VIANNA GARCIA; MARCELO BISPO DE JESUS; NELSON EDUARDO DURÁN CABALLERO.

(57) Resumo: PROCESSO DE OBTENÇÃO DE NANOPARTÍCULAS BIOSSINTÉTICAS DE PRATA, NANOPARTÍCULAS BIOSSINTÉTICAS DE PRATA OBTIDAS E SEU USO. A presente invenção refere-se a um processo de obtenção de nanopartículas biossintéticas de prata através da redução da prata por enzimas e substratos presentes em solução obtidas após a filtração da biomassa do fungo Fusarium oxysporum. Adicionalmente, a presente invenção refere-se as referidas nanopartículas obtidas, assim como ao uso das mesmas para o preparo de um medicamento para tratar o câncer de bexiga.

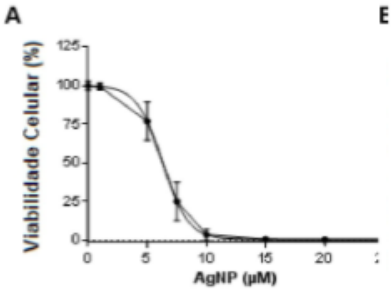

3. Resumos apresentados em congressos

Sociedade Brasileira de Bioquímica e Biologia Molecular — SBBq

45ª Reunião Anual da SBBq
18 a 21 de junho de 2016 - Natal, RN

Endocytosis and intracellular trafficking of Solid Lipid Nanoparticles gene delivery system in HEK cells

Radaic, A.; Ferreira, L.A.B.; Campese, G.; de Jesus, MB

Nano-Cell Interactions Lab., Department of Biochemistry and Tissue Biology,

Institute of Biology, University of Campinas, UNICAMP, Campinas, SP, Brazil

INTRODUCTION: Plasma membrane is selectively permeable, which makes it impermeable for most of nanomaterials. Therefore, nanomaterials must exploit endocytic pathways to gain entry into the cell. Determining the specific endocytic pathway of the nanoparticles is important to understand the mechanisms involved in their intracellular fate, biological effect and possible toxicity. **OBJECTIVE:** We aim to determine the endocytic pathway and intracellular trafficking solid lipid nanoparticles as gene delivery system in HEK cells. **MATERIAL AND METHODS:** We used labeled nanoparticles in presence of inhibitors to determine the internalization pathway. Co-localization of nanoparticles with lysosomalassociated membrane protein 1 (LAMP1) was performed using confocal microscopy. Finally, we used chloroquine, a lysosomotropic agent that prevents endosomal acidification, to test the endosomal acidification in DNA release mechanism. **RESULTS AND DISCUSSION**: Internalization in presence of inhibitors showed that chlorpromazine, inhibitor of clathrin-mediated endocytosis, significantly decreased the uptake and the transfection efficiency of solid lipid nanoparticles in HEK cells. Co-localization with LAMP1 reached the higher levels after 6h of treatment. The lysosomotropic agent dropped significantly the transfection efficiency, indicating that endosomal acidification could be associated to DNA release mechanism. **CONCLUSION:** Solid lipid nanoparticles gained access into HEK cells mainly via clathrin-mediated endocytosis. Nanoparticles were driven to lysosomal compartment within 6h. Finally, the acidification can be vital for DNA release, as indicated by transfection in presence of chloroquine.

Keywords: solid lipid nanoparticles, transfection, gene delivery, intracellular trafficking, endocytosis.

Support: FAPESP, CNPq and CAPES

II Workshop in Environmental Nanotechnology
December 07th to 09th, 2016 - Auditorium of UNESP - Campus Sorocaba

Biogenic silver nanoparticles induce oxidative stress, autophagy and necropstosis death in primary elicited peritoneal macrophages

Ferreira, L.A.B.[1], Farias, A.S.[2], Duran, N.[3], Marcato, P.D.[3,4], de Jesus, M.B.[1]

[1] Department of Structural and Functional Biology, University of Campinas, Campinas, SP, Brazil;
[2] Department of Genetics, Evolution and Bioagents, University of Campinas, Campinas, SP, Brazil;
[3] Biological Chemistry Laboratory, Institute of Chemistry, University of Campinas, Campinas, SP, Brazil; [4] Faculty of Pharmaceutical Sicience Ribeirão Preto, University of São Paulo, Ribeirão Preto, SP, Brasil

Silver Nanoparticles (AgNPs) have been incorporated into many products due to its broad-spectrum antimicrobial activity. However, the increased use of this nanomaterial has grown the concern about its exposure, disposal, and possible toxic effects. The knowledge about toxic effects and the mechanisms of cellular response is critical for achieving safe applications of nanomaterials. In this work, we investigated the cytotoxic molecular mechanisms of biogenic silver nanoparticle in thioglycollate-elicited peritoneal macrophages. We determined that the cytotoxic effects of AgNP are dose and time-dependent (IC_{50} of 25 µM at 6 h of treatment). Several biochemical alterations were found upon AgNP treatment within 6 h; for example, the generation of ROS, lipid peroxidation of cell membrane and mitochondrial depolarization. In addition, we observed the increase in LC3-II expression within 3 hours, which could be related to the stimulation of autophagic flux. Finally, AgNP induced necroptosis cell death in macrophages, showed by the absence of DNA degradation (a biochemical hallmark of apoptosis) and the mitigation of the cytotoxicity in the presence of necroptosis inhibitor (RIP-1). Therefore, this acute cytotoxic dosedependent effect of biogenic AgNP is a potential risk factor for the maintenance of cellular homeostasis, contributing to many intracellular events leading to cell death. Elucidating these mechanisms is a key for the development of safer nanomaterials application and more effective anti-microbial products in the future.

Keywords: Silver nanopartícles, biogenic, elicited peritoneal macrophages, cytotoxic molecular mechanisms
Financial Support & Acknowledgements: CAPES

- **Premiação de melhor pôster do evento**

BIOGENIC SILVER NANOPARTICLES INDUCE HEPATIC TOXICITY AND OXIDATIVE STRESS IN MALE WISTAR RATS

Luiz A. B. Ferreira[1]; Monique C. P. Mendonça[1]; Ângela G. Batista[2], Emanueli do Nascimento da Silva[3]; Mário R. M. Junior[2]; Maria A. da Cruz Hofling[1]; Solange Cadore[3]; Nelson Duran[4]; Marcelo B. de Jesus[1]*

[1]Department Biochemistry & Tissue Biology, Biology Institute, University of Campinas, Campinas, SP, Brazil.
[2]Department of Food and Nutrition, School of Food Engineering, University of Campinas, Campinas, SP, Brazil.
[3]Department of analytical chemistry, Institute of Chemistry, University of Campinas, Campinas, SP, Brazil.
[4]Biological Chemistry Laboratory, Institute of Chemistry, University of Campinas, Campinas, SP, Brazil.

Key Words: *Biogenic silver nanoparticle, hepatic toxicity, cytotoxic effects.*

Silver nanoparticles show broad antimicrobial spectrum and have been incorporated into many products, such as food, textiles, cosmetics, and healthcare. The long-term exposure to nanosilver products contrasts with the lack of knowledge about the toxic effects to human health. In this work, we investigated the molecular mechanisms of cytotoxicity of biogenic silver nanoparticle *in vivo* (male Wistar rats) and *in vitro* (Huh-7 hepatocarcinoma cell line). *In vivo* studies showed that animals treated with sub-lethal doses of AgNP (5mg/kg IV) increased hepatic toxicity markers levels (ALT, AST, and Alkaline phosphatase) and the antioxidant enzymes (GSH and TBARS). Furthermore, the atomic absorption spectrometry graphite furnace analysis demonstrated the accumulation of silver in the liver, which corroborates the increase in toxicity. *In vitro* studies showed that the cytotoxic effects of AgNP are dose-dependent (IC_{50} 10 µM) and related to the reactive oxygen species level increase. Therefore, this acute toxicity effect of biogenic AgNP is a potential risk factor for the maintenance of cellular homeostasis. Elucidating these mechanisms is a key for the development of safer nanomaterials application and more effective anti-microbial products in the future.

A91249Md

N-Acetylcysteine as antidote for silver nanoparticles intoxication

MENDONÇA Monique C. P. [1], FERREIRA Luiz Bandeira [1], RIZOLI Cintia [1], SILVA Emanueli do Nascimento [2], DURÁN Nelson [2,3], CADORE Solange [2], CRUZ-HÖFLING Maria Alice [1], **DE JESUS Marcelo Bispo** [1]

(1) University of Campinas, Institute of Biology, Department of Biochemistry and Tissue Biology, 13083-862, Campinas, Brazil., Campinas, Brazil; (2) Institute of Chemistry, University of Campinas, Campinas, SP, Brazil, Campinas, Brazil; (3) Nanomedine Units, Federal University of ABC (UFABC), Santo André, Brazil

The use of silver nanoparticles (AgNP) in consumer products is growing exponentially. Consequently, increases the human exposure to AgNP significantly when handling during manufacturing, using and disposing of AgNP-containing products. In cases of AgNP poisoning, the medical procedure is not established yet. We found that thiol-containing antioxidants NAcetylcysteine (NAC) could act as chelating agent in vitro for AgNP, reverting their cytotoxic effects. Here, we hypothesized that NAC could act as an antidote for AgNP intoxication in vivo. AgNP (5 mg/kg) led o increase in serum biochemical parameters of the hepatic function (aspartate aminotransferase (AST), alanine aminotransferase (ALT), and alkaline phosphatase (ALP)) in adult male Wistar rats compared to control. All biochemical parameters showed physiological values after a single administration of NAC (1g/kg) one hour after injection of AgNP. In accordance with liver biochemistry results, the hepatic tissue of AgNP group exhibited inflammatory cell infiltration at the hepatic portal system, while no visible alteration was observed in hepatic parenchyma of the AgNP+NAC group. Immediately after AgNP injection, the hind paws exhibited a dark bluish color suggesting inadequate oxygenation of the blood. Compared to the control group, AgNP group showed a decrease in many blood parameters such as red blood cells, hemoglobin, hematocrit levels, and platelet count. No alterations in hematological parameters were found in the animals treated with AgNP+NAC. The white blood cells (WBC) count was higher in the AgNP group when compared to control, NAC and AgNO3 groups. Typically, an increased number of WBC is associated with inflammation, whose was shown above at the liver portal system of AgNP-treated animals. A significant density of Kupffer cells was found nearby the portal area; although, in animals treated with AgNP+NAC, the population of Kupffer cells was more rarefied. The treatment with NAC led to an altered silver biodistribution, which would avoid their accumulation in the liver while increasing their renal excretion. Overall, we conclude that NAC reversed toxic effects of AgNP, and could to be a potential candidate for early intervention in cases of AgNP intoxication.

A91250Md

Thiol-antioxidants binding to silver nanoparticles interfering with cytotoxicity assessment

FERREIRA Luiz Bandeira [1], BERNARDES Juliana da Silva [4], DURÁN Nelson[2,3], **DE JESUS Marcelo Bispo** [1]

(1) University of Campinas, Institute of Biology, Department of Biochemistry and Tissue Biology, 13083-862, Campinas, Brazil., Campinas, Brazil; (2) Institute of Chemistry, University of Campinas, Campinas, SP, Brazil, Campinas, Brazil; (3) Nanomedine Units, Federal University of ABC (UFABC), Santo André, Brazil; (4) Brazilian Center for Research in Energy and Materials, CNPEM, Campinas, Brazil

Cytotoxicity of chemically and biologically synthesized silver nanoparticle (AgNP) have been broadly investigated, and the oxidative stress is generally presumed as the primary mechanism of cell death. Most of these studies rely on antioxidants to establish this cause-and-effect relationship; however, details on how these antioxidants interact with AgNP are often neglected. Therefore, we decided to study interferences of interaction between thiolantioxidants (N-acetyl-L-cysteine, L-cysteine, and glutathione) or non-thiol-antioxidants (Trolox and ascorbic acid) with AgNP. Our results showed that both antioxidants families mitigated the production of ROS in Huh7 hepatocarcinoma cells upon AgNP treatment. However, thiolantioxidants can reverse the cytotoxic effect, whereas non-thiol-antioxidants are unable to reverse the cytotoxic effect. Further, we found that the mitigation of cytotoxicity correlates with the chelation capacity of the antioxidant, demonstrated through the aggregation assays using dynamic light scattering technique and silver-thiol bonding confirmed by X-ray photoelectron. Our findings show that the care should be taken in the interpretation of cytotoxicity when studying metallic nanoparticles with thiol-antioxidants. Determining the correct mechanisms underlying the cytotoxic effects of nanoparticles is critical to promote the progress of nanotechnology.

A91688WF

Association of Graphene Oxide Derivatives for Non-Muscle Invasive Bladder Cancer (NMIBC) Treatment.

FÁVARO Wagner [1,2], DE SOUZA Joel G. [1], MATSUMOTO Mirian Y. [1], FERREIRA Luiz A.B. [3], DE JESUS Marcelo B. [3], DURÁN Marcela [1,2], DURÁN Nelson [1, 2, 4]

(1) Laboratory of Urogenital Carcinogenesis and Immunotherapy, Department of Structural and Functional Biology, University of Campinas (UNICAMP), Campinas-SP, Brazil; (2) NanoBioss, Institute of Chemistry, University of Campinas (UNICAMP), Campinas-SP, Brazil;
(3) Department of Biochemistry and Tissue Biology, Institute of Biology, University of Campinas (UNICAMP), Campinas-SP, Brazil; (4) Nanomedicine Research Unit (Nanomed), Federal University of ABC (UFABC), Santo André-SP, Brazil

The most widely used therapy modality for the treatment of bladder cancer (BC) is based on the intravesical administration ofBacillus Calmette-Guérin (BCG) associated with transurethral resection. Despite the anticancer activity of BCG, a significant number of patients exhibited intolerance, besides potentially fatal complications, such as systemic BCG infection. Furthermore, 50% of non-muscle invasive bladder cancer (NMIBC) tumors have recurrence within 4 years after treatment. Doxorubicin (DOX) is a chemotherapeutic agent in transitional cell carcinoma of the urinary bladder, but when this drug is administered systemically in certain doses it can induce cardiac toxicity and myelosuppression. Besides DOX, after the recent discovery of interference RNA (siRNA), these substances started to be studied by silencing genes associated with cancer. In this work, we developed graphene oxide (GO) hybrids for administration of DOX and siRNA for VEGF (vascular endothelial growth factor). Furthermore, we associated GO hybrids containing DOX and siRNA. For the transport of DOX, GO was initially carboxylated in order to bind DOX through amide bond formation. For the delivery of siRNA for VEGF, GO was covalently bonded to polyethylene glycol (PEG), and also to the cationic polyethyleneimine (PEI) for allowing complexation. Ultimately, the hybrids were administered in vivo (Fischer 344 rats) in order to investigate the antitumor effect against NMIBC. The ultrasonography of the rat´s bladder revealed that 60% of the animals treated with GO carboxylated and DOX did not show apparent signs of lesions, while 100% of the animals treated with free DOX showed those signs. Concerning the animals which were treated with GO-PEG-PEI-siRNA, only 20% of them showed signs of lesions. Finally, the association compound GO-PEG-PEI-siRNA-DOX resulted in the absence of lesions. Histopathological analyzes showed that GO derivatives containing DOX or siRNA reduced the aggressiveness of NMIBC. It is worth to mention that the association between GO-COOH-DOX and GO-PEGPEI / siRNA potentiated the action on the reduction of the aggressiveness of the tumors, since 60% of the animals treated with this association showed no signs of lesions. Therefore, the GO derivatives represent a promising strategy for NMIBC.

Acknowledgement: This work was supported by NanoBioss/Sisnano (CNPq-Brazil, Process number 402280/2013-0), INOMAT (CNPq/MCTI), Brazilian Network of Nanotoxicology (CIGENANOTOX) and FAPESP.

A91686WF

NANOTOXICOLOGICAL ASPECTS OF BACILLUS CALMETTE-GUÉRIN THERAPY ASSOCIATED TO PLATELET-RICH PLASMA 16-970 nm ON BLADDER CANCER

FÁVARO Wagner J. [1,2], LUZO Ângela C.M. [3], VOLPE Bruno B. [1,3], GALDAMES Sofia E.M. [4], FERREIRA Luiz A.B. [5], DURÁN Marcela [1,2], DURÁN Nelson [1,2,6], DIAS Lara P. [1] (1) Laboratory of Urogenital Carcinogenesis and Immunotherapy, Department of Structural and Functional Biology, University of Campinas (UNICAMP), Campinas-SP, Brazil; (2) NanoBioss, Institute of Chemistry, University of Campinas (UNICAMP), Campinas-SP, Brazil; (3) Public Umbilical Cord Blood Bank, Haematology Hemotherapy Center/INCT do Sangue, University of Campinas (UNICAMP), Campinas-SP, Brazil; (4) Department of Engineering of Materials and Bioprocesses, School of Chemical Engineering, University of Campinas (UNICAMP), Campinas-SP, Brazil; (5) Department of Biochemistry and Tissue Biology, Institute of Biology, University of Campinas (UNICAMP), Campinas-SP, Brazil; (6) Nanomedicine Research Unit (Nanomed), Federal University of ABC (UFABC), Santo AndréSP, Brazil

For many years on Bacillus Calmette-Guérin (BCG) intravesical immunotherapy is using on non-muscle invasive bladder cancer (NMIBC). Our study describes the effects of a promising therapeutic alternative for this standard treatment. A new combination of BCG with Plateletrich plasma (PRP) (16 nm [exosomes], 105 nm [microparticles] and 972 nm [microaggregates] with 2%, 26% and 72%, respectively) 1 in an animal model was studied. Interesting, this study describes the possible mechanisms of this therapeutic combination involving Toll-like Receptors (TLRs) 2 and 4 signaling pathways. NMIBC was induced by treating female Fischer 344 rats with N-methyl-N-nitrosourea (MNU). The animal experiments were approved by an institutional Committee for Ethics in Animal Use (CEUA/UNICAMP, protocol no. 3901-1. After treatment with MNU, the animals were distributed into four experimental groups: Control (without MNU) group, MNU (Cancer) group, MNU+PRP group, MNU+BCG group and MNU+PRP+BCG group. Data from in vitrostudy demonstrated that PRP treatment alone or associated with BCG triggered significant cytotoxicity in bladder carcinoma cells (HTB-9). Sixty female Fischer 344 rats seven weeks old treated with PRP associated to BCG clearly showed better histopathological recovery from the cancer state and decrease of urothelial neoplastic lesions progression in around 70-75% of rats when compared to groups that received the monotherapies administered separated. The rats from Control and Control+PRP groups showed intense and moderate TRIF and IRF3 immunoreactivities, respectively in relation to MNU group, which exhibited weak immunoreactivities. The animals from MNU+BCG and MNU+PRP exhibited moderate immunoreactivities for theses antigens. The combined treatment with PRP and BCG was able to increase TRIF and IRF3 immunoreactivities. Besides this, therapeutic association led to distinct activation of immune system TLRs 2 and 4mediated, resulting in increased MyD88, TRIF, IRF3, IFN-γimmunoreactivities. In conclusion, our results obtained suggest that interferon signaling pathway activation by PRP treatment in combination with BCG immunotherapy may allow novel therapeutic boards for non-muscle invasive bladder cancer.Acknowledgement: This work was supported by NanoBioss/Sisnano (CNPq-Brazil, Process number 402280/2013-0), INOMAT (CNPq/MCTI), Brazilian Network of Nanotoxicology (CIGENANOTOX), and FAPESP.

Reference: 1. Maurer-Spurej, E. et al. Transf. Apheresis Sci. 55, 35 (2016)

A91687WF

NANOSTRUCTURED LIPID CARRIER Co-LOADED WITH DOXORUBICIN AND siRNA: ITS TOXICITY AND ANTITUMOR ACTIVITY AGAINST BLADDER CANCER

FÁVARO Wagner [1,2], DE SOUZA Joel G. [1], DINI Alzira X.P. [2], MUNIZ Miriam S. [1], MATSUMOTO Mirian Y. [1], FERREIRA Luiz A.B. [3], DE JESUS Marcelo B. [3], DURÁN Nelson [1,2,4]

(1) Laboratory of Urogenital Carcinogenesis and Immunotherapy, Department of Structural and Functional Biology, University of Campinas (UNICAMP), Campinas-SP, Brazil; (2) NanoBioss, Institute of Chemistry, University of Campinas (UNICAMP), Campinas-SP, Brazil;
(3) Department of Biochemistry and Tissue Biology, Institute of Biology, University of Campinas (UNICAMP), Campinas-SP, Brazil; (4) Nanomedicine Research Unit (Nanomed), Federal University of ABC (UFABC), Campinas-SP, Brazil

The nanostructured lipid carrier (NLC) was prepared from two solid lipids Cupuaçu butter and bis-diglyceryl polyacyladipate-2 at 60:40 and buriti oil (25%) as liquid lipid and stabilized by a surfactant 1.5% of Pluronic F68 and behentrimomiun chloride (cationic surfactant) loaded with Doxorrubicina (DOX) in a high pressure homogenizer at 5.000 a 20.000 rpm. The use of NLC with DOX and the histopathological analyses showed on induced rats with non-muscle invasive bladder cancer (NMIBC) that 20% of the rats exhibited benign lesions (papillary hyperplasia) and 80% malignant lesions. Besides this, considering the malignant lesions, 40% were Highgrade Papillary Carcinoma (pTa), 20% Low-grade Papillary Carcinoma (pTa) and 20% lesions of Urothelial Carcinoma with invasive of lamina Propria (pT1). The histopathology analyses of the treatment only with free DOX demonstrated a 25% of animals exhibited papillary hyperplasia, 50% High-grade Papillary Carcinoma (pTa) and 25% Urothelial Carcinoma with invasive Lamina propria. The use of NLC/siRNA (vascular endothelial growth factor (VEGF)) showed 40% of the animals exhibited benign lesions (Papillary hyperplasia) and 60% malignant lesions. However, the malignant lesions 20% were of the Papillary Carcinoma in situ (pTis) and 40% of Low-grade Papillary Carcinoma (pTa) (Table 1). Our results are indicative that NLC/siRNA reduced the severity of NMIBC related to free DOX as also with DOXIL®. Then, the NLC/siRNA/DOX appears as an excellent anticancer nanocarrier with very low toxicity.

Acknowledgement: This work was supported by NanoBioss/Sisnano (CNPq-Brazil, Process number 402280/2013-0), INOMAT (CNPq/MCTI), Brazilian Network of Nanotoxicology (CIGENANOTOX – MCTI/CNPq), and FAPESP.

Histopathology	Squamous metaplasia and urothelial carcinoma with invasion of the lamina propria (pT1)	Urothelial carcinoma with invasion of the lamina propria (pT1)	High grade papillary carcinoma (pTa)	Low-grade papillary carcinoma (pTa)	Carcinoma in situ (pTis)	Papillary hyperplasia	Normal
Injury type	Malignant	Malignant	Malignant	Malignant	Malignant	Benign	———
Control n=5	———	———	———	———	———	———	5 (100%)
MNU Cancer n=5	———	3 (40%)	2 (40%)	1 (20%)	———	———	
DOX n= 4	———	1 (25%)	2 (50%)	———	———	1 (25%)	
NCL n=5	1 (20%)	1 (20%)	2 (40%)	1 (20%)	———	———	
NCL-DOX n=5	———	1 (20%)	2 (40%)	1 (20%)	———	1 (20%)	
NCL-DOX-siRNA n=5	———	———	———	2 (40%)	1 (20%)	2 (40%)	
BCG n=5	3 (60%)	2 (40%)	———	———	———	———	

A91690WF

CYTOTOXICITY AND ANTIUMOR ACTIVITY OF BIOGENIC SILVER NANOPARTICLES AGAINST NON-MUSCLE INVASIVE BLADDER

BANDEIRA Luiz A.B. [1], FÓSSA Fernanda G. [1], DE JESUS Marcelo B. [1], DURÁN Nelson[2,3,4], **FÁVARO Wagner J.** [2,3]

(1) Nano-cell Interactions Lab.; Department Biochemistry & Tissue Biology, Biology Institute, University of Campinas (UNICAMP), Campinas-SP, Brazil; (2) Laboratory of Urogenital Carcinogenesis and Immunotherapy, Department of Structural and Functional Biology, University of Campinas (UNICAMP), Campinas-SP, Brazil; (3) NanoBioss, Institute of Chemistry, University of Campinas (UNICAMP), Campinas-SP, Brazil; (4) Nanomedicine Research Unit (Nanomed), Federal University of ABC (UFABC), Campinas-SP, Brazil

Bladder cancer is the fifth most common form of malignancy in the United States, and for most of the last three decades, the treatment and outcomes for patients with this disease have not changed. Nanomedicine aims to provide the means to target chemotherapies directly and selectively to cancerous cells and enhance their therapeutic efficacy. In this scenario, we employed biogenic Silver Nanoparticles (AgNPs) as an anticancer agent against non-muscle invasive bladder cancer (NMIBC). Bladder cancer was chemically induced with N-methyl-Nnitrosourea (MNU) on C57BL/6Junib female mice and treated by intravesical route with biogenic silver nanoparticles concentrations of 0.5, 0.2, and 0.05 mg/mL. The histopathological analyzes showed the treated with AgNP 0.5 group presented 50% of pTa and 50% of pTis, indicating that this treatment was not effective in regressing the neoplastic lesions. MNU + AgNP 0.2 group showed 50% of tumor regression, and 50% of the animals presented flat hyperplasia. Finally, treatment with 0.05 AgNP led to 100% tumor regression, with 50% of the animals showing normal urothelium and 50% showing flat hyperplasia, considering a benign lesion. Further, to understand the antitumor effect of AgNPs, we evaluated the molecular mechanism of cytotoxicity in human bladder carcinoma 5637 cell. The results showed the dose-time dependent cytotoxicity, and detailed analysis demonstrated induction of cell death via apoptosis. Besides, we found that AgNP inhibition in cell migration and proliferation. Thus, these findings confirm the antitumor properties of AgNPs, and suggest that they may be a costeffective alternative and promising candidate for the treatment of bladder cancer.

Keywords: Biogenic silver nanoparticle; bladder cancer; apoptosis.

A91712WF

CELL VIABILITY OF THE ONCOTHERAD IMMUNOTHERAPY ON URINARY BLADDER CARCINOMA CELLS: NEW THERAPEUTIC PERSPECTIVE FOR BLADDER CANCER

FÁVARO Wagner J. [1, 2], FERREIRA Luiz A.B. [3], DURÁN Nelson [1,2,4]

(1) Laboratory of Urogenital Carcinogenesis and Immunotherapy, Department of Structural and Functional Biology, University of Campinas (UNICAMP), Campinas-SP, Brazil; (2) NanoBioss, Institute of Chemistry, University of Campinas (UNICAMP), Campinas-SP, Brazil; (3) Nano-cell Interactions Lab., Department Biochemistry & Tissue Biology, University of Campinas (UNICAMP), Campinas-SP, Brazil; (4) Nanomedicine Research Unit (Nanomed), Federal University of ABC (UFABC), Santo André-SP, Brazil

The treatment of non-muscle invasive bladder cancer (NMIBC) remains a challenge in the pharmaceutical field due the recurrence and progression of the disease, as well as the pronounced side effects still associated to the available therapeutic modalities. OncoTherad (MRB-CFI-1) is a nanostructured inorganic phosphate complex (CFI-1) associated to glycosidic protein (P14-16), which exhibits immunomodulatory and antitumor properties, developed by our research group1. Thus, this study describes cell viability of the OncoTherad (MRB-CFI-1) and its components (CFI-1 and P14-16) on urinary bladder grade II carcinoma cells (5637 cell line), after 24 hours of incubation. The cell viability of OncoTherad (MRB-CFI1)and its components, CFI-1 and protein P14-16, was 76.01% ± 12.39, 68.63% ± 9.47 and 75.71% ± 11.52, respectively, using the maximum concentration of 12.5 mg, as demonstrated in the MTT reduction assay (Figure 1A). Also, the impact of OncoTherad (MRB-CFI1)treatment on cell membrane integrity was verified, where calcein negative cells were observed, indicating loss of cell viability, and propidium iodide (PI) positive cells, indicating cell death (Figure 1B). The results with 12.5 mg of the OncoTherad (MRB-CFI-1) showed 75.25% ± 6.19 calcein positive and 25.50% ± 2.52 positive PI for cell death. Therefore, all techniques reported comparable dose–response relationship and the OncoTherad (MRB-CFI-1) immunotherapy showed low toxicity, as expected from immunomodulatory drugs. Taken together, the data obtained demonstrated that OncoTherad (MRB-CFI-1) immunotherapy could be considered a safe and effective therapeutic option for patients with bladder cancer.

[1] Fávaro, W.J., Durán N. Brazilian Patent PIBR 10 2017 012768 0 (2017).

4. Comitês de Ética

UNICAMP

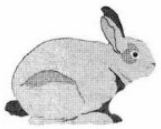

CEUA/UNICAMP

C E R T I F I C A D O

Certificamos que o projeto intitulado **"Citotoxicidade, endocitose e processamento celular de nanopartículas biossintéticas de prata em macrófagos peritoneais"**, protocolo nº **4014-1**, sob a responsabilidade de **Dr. Marcelo Bispo de Jesus / Luiz Alberto Bandeira Ferreira**, que envolve a produção, manutenção e/ou utilização de animais pertencentes ao filo *Chordata*, subfilo *Vertebrata* (exceto o homem) para fins de pesquisa científica ou ensino, encontra-se de acordo com os preceitos da **LEI Nº 11.794, DE 8 DE OUTUBRO DE 2008**, que estabelece procedimentos para o uso científico de animais e do **DECRETO Nº 6.899, DE 15 DE JULHO DE 2009**, e com as normas editadas pelo **Conselho Nacional de Controle da Experimentação Animal - CONCEA**, e foi aprovado pela **Comissão de Ética no Uso de Animais** da **Universidade Estadual de Campinas - CEUA/UNICAMP,** em reunião de **19 de outubro de 2015**.

Vigência do projeto: 11/2015-05/2019
Espécie/Linhagem: Camundongo isogênico / C57BL/6JUnib
No. de animais: 40
Idade/Peso: 04 semanas / 10g
Sexo: fêmeas
Origem: CEMIB/UNICAMP

A aprovação pela CEUA/UNICAMP não dispensa autorização prévia junto ao **IBAMA**, **SISBIO** ou **CIBio**.

Campinas, 19 de outubro de 2015.

Profa. Dra. Liana Maria Cardoso Verinaud
Presidente

Fátima Alonso
Secretária Executiva

UNICAMP

CEUA/UNICAMP

CERTIFICADO

Certificamos que a proposta intitulada **Avaliação nanotoxicológica in vivo das nanopartículas de prata**, registrada com o nº **4410-1**, sob a responsabilidade de **Prof. Dr. Marcelo Bispo de Jesus e Luiz Alberto Bandeira Ferreira**, que envolve a produção, manutenção ou utilização de animais pertencentes ao filo *Chordata*, subfilo *Vertebrata* (exceto o homem) para fins de pesquisa científica (ou ensino), encontra-se de acordo com os preceitos da **LEI Nº 11.794, DE 8 DE OUTUBRO DE 2008**, que estabelece procedimentos para o uso científico de animais, do **DECRETO Nº 6.899, DE 15 DE JULHO DE 2009**, e com as normas editadas pelo **Conselho Nacional de Controle da Experimentação Animal (CONCEA), tendo sido** aprovada pela **Comissão de Ética no Uso de Animais** da **Universidade Estadual de Campinas - CEUA/UNICAMP,** em **13 de dezembro de 2016**.

Finalidade:	**( ) Ensino (X) Pesquisa Científica**
Vigência do projeto:	**01/01/2017-01/01/2019**
Vigência da autorização para manipulação animal:	**01/01/2017-01/01/2019**
Espécie / linhagem/ raça:	**Rato heterogênico / HanUnib: WH (Wistar)**
No. de animais:	**128**
Peso / Idade:	**06 semanas / 200g**
Sexo:	**machos**
Origem:	**CEMIB/UNICAMP**

A aprovação pela CEUA/UNICAMP não dispensa autorização prévia junto ao **IBAMA**, **SISBIO** ou **CIBio** e é **restrita** a protocolos desenvolvidos em biotérios e laboratórios da Universidade Estadual de Campinas.

Campinas, 13 de dezembro de 2016.

Profa. Dra. Liana Maria Cardoso Verinaud
Presidente

Fátima Alonso
Secretária Executiva

IMPORTANTE: **Pedimos atenção ao prazo para envio do relatório final de atividades referente a este protocolo: até 30 dias após o encerramento de sua vigência. O formulário encontra-se disponível na página da CEUA/UNICAMP, área do pesquisador responsável. A não apresentação de relatório no prazo estabelecido impedirá que novos protocolos sejam submetidos.**

5. Declaração de não infringência sobre os direitos autorais

Declaração

As cópias de artigos de minha autoria ou de minha co-autoria, já publicados ou submetidos para publicação em revistas científicas ou anais de congressos sujeitos a arbitragem, que constam da minha Dissertação/Tese de Mestrado/Doutorado, intitulada **MECANISMO DE MORTE CELULAR E TOXICIDADE IN VIVO DE NANOPARTÍCULAS BIOSSINTÉTICAS DE PRATA**, não infringem os dispositivos da Lei n.° 9.610/98, nem o direito autoral de qualquer editora.

Campinas, 10 de dezembro, 2019

Assinatura : _____
Nome do(a) autor(a): **Luiz Alberto Bandeira Ferreira**
RG n.° 40.293.297-7

Assinatura : _____
Nome do(a) orientador(a): **Marcelo Bispo de Jesus**
RG n.° 32.591.974-4